DESIGN AND ANALYSIS OF A LIGHTWEIGHT PARALLEL CABLE-CONTROLLED MANIPULATOR

by

ROBERT H. MONTGOMERY

B.F.A., Sculpture
Rhode Island School of Design
(1971)

B.S. Mechanical Engineering
Southeastern Massachusetts University
(1984)

SUBMITTED IN PARTIAL FULFILLMENT OF THE REQUIREMENTS FOR THE DEGREE OF

MASTERS OF SCIENCE IN MECHANICAL ENGINEERING

at the

Massachusetts Institute of Technology
December 1987

Signature of Author _____
Department of Mechanical Engineering
December 1, 1987

Certified by _____
Thomas B. Sheridan
Thesis Supervisor

Accepted by _____
Ain A. Sonin
Chairman, Department Committee

DESIGN AND ANALYSIS OF A LIGHTWEIGHT
PARALLEL LINK CABLE-CONTROLLED MANIPULATOR

by Robert H. Montgomery

Submitted to the department of Mechanical Engineering on December 1, 1987 in partial fulfillment of the requirements for the Degree of Master of Science in Mechanical Engineering.

ABSTRACT

The utility and pitfalls of lightweight, electric motor driven, cable controlled parallel manipulators for low power applications such as outer space have been investi--gated using analysis and the results from experimentation with a 3 DOF test robot. The limitations of power consumption and flexibility imposed by the outer space environment coupled by the potential for very large inertial loading presents substantial design challenges to robots. Presently serial manipulators while able to meet the power limitations are also quite flexible for the low mass and large sizes required. A cable-controlled parallel manipulator, which directly controls the endpoint through cables, may be stiffer than a similarly sized serial manipulator. Unfortunately to maintain tension in the cables a central spine which applies outward force and consumes power is necessary.

The power analysis shows that if the spine force is actively controlled to an optimal minimum then the cable controlled parallel manipulator can approach the power consumption of a parallel manipulator which has compressive and tensile links such as hydraulic cylinders instead of cables.

The endpoint flexibility of the parallel manipulator depends on the stiffness of the cable drives and not the stiffness of the spine. Analytic comparisons of dynamic endpoint oscillations with a 'dynamically equivalent' serial manipulator show a 1/2 to 1/3 reduction in magnitudes of oscillation for the parallel manipulator. Furthermore the oscillations in the parallel manipulator can be reduced significantly by increasing cable stiffness.

Thesis Supervisor: Dr Thomas B. Sheridan
Professor of Engineering and
Applied Psychology

TABLE OF CONTENTS

LIST OF FIGURES

Chapter 1
PURPOSE AND INTRODUCTION

Purpose

Investigate , demonstrate and analyze the utility and pitfalls of lightweight electrically powered cable -controlled parallel link manipulators for low power applications such as outer space.

Introduction

The first cable-controlled parallel link robot was designed and built in the MIT Man Machine Lab [1] as a manipulator arm for a remotely operated midget ubmarine, fig 1.1. This hydraulically powered arm has surpassed all expectations proving itself faster, stronger, stiffer, lighter, and more accurate than comparably sized serial link robot arms. The inherent stiffness and lightness of these parallel robots has suggested a possible utility in outer space.

Space Shuttle Robot Arm

The present space shuttle uses a six degree of freedom (DOF) serial link robot arm with a reach of 50 feet, fig 1.2. The design load is 30,000 lbm, 15 ft diameter, and 60 ft length in a weightless environment. The arm is built so lightly that it cannot support its own weight on the surface of earth.

This arm has been described as quite flexible and is normally operated with either the wrist 3 DOF or the shoulder and elbow 3 DOF locked. The arm is generally positioned with the translational DOF and fine operations are performed with the rotational DOF. The total arm mass is 795 lbm and the total energy budget for actuation is 535 watts. The actuators are back-drivable geared brushless DC electric motors with gear ratios up to 1842:1 [9].

At the full 50 ft extension the translational stiffness is approximately 15 lbf/in. Assuming the extended arm behaves like a cantilever beam the unloaded arm's natural frequency is .9 hz while the fully loaded arm's is .07 hz. It is likely that the structural modes will be close to the bandwidth of all but the slowest controls.

Parallel Space Robot

The limitations of power consumption and flexibility imposed by the space environment coupled with the potentially very large inertial loads present substantial design challenges for robots. Parallel actuated robots may provide additional stiffness by controlling the endpoint directly with cables. To investigate the performance of long and flexible cable-controlled parallel manipulators a test 3 DOF parallel robot was built, fig 1.3. Experimentation with the test robot provided the experience and indicated where analytic techniques could be meaningfully applied. This thesis will describe the design and performance of this test robot, an analysis of power consumption and compliance, and a comparison of endpoint position control between the parallel manipulator and a 'dynamically equivalent' serial manipulator.

Chapter 2
DESIGN SPECIFICATIONS

Broad Guidelines

The test robot 'design task' is to demonstrate the potential of parallel robots for outer space. The size and performance requirements grew from considerations of intent, size practicality, and cost limitations. Broad guidelines for the project were:

1) Price ceiling of $2000.
2) Positioning of an 1 lbm inertial design load at a reasonable bandwidth.
3) Electric motor driven actuators.
4) Bigger than a bread box, smaller than a refrigerator, with the final dimensions as determined by preliminary analysis and motor choice. A base radius of 1 foot will serve as a starting point.
5) Start with a 3 DOF manipulator which can be expanded to 6 DOF at a later date.
6) Identify potential outer space operational problems with the test robot. Analyze these problems.
7) Further evolve the hardware design of the original parallel robot.

Preliminary Static Analysis

Broad generalizations of the design limits can be derived from static analysis of the existing 6 DOF parallel robot, fig 1.1. The terms used in the following analysis are defined in fig 2.1. The base radius Rb is the radius

of the circle defined by the intersection of the cables with the base. Likewise, the platen radius Rp is defined by the intersection of the cables with the platen. The spine angle ß is the angle the spine has rotated from the vertical position. The spine length R is the distance from the gimbal to the platen. The base angle α is the angle the endpoint has rotated from the Xb axis in the XYb plane. To make the analysis general the spine length and platen radius are normalized by the base radius Rb. Hence a normalized spine length of 8 is a spine length which is 8 times the base radius.

Using the equations of statics outlined in [1] the cable tensions and the corresponding spine force necessary to maintain tension in all the cables are found as a function of varying spine length, spine angle, and platen radius for a set of unit force and unit moment loads in XYZb directions. The unit moments are a unit force times a unit length where a unit length is defined as the base radius Rb. The cable tensions and spine forces are in unit forces. Hence if a unit force is 1 lbf and the base radius is 1 foot then a unit moment is 1 ft lbf; likewise, the cable tension and spine force are in lbf. These force and moment loads are intended to loosely represent the gravitational and inertial loading reflected to the motors and spine.

There are five notable results from this analysis:

1) For a constant spine angle, base radius, and platen radius, the maximum cable tension and corresponding spine force increase linearly with increasing spine length for both force and moment loading, fig 2.2.
2) For a constant spine length, base radius, and platen

radius, the maximum cable tension and corresponding spine force due to both force and moment loading are constant for spine angles less than 30 degrees but increase linearly for spine angles greater than 30 degrees, fig 2.3

3) For a constant spine length, base radius and spine angle, the maximum cable tension and corresponding spine force increase inversely for decreasing platen radius under moment loading but are constant for force loading, fig 2.4

4) For a constant base radius, the maximum cable tension and corresponding spine force due to force loading in the gravitational direction increase linearly with increasing spine length and angle, fig 2.5. Below 30 degrees spine angle the effects of gravitational loading are less than loads in the other directions, compare fig 2.3 with fig 2.5

5) The spine force is generally two to five times larger than the maximum cable tension for a given load set.

Counterbalance

It is apparent that the 1 lbm design load will present problems due to gravitational loading. If we assume a massless spine of normalized length 8 at 60 degrees spine angle, a minimum spine force of 30 lbf and maximum cable tension of 10 lbf will be necessary. A slightly more realistic spine of 1 lbm at the endpoint requires 60 lbf spine force and 20 lbf cable tension. The gravity loading will drive the design to much larger sized components than would be necessary in a gravity free environment. This heftier robot will be more expensive and, worse, may not have the flexible qualities of a space robot. To circumvent this problem a counterbalance is added to the spine which

negates as much of the gravity loading as possible. A counterbalance which balances the spine and load at half its extension length which will lower the necessary tensions and spine forces by 1/3. The trade off is a larger inertial load which will tend to flex the spine. Given the purpose of the test robot this added flexing is an advantage. The actual inertial increase due to the counterbalance is not large, 20% at a spine length of 60 inches.

Active and Passive Spine

The spine force can be passive or actively controlled. An example of a passive spine is a constant force spring which exerts an approximately constant force regardless of position, orientation or load. An active spine exerts a force as demanded by a control system. In the passive case a worse case spine force over the operating envelope is necessary to always maintain tension in the cables. To accommodate a reasonable workspace and load this passive force may become quite large. Most of the time the major portion of the power expended by the cable winches is used to restrain the passive spine force. In space spine force or cable tension is necessary only when the robot is moving or performing a work task like drilling. It seems reasonable that to minimize power consumption and weight an actual space robot should have some form of an active spine which will exert some optimized spine force. The practicality and pitfalls of an active spine will be demonstrated with an electrically powered active spine.

Other Six DOF Ideas

There are inherent workspace limitations of the existing 6 DOF robot which can be minimized with other cable actuated parallel forms. The rotational capability of the existing parallel robot is limited to ±30 degrees in the spine direction [1]. Moment loading capability is dependent on platen radius but large platens limit the workspace. An alternative design which could minimize these limitations is a hybrid arm with 3 translational DOF provided by cables and 3 rotational DOF provided by a conventional 3 roll wrist or even a short spherical arm mounted on the end, fig 2.6. These configurations would have very simple kinematics and dynamics which would be solvable in both the forward and inverse forms. The notable disadvantage of these hybrid manipulators is that the spine would have to be capable of absorbing additional moment loading from the wrist. This project will use a 3 DOF spine leaving the option for the final 6 DOF form open for future research, fig 1.3

Chapter 3
KINEMATICS

Kinematics in General

Kinematics can be defined between any two coordinate spaces. Of particular interest on the parallel robots are the relationships of end point position to joint displacement, end point position to cable length, and joint displacement to cable length In open chain serial link robots forward kinematics are the geometric equations which define endpoint position in terms of joint displacement, while inverse kinematics define joint displacement in terms of end point position. While parallel robots can be analyzed by the same kinematic methods as the serial robots the added complexity of both cable length and joint displacement creates confusion as to which are forward and which are inverse kinematics. To avoid the problem the terms forward and inverse will not be used in this thesis.

All kinematics for the 3 DOF parallel robot are straightforward and solvable as is generally the case for 3 DOF robots. The solvability of kinematics in 6 DOF serial manipulators can be guaranteed where the last three joint axis coincide at a point [3]. The hybrid robot of fig 2.6 would fall into this category whereas the full cable 6 DOF parallel robot of fig 1.1 would not.

Definitions

Previous research [1] has defined the cables as links. This method does not explicitly include the spine in the analysis and the spine mass must be neglected or lumped at the endpoint. Since the space and test parallel robots will have a large spine, no platen, small load, and light cable it makes more sense to define the spine and gimbal as links , fig 3.1. This choice adapts nicely to Denavit-Hartenberg notation and provides a bridge to existing theory developed for serial link robotics.

Spherical coordinates which seem to be the natural coordinate system of the robot, will be used to describe endpoint position but they cannot be used for the analysis. Spherical coordinates by a quirk in math are redundant and hence singular at the vertical spine position where the spine angle β is zero. In this position a unique position in 3 dimensions can be described with only two coordinates, R, spine length and β, spine angle. A better set of coordinates which can be used later for generalized coordinates in the dynamic analysis are the gimbal joint displacements $\theta 1$, $\theta 2$, and spine length R, fig 3.1.

Kinematics of Joint Space to End Space:

In the base coordinate system, fig 3.1, the position of the endpoint as a function of the joint displacements is ,

$$\underline{Xe} = \begin{matrix} xe \\ ye \\ ze \end{matrix} = \begin{matrix} R \sin\theta 1 \sin\theta 2 \\ -R \cos\theta 2 \\ R \cos\theta 1 \sin\theta 2 \end{matrix} \quad . \qquad (3.1)$$

Infinitesimal motions and velocities of the endpoint due to joint motions are related by the Jacobian where,

$$d\underline{Xe} = \underline{J}_{\theta} \, d\underline{\theta} \; . \qquad (3.2)$$

A Jacobian is essentially a matrix of the first order terms in a Taylor Series evaluated at a point, the Jacobian in eq. 3.2 can be expanded to,

$$d\underline{Xe} = \begin{bmatrix} dxe \\ dye \\ dze \end{bmatrix} = \begin{bmatrix} \delta xe/\delta R & \delta xe/\delta\theta 1 & \delta xe/\delta\theta 2 \\ \delta ye/\delta R & \delta ye/\delta\theta 1 & \delta ye/\delta\theta 2 \\ \delta ze/\delta R & \delta ze/\delta\theta 1 & \delta ze/\delta\theta 2 \end{bmatrix} \begin{bmatrix} dR \\ d\theta 1 \\ d\theta 2 \end{bmatrix} . \qquad (3.3)$$

The terms after the indicated differentiation are,

$$\underline{J}_{\theta} = \begin{bmatrix} S\theta 1 \; C\theta 2 & R \; C\theta 1 \; S\theta 2 & R \; S\theta 1 \; C\theta 2 \\ -C\theta 2 & 0 & R \; S\theta 2 \\ C\theta 1 \; S\theta 2 & -R \; S\theta 1 \; \theta 2 & R \; C\theta 1 \; C\theta 2 \end{bmatrix} . \qquad (3.4)$$

This particular Jacobian will be useful in the dynamic analysis.

Kinematics of End and Joint Space to Cable Space

The cables and coordinate vectors are shown in fig 3.2. Cable vectors L1, L2, and L3 are the vector differences between tie point vectors I, II, and III and the end point vector Xe.

$$\begin{aligned} \underline{L1} &= \underline{Xe} - \underline{I} \\ \underline{L2} &= \underline{Xe} - \underline{II} \\ \underline{L3} &= \underline{Xe} - \underline{III} \; . \end{aligned} \qquad (3.5)$$

Jacobians linking infinitesimal motions in end space or joint space to infinitesimal motions in cable space can be defined such that,

$$\begin{aligned} d\underline{L} &= \underline{J_{\theta}} \; d\underline{\theta} \\ \text{or} & \qquad , \\ d\underline{L} &= \underline{J_{x}} \; d\underline{Xe} \quad . \end{aligned} \tag{3.6}$$

The terms of these Jacobians are in Appendix 3.1. Note that the vector dL is composed of the three scalar lengths of cables L1, L2 and L3,

$$d\underline{L} = \begin{bmatrix} dL1 \\ dL2 \\ dL3 \end{bmatrix}. \tag{3.7}$$

The inverse of the previous kinematics are useful in static and dynamic analysis. End point position can be found as a function of cable length, the algebra is straightforward but involved and the results are in Appendix 3.2. The Jacobian linking cable length to end point position is defined,

$$d\underline{Xe} = \underline{J_{L}} \; d\underline{L}. \tag{3.8}$$

It is important to note that the Jacobians $\underline{J_{x}}$ and $\underline{J_{L}}$ are inverses,

$$\underline{J_{x}} = \text{INV } \underline{J_{L}} \; . \tag{3.9}$$

It is very handy to be able to calculate this without resorting to analytical inversion.

Chapter 4
STATICS

The equations in this chapter are a restatement of equations in S. Landsberger's thesis [1] in a standard notation which simplifies later work. The equations are general in nature and with the proper expansion of the vectors and Jacobians to include rotations and moments these equations can be used for six DOF manipulators [2].

Static Equation of Equilibrium

Static equilibrium is guaranteed by a balance of forces at the endpoint E of the manipulator, fig 4.1. The forces acting on E are the cable tensions TL, the external forces -Fe, the spine force Fs. The sign convention for Fe is positive for the force which the manipulator exerts on the environment and negative for the force the environment exerts on the manipulator. The sign convention for the cable tension TLi is positive for compression which corresponds to increasing cable length, This sign convention yields positive work for pulling in or pushing out (impossible) cable. The sign convention of spine force Fs is positive in the direction the spine exerts force on the endpoint, E. Gravity components of the spine, cable or load can be added to either the external forces or the spine force.

The equation for static equilibrium can be found from the principal of virtual work [2],

$$\delta \text{Work} = \underline{TL}^T \, \delta \underline{L} + \underline{Fs}^T \, \delta \underline{Xe} - \underline{Fe}^T \, \delta \underline{Xe} \; . \qquad (4.1)$$

The virtual displacements in cable space can be transformed to end space by eq. 3.6. The equation of equilibrium is found by letting the virtual work go to zero,

$$\underline{J}_{\underline{x}}^T \, \underline{TL} + \underline{Fs} = \underline{Fe} \qquad (4.2)$$

This could be alternatively expressed as

$$\underline{J}_{\underline{x}}^{-T} \, (\underline{Fe} - \underline{Fs}) = \underline{TL} \qquad (4.3)$$

Relationship Between Spine Force and Cable Tension

Cable tension is maintained by the spine force. There is a minimum spine force Fs at which cable tension(s) become zero and the manipulator is on the verge of collapse. This spine force can be found by resolving $\underline{Fs}$ into a magnitude and a direction and inserting them into eq 4.3

$$\underline{TL} = \underline{J}_{\underline{x}}^{-T} \, (\underline{Fe} - Fs \, \underline{Fsd}) \; . \qquad (4.4)$$

There are three independent equations for the tensions in each cable. The largest Fs for which yields zero tension in one of the cables is the minimum spine force for rigidity,

$$Fsmin = \max Fsi = \max \left[\frac{[\, \underline{J}_{\underline{x}}^{-T} \, \underline{Fe} \,] \text{ ith component}}{[\, \underline{J}_{\underline{x}}^{-T} \, \underline{Fsd}] \text{ ith component}} \right] . \qquad (4.5)$$

Likewise the maximum load Fe can be found by separating Fe into magnitude and direction. The largest Fe will be the smallest Fe which yields zero tension in one of the cables

$$Fsemax = \min Fei = \max\left[\frac{[\ J\mathfrak{E}^{-T}\ Fs\ ]\ \text{ith component}}{[\ J\mathfrak{E}^{-T}\ Fed]\ \text{ith component}} \right]. \qquad (4.6)$$

Results

To design the winches and choose the motors a sense of the cable tensions over the workspace for the 3 DOF test robot is necessary. The equations of equilibrium for the 3 DOF test robot have been solved over the work space for the following conditions: with and without the spine gravity loading; with and without the counterbalance; with and without a 1 lbm load; and finally with and without a constant spine force of 25 lbf.

The particulars of the actual spine are in chapter 5 Hardware Design. The spine is counterbalanced for no load at a 20 inch rod extension using a 12.5 lb weight, fig 5.6. The base radius is 1 foot so a spine length of 5 is now more specifically a spine length of 5 feet, or 60 inches.

The cable tensions and spine forces for a spine angles up to 60 degrees and spine lengths to 8 feet are presented in fig 4.2 to 4.6 . Included in this study are the effects of: the counterbalance; fixed spine force; and load. The results can be summarized :

1) The uncounterbalanced spine has a linear relationship between cable tension and both spine length and spine angle. The counterbalanced spine also has a linear relationship between cable tension and spine angle but shows a minimum at the spine length where the spine is counterbalanced.

2) Maximum cable tensions are reduced significantly by the counterbalance. For the minimum spine force cases at a spine angle of 60 degrees the tension reductions are approximately 15 lbf loaded and 30 lbf unloaded.

3) Maximum spine force is reduced by the counterbalance. For both the loaded and unloaded case the difference is about 25 lbf.

4) A constant passive spine force of 25 lb will work over the entire work space for the unloaded case and over all but extensions over 5 feet at 60 deg spine angle for the loaded case.

5) The design cable tension will be 10 lb for the unloaded case and 15 lb for the loaded case. The design spine force is 30 lbf.

6) In zero gravity when the manipulator is at rest without external loading neither spine force nor cable tension are necessary to maintain equilibrium. Cable tension is also independent of the counterbalance and load mass at the endpoint. For a spine force of 25 lbf and spine lengths above 3 feet the maximum tensions are below 10 lbf for all spine angles, fig 4.6. The unloaded counterbalanced case , fig 4.3, is very similar to this weightless case.

Chapter 5
HARDWARE DESIGN

The test robot is a piece of laboratory hardware which is used for experimentation in a friendly environment. The hardware was designed and laid out to accommodate change easily as future experiments take shape. The pieces are as independent as possible so they can be moved or replaced without affecting other parts. There is a conscious effort to reduce the number of parts and the machine work necessary to make each part. Critical dimensions are held to the bare minimum. Aesthetically the test robot is intended to emphasize simplicity and potential utility of this very simple type of manipulators.

Motors

Permanent Magnet DC Gearmotors were chosen to power the cable winches and active spine on the basis of simplicity, availability and cost. In a real space application Brushless DC Gearmotors [6] would be the probable choice for superior performance, heat dissipation, size, and weight. For this application the brushed motors are more than sufficient.

There are two basic equations for the analysis of DC brushed motors . From the DC Motor model, fig 5.1 Kirchoff's voltage law yields the first basic motor equation,

$$E = I\ Rt + Ke\ w + L\ dI/dt\ . \qquad (5.1)$$

where: E = applied voltage
I = motor current
L = motor inductance
Rt = winding resistance
Ke = back emf constant
w = motor speed

The second equation expresses that the torque is proportional to the current in a permanent magnet motor,

$$\tau l + \tau m = Kt\ I\ . \qquad (5.2)$$

where: τl = torque applied to the load
τm = internal motor torque losses
Kt = motor torque constant

This relationship has two very useful consequences. The torque output of a DC motor can be limited by a current limit in the servo amplifier and the torque output can be calculated from the current. The torque calculation becomes difficult in the case of inexpensive gearmotors due to the never-ending presence of static and dynamic friction.

These two equations can be combined and rearranged into a form commonly used to generate motor performance curves,

$$w = \frac{E}{Ke} - \frac{Rt}{Kt\ Ke}(\tau l + \tau m) \qquad (5.3)$$

.

Motor speed is the linear combination of both applied voltage and torque. The typical performance curves drawn from this equation are shown in fig 5.2. For the ideal case with no internal torque losses and constant input voltage the motor will operate more or less along a straight line between no load speed and stall torque. Inspection of the curves shows that for low speeds these motors can potentially exert large torques. Unfortunately there are thermal limitations, the I squared R winding losses must be dissipated or the windings will burn out. The continuous torque limitations are a function of how much heat the motor can dissipate [5],

$$r_{con} = K1\ Km \left(\frac{Tmax - Tamb}{Zt} - \frac{r_m w}{K2} \right)^{.5} - r_m \qquad (5.4)$$

where: Tmax = max winding temperature
Tamb = ambient temperature
Zt = motor thermal impedance
Km = motor constant = $Kt/\sqrt{Rt}$
K1 = constant dependent on magnet material
K2 = unit conversion

The continuous torque limitations and the effects of current limiting by the servo amplifier are included on the performance curves , fig 5.2. The continuous operation area is a small percentage of the potential motor capability. The continuous torque capacity can be enlarged with various cooling schemes for the windings such as forced air. The brushed motors are difficult to cool since the windings are on the rotating armature which can only be cooled by convection. The torque above the continuous zone but below current limiting can be considered the

transient zone. It is apparent that these motors have considerably more transient than continuous capability. Since the dynamic loading on the motors is an order of magnitude less than the static loading [1] and the transient capability of the motors is much greater than the continuous capability, the motor choice will be determined by the static loading. The question which remains unanswered is how continuous is continuous, the curves calculated by these equations will give a very continuous nonstop, day in and day out torque capacity. This capacity is probably overkill since the test robot will not be operated for long periods especially in the extreme operating zones and the experimental nature of the robot encourages pushing the hardware.

The motors chosen are Pittman GM9434 DC gearmotors whose performance curves are the ones presented in fig 5.2. This gearmotor has an 11.5:1 gear ratio, a winding voltage rating of 30 v and max stall current of 6.5 amps. The other motor constants are in Appendix 5.1. These motors have a maximum continuous torque at zero speed of 4 in lbf which translates to 8 lbf cable tension. This is less than the static design tension of 10 lbf unloaded and 15 lbf loaded, but the availability, extremely low price of $20, intermittent use, and fall back position of adding cooling or even mounting two motors per winch made the chance worth taking. The overhung load translated to 800 psi at the outboard bearing which is not excessive for the bronze bearings. The standard gearing is rated for 10 in lb output torque or 20 lb cable tension.

Typically electric motors do not operate smoothly around zero speed. Static friction can cause the motors to

stick or cog at very low speeds. There are design techniques to minimize the friction effects such as increasing and skewing the slots on the armature; and using ball bearings. These motors have seven skewed slots and bronze bearings. Clearly there are limits of what $20 buys. The friction due to the brushes is unavoidable though and on such small motors it can become a sizable percentage of the total torque losses. In the control section this frictional loss is measured.

Servo Amplifiers

Aerotech Model 3010 Linear Servo Controllers were chosen to drive each motor. These amplifiers are rated at ±30 volts with ±10 amps peak and ±3 amps continuous output. The power dissipation rating is 350 watts peak and 70 watts continuous This will more than drive the motors since the 3 amps correspond to 28 lbf cable tension. Each amplifier has its own power supply to transform and rectify 125 VAC. There is a 741 op-amp based preamplifier which provides a DC open loop voltage gain of 100db, an inverting summing junction for three single ended inputs, and provisions for a standard compensation. Two of the inputs have adjustable gains. The power amplifier is configured in a current feedback mode which yields a 1.2 amps/volts gain out to a 2 Khz bandwidth. The power amplifier maintains a current output proportional to a voltage input. Since the motor torque depends on current, the inner closed current loop yields much faster torque response than a voltage to voltage amplifier. The amplifier is protected from downstream short-circuits by output current fusing. Adjustable current limits on the outputs provide motor protection. There are ±15v power outlets to run additional external control circuitry.

Potentiometers

Helipot AJ ten turn, 100 kΩ linear potentiometers are used for position feedback. The pots are driven by the winch drum with a 2.75:1 spur gear reduction to account for the full cable capacity. The pot linearity is .075% which could amount to a .07 inch error in cable length from beginning to end of the full 92 inches. This error is negligible for a system as flexible as this manipulator.

Tachometers

Harowe 1211-003 DC tachometer were used to provide rate feedback to the position controls. These tachometers have a .1% linearity and a 3% maximum ripple. Originally I wasn't going to use rate feedback but it was necessary as will be explained in the control section. The tachometers are driven by a belt from the winch drum at a 1:1 ratio. The output from the tachometer is 20.8 v/1000 rpm.

Cable

The design cable tension of 15 lbf is handled by a 1/32 diameter stainless 7 by 7 aircraft cable with a minimum breaking strength of 120 lbf which yields an acceptable safety factor of 8 [4]. The minimum recommended bend radius for this diameter cable is 15/16 inches or 30 diameters for 7 by 7 cable.

Winch Drums

The winch drums must be large enough to hold all the cable; as small in diameter as possible to provide gear reduction; and short enough to minimize the overhung load on the motor shaft without an extra outboard bearing. The winch drums are shown in fig 5.3. The winch diameter is 1 inch to satisfy the minimum bending radius of the cable. For a spine length capability of 2 to 8 ft and a spine angle capability of 60 degrees it is necessary to store 92 inches of cable. This cable length corresponds to 29 wraps on the 1 inch diameter drums, drum lengths of 1 3/8 inches will be sufficient to handle the length plus provide room for a belt to drive a tachometer. There are .5 inch high flanges on each end of the drum to encourage loose cable to remain on the drum. A through hole is provided at the end opposite the motor for cable mounting via a dead end crimp. A small stub shaft with a ten tooth gear is mounted on the end opposite the motor to drive the potentiometer. Both the motor and the stub shaft are slip fit into a .250 inch hole reamed through the center of the drum. Shaft attachment is provided by set screws tightened upon flats ground on the shaft.

Winches

Each winch assembly has a motor, potentiometer, tachometer, winch drum, and base, fig 5.4. The winches are self contained and surface mounted with four bolts to the lab stand top. The winches can be easily repositioned on the lab stand to try different configurations. The winch drum axes are horizontal to take advantage of gravity in

cable winding, hence minimizing keepers and followers. The wire on a vertical drum would slide downwards every time the tension was relaxed unless the drum was grooved and there was some method to maintain tension at the drum face. It would be very difficult to keep such thin cable in grooves without some fairly sophisticated tensioning and tracking devices. Cable tension during brief transients where the winches momentarily over-run the spine is maintained by tracking springs made of .012 inch music wire. The motor, potentiometer, and, and tachometer are mounted so that they can be changed independently.

As mentioned before, the fall back position in case one motor was insufficient is two motors per winch. These winches could easily be transformed to two motor drive by offsetting the potentiometer with a geared belt or chain drive. The drum would be mounted between the motors directly on the motor shafts. The motors proved powerful enough so this wasn't necessary but the technique was used successfully for the active spine

Flag Bocks

One flag block per winch is necessary to lead the cable from the manipulator endpoint onto the winches. An attempt at just using a simple block and eyebolt was not satisfactory since this arrangement added unwanted flexibility in the actuators. Ultimately six piece flag blocks were necessary, fig 5.5. Notable are the keeper which 'keeps' the wire centered and the wire spring lead, which insures that whichever direction the manipulator pulls a slack cable that cable will lead onto the pulley

and lift the block. An additional ball bearing may be warranted at the block swivel to eliminate drag which prevents the block from pointing directly towards the manipulator endpoint when the cable tension is low.

Passive Spine and Gimbal

The spine is the core of the test robot. The spine should be as long, light and flexible as is possible to simulate space operation . A 1 1/8 in diameter by 42 inch stroke Aro pneumatic cylinder was chosen for the spine, fig 5.6. This cylinder is 84 inches long fully extended, The cylinder is mounted in a two axis gimbal with the pivot at 6.5 inches up the cylinder, the full reach above the pivot will be 6.5 feet. There is a 12.5 lb counterbalance on the lower end of the cylinder below the pivot.

The rod is steel, 3/8 in diameter 46 inches long. The Euler buckling load is 40 lbf. at a full rod extension of 42 inches. This rod is quite limber with a fully extended unloaded natural frequency between 1 and 2 hz .

The passive spine force is supplied by connecting the cylinder to an a 6 gallon air tank which is charged with pressurized air. The air tank acts as an accumulator, the much larger tank volume ensures that there is very little change in spine force as the cylinder extends and retracts. The air pressure difference measured in the tank between full extend and retract is 4%. The rod is protected from buckling since the spine force is limited by the air pressure. Before the rod will buckle, an overloaded spine will retract and the cables will go slack.

Active Spine

A passive spine necessitates finding a worse case spine force over the operating range which will cause static cable tensions higher than necessary most of the time. In a weightless environment there are only dynamic forces which need to be satisfied. When the arm is stationary the spine force could be reduced to near zero. Additionally dynamic response could be improved if the spine force could be varied. Consider a transient of pure extension or contraction, increasing or decreasing the spine force could speed these up.

The passive system described above while well suited for the test robot is probably not practical in outer space, where there is certainly a problem recharging the air tank. The present shuttle arm is all-electrically actuated. It is likely that the outer space spine whether active or passive should be electrically actuated. Once the spine is electrically actuated making it passive probably necessitates an active control anyway.

There are numerous very different possibilities for designing an electric spine, ball screws, rack and pinion gear drives, and linkage drives to mention a few. A very simple possibility which requires no precision mating is a variation of the 'Sign Crane', which is a telescoping cable driven crane used for lifting light loads up to high positions. These cranes collapse to a fraction of their extended height. Six telescoping sections are not uncommon. An ingenious cable drive lifts all of the sections simultaneously. This type of mechanism can be adapted into an active spine with the addition of a force measuring device, fig 5.7.

Before embarking on designing and building the active spine described above it was necessary to demonstrate the concept of the active spine. There were unresolved issues which needed exploring such as: how will the force be measured; will there by a dynamic interaction between the position cable controls and the force controlled spine; what kind of bandwidth can be expected of the force control; will the spine cables turn into a tangle; will frictional losses make this design unworkable; and finally how will safety be provided to ensure that the cable winches are not overpowered and that the rod is not buckled?

To answer these concerns an interim active test spine was designed and built, fig 5.8. This spine is an adaptation of the present pneumatic cylinder passive spine. A pulley is fitted to cylinder end over which a cable is passed , led down the inside of the cylinder, and attached to the rod base. To pull this cable a winch is attached to the outside of the cylinder far enough down to provide adequate lead to the pulley and far enough up so as to not limit the workspace. For simplicity the same cable winch motors are used but there are two of them with a winch drum mounted between them. Force feedback is provided by mounting the winch on a pivot and holding it in place with a cable. In the middle of the cable is a simple 'C' clamp style 'load cell'. A strain gage is mounted on the back of the 'C' where bending is proportional to cable tension. This method while not measuring the rod force directly is close enough if friction between the sections can be kept at an acceptable minimum. Originally I intended to measure the tensile force in the rod but the dynamic bending in the rod made this a measuring

nightmare. The strain gage signal is conditioned with a Wheatstone bridge and Analog Devices AD524 instrument amplifier. For reasons which will be enumerated on in the control section a tachometer is used to provide damping.

Base and Layout

The servo amps and manipulator are mounted on a wheeled table, fig 5.9. The base radius of the flag blocks is 1 foot. The distance of the winches to the flag blocks is limited to a minimum of about a foot to allow for a fair lead onto the winches. The winches are laid out as they would conveniently fit on the table top and the flag blocks were positioned to lead the cable from the rod end to the winches for all arm positions. The spine counterweight and gimbal are mounted through an 8 by 12 inch hole in the table top. The servo amplifiers are mounted in the bottom of the cart. The amplifiers are protected from a falling counterweight by a shelf. Two 12 foot cables connect the table born electronics to the control interface box and computer.

Electronics and Wiring

The electronics of the system are broken into six distinct entities. The motors, feedback signals, servo amplifiers, input signals, interface box, and computer control, fig 5.10. The motors, feedback transducers, and servo amplifiers have been previously discussed. The computer is an Intel 310 with a 16 channel 12 bit a/d and a 8 channel 12 bit d/a. The command signals are supplied by

four 40k Ω potentiometers pirated off an old analog computer. The interface box connects the table born electronics with the computer and input signals. In this box are three boards with twelve 741 op-amps each. These amplifiers are used to buffer the input commands into and out of the computer, adjust gains on tachometer signals, and provide 50 radian/sec double pole anti aliasing filters for signals going into the computer. The control electronics are powered by a separate ±15 V power supply.

Chapter 6
CONTROL DESIGN

Cable Control Configuration

Currently the3 DOF endpoint position is controlled with three uncoupled closed loop cable length controls, fig 6.1. Endpoint position commands from the control board potentiometers are transmitted into the digital computer where the three cable lengths are calculated. The cable length commands are sent to the 3 servo amps which then close position loops with the potentiometer feedback. Additionally, there is rate feedback provided by the tachometers. Each servo amplifier has built in control circuitry which provides a summing junction for 3 inputs.

The control was developed on a 1 DOF system where only one cable was attached to a winch, the other two were tied off to cleats. Conceptually the two tied off cables are the perfect controls, they maintain cable length in the face of all disturbances. For a given combination of fixed cable lengths the trajectory is an arc with the radius dependent on the triangle formed by the two fixed cables. This circular trajectory can be routed through the workspace in many directions, spine lengths and spine angles giving the control and cable handling hardware a fairly decent workout before the final winch design and control design were expanded to 3 DOF.

A variety of control schemes were tried out during the 1 DOF development stage. Originally I hoped to do some sound modeling and analytic control design which would then

be implemented, tested, correlated, evaluated, and readjusted. Fortunately time and common sense prevailed; it proved far more efficient to allow the hardware and intuition to drive the the design and then later explain the phenomena with analysis. All of this was fine with me since by definition the robot is a perfect nonlinear model, and playing with the robot is far more fun than contending with some dreary computer model.

Endpoint position ,velocity, and acceleration of a typical serial link robot can be reflected to joint displacements. Typically the joints are directly driven by actuators. In a vector sense these actuators point in the same direction as the joints. Generally though independent joint angles can be defined the joints are dynamically coupled either by the dynamic link interaction or by centrifugal and Coriolis effects. The former coupling is characterized by non-diagonal elements in the inertia matrix; torque in one joint will cause torques and accelerations in other joints. The latter coupling is characterized by a configuration dependent inertia matrix; the product of two joint velocities induce joint torques due to centrifugal and Coriolis effects .

A truly uncoupled manipulator would have a diagonal-configuration-independent inertia matrix. The 2 DOF test robot has a diagonal inertia matrix for joint acceleration, chapter 9. This quality, which is not easily attained in serial robots but natural to the parallel robots, is due to having three coincident and orthogonal joint axis. The inertia is configuration-dependent, resulting in coupling due to centrifugal and Coriolis acceleration. In a very stiff parallel robot this dynamic

decoupling is lost by the choice of actuator direction. The parallel robot is not driven at the joints but by cables which do not point in the direction of any of the joints. Most trajectories, with the exception of the previously mentioned 1 DOF arc trajectories, need length changes in all three winches. A change in length in any one cable will generally change all three joint displacements. An acceleration at any joint is accompanied by torques in all three winches. Likewise an acceleration in any cable will induce torque in the two remaining winches.

The 3 DOF parallel robot is dynamically coupled from cable length to either the end point or joint displacements. This coupling is outside of the closed loop since the loops are not closed on joint angle or endpoint feedback but instead on cable position. The entire system is stable since the robot is open loop stable from cable position to endpoint position. The robot presents disturbance loading to the actuator loops which will be accepted or rejected on the merits of the individual loops. This does not imply that the output of the robot is uncoupled from the cable actuators but that the cable loops are interconnected only by coupled disturbances [1]. The assumption is that enough is known about the robot to ensure that a desired output can be attained from knowing where the actuators are. In the case of rigid robots this is probably true.

It has been shown but is hard to believe that local position controls such as uncoupled PD on each joint axis will be stable and robust to coupled manipulators even though the controls were designed without consideration of

the coupling [2]. These local PDs behave like springs and dampers at each joint centered at the command position. Eventually all of the joints will assume the desired endpoint position. If a large step in displacement is given the manipulator can assume some fairly wild configurations during the transient since the trajectory of the links is not directly controlled . When these local position controls are used for trajectory tracking a continuous stream of positions is given which each joint will follow with varying degrees of success depending on the bandwidth of the command and the control and disturbance rejection capabilities of each control.

Linear Model

The closed position loop for one cable winch is shown in fig 6.2. The dynamic plant model from force to speed is a first order lag where an equivalent mass Me ,and equivalent damping Beq for the entire system are used. This is an extension of the standard motor model of eq 5.3. The total inertia of the spine, motor, and drive are lumped into an equivalent mass Meq at the winch surface. Likewise all displacements, velocities and accelerations are reflected to equivalent cable motions while all torques and forces are reflected as equivalent forces at the winch surface.

Most of the equivalent damping is due to the motor back emf since this damping reflects as the square of the gear ratio through the gearbox. Calculation of this term is nearly impossible since the current feedback amplifier is dynamically inside the motor voltage loop and the effect of the back emf is dynamically coupled to the current. The

equivalent damping was found experimentally by finding the break point of the motor lag with frequency response and recognizing that the motor time constant Tm is a function of the motor inertia and the equivalent damping,

$$Tm = M(motor)/Beq \qquad (6.1)$$

Both the motor inertia and damping are reflected to the winch surface. The values of Tm, M(motor) and Beq are in Appendix 6.1.

Non Linear Friction Effects

The effects of static friction are shown as deadbands placed on the motor force and spine force right before the force summation, fig 6.2. These deadbands are very large and have a pronounced effect on stability and performance. The deadband was measured for the loaded motor, spine and the motor spine combination, Table 4.1.

TABLE 4.1

Measured Deadband

	linear force	friction force
motor alone	9.8 lbf	±3.2 lbf
spine alone	8.4 lbf	±1.5 lbf
motor and spine	8.4 lbf	±4.7 lbf

25 lbf spine force, 20 inch rod extension, vertical

At this operating point there is a 32% friction to linear force loss in the motor, 17% in the spine and a total loss

reflected at the motor of 55%. Physically these deadbands mean that an incremental increase in force may not get passed on to the manipulator. In terms of stability and performance the deadband appears as a gain reduction. Especially for very small deviati ns, this will tend to stabilize the system but at the expense of steady state error. A small position error may generate a torque but that torque may not get through the deadband. The system has a natural open loop integrator from motor speed to position. In the absence of friction this integrator would yield zero steady state error to position. Effectively the dead band limits maximum integrator gain at low frequency

Proportional Control

The first control scheme tried was proportional. The potentiometer feedback is summed with a cable length command, fig 6.2. On the root locus as the forward loop gain Kol is increased the motor pole and the integrator come together and split, fig 6.6. In the absence of any other dynamics this control will be stable but increasingly less damped as the gain increases. The open and closed loop transfer functions are,

$$L/Lref(ol) = \frac{Klv\ Kol\ /\ Beq}{S\ (\ Meq/Beq\ S + 1\ )}\ , \qquad (6.2)$$

$$L/Lref(cl) = \frac{Klv\ Kol\ /Meq}{(\ S**2 + Beq/Meq\ S + Klv\ Kol/Beq\ )}\ . \qquad (6.3)$$

The values for the gains and conversions used in this chapter are tabulated in Appendix 6.1. The force disturbances due to loading and spine force enter at the force balance after the control. Because the disturbance is injected upstream of the integrator there will be a steady state error. The closed loop from force disturbance to cable length is,

$$L/Fd = (1/Kol)\ [L/Lref(cl)]\ . \qquad (6.4)$$

The cable length will follow the force disturbance attenuated by the open loop gain as if it were a reference signal. It is apparent that for small steady state error a large forward loop gain is required.

Open Loop gains up to 1000 were implemented in the controller. For spine loads of 25 lbf with and without the 11bm load as predicted there were unacceptably large steady state errors for low gains. The best performance was obtained at a gain of 1000 which corresponds to a steady state error of .0013 in/lbf disturbance. Open and closed loop bode plots for this gain predict very low phase margin corresponding to wild underdamped poles at a 188 rad/sec, with a damping ratio of .04, fig 6.3.. These poles are practically on the jw axis but they did not cause the expected wild oscillations in the test robot due to the stabilizing effect of the deadband caused gain reduction.

Even though the arm seemed stable performance was very poor. The arm did not move smoothly but rather jittered along. The static friction would hold the arm until the error was large enough to produce a control force which would overcome static friction. The static friction force

decreases as the arm starts to move and the arm accelerates rapidly until the error closes and the arm stops. The cycle then repeats as the reference signal is ramped along. The arm never seemed to overshoot the reference signal as predicted by the linear analysis. This is due to the gain reduction of the deadbands at small errors. As the robot approaches the reference the torque becomes swallowed by the deadband. While the system is outside of the deadband it performed as the linear analysis predicted, inside the deadband the system changes character as the gain deteriorates. At lowered open loop gains these jitters became very long hesitations followed a very fast transient to catch up. This control scheme was thereby deemed unworthy and an alternative was sought.

Proportional and Derivative Control

It was apparent from the time response that if the control signal could be reduced as the velocity increased that the jittering may be dampened out of the response. In control this translates to introducing rate feedback for viscous damping, fig 6.4. The effect of rate feedback can be seen from linear analysis even though I first saw it by attaching a tachometer and letting the fur fly. The open and closed loops are

$$L/Lref(ol) = \frac{Klv\ Kol\ /\ (Beq + Kol\ Kfv)}{S\ [\ (Meq/(Beq + Kol\ Kfv))S + 1)]} \qquad (6.5)$$

$$L/Lref(cl) = \frac{Klv\ Kol\ /\ Meq}{S^{**}2 + (Beq + Kol\ Kfv)\ S + Klv\ Kol} \qquad (6.6)$$

Again, the values for these gains and conversions are tabulated in Appendix 6.1. The same relationship holds for disturbance rejection as eq 6.4 so it is apparent that a high open loop gain will be desirable. Inspection of the open loop transfer function gives an indication of the effect of the tachometer. The position of the motor pole is now dependent on the rate feedback gain. By increasing the rate feedback the motor pole can be placed above the system bandwidth and with a potential gain of up to 90 degrees of phase. Both bandwidth and phase margin can be independently set with the two feedback gains. For a open loop gain of 1000 and a rate feedback gain of .016 v/(in/sec) the open loop and closed loop bode plots show a crossover frequency and bandwidth of about 44 rad/s (7 hz). The system is overdamped with 90 degrees phase margin. The motor pole has moved out to 1000 r/s, and the closed loop bandwidth appears as two real poles at 44 r/s and 790 r/s. See the Bode plots in fig 6.5 and root locus in fig 6.6.

In reality the rate feedback gain was not determined from the linear analysis but by cranking up the gain until the jittering went away. The performance improvement with rate feedback is dramatic. The cable length controls now follows a ramp very smoothly without jerking and bouncing.

This bandwidth is driven by the requirement for steady state gain in the face of disturbances. This bandwidth is still too high for the hardware and the possible spine force. The cable winches still respond to hand tremors on the potentiometers and out-race the spine's ability to maintain tension. To artificially lower the bandwidth further the command signals are filtered digitally with a

single pole filter at 6.2 r/s (1hz). This lowers the bandwidth to the 1 to 2 hz range which is still a lot faster than hand guided transients are going to be. The 98% rise time for this bandwidth is .3 seconds.

Other Methods Tried and Lessons Learned

Before arriving at the tachometer solution a few other solutions were tried without notable success, but are worthy of brief mention.

A PID with the gains found using LQR methods was tried. The added integrator and its attendant phase loss introduced the possibility of instability for elevated gains. The gains were much lower than the gains used in the PD but the steady state error would be taken care of by the software integrator. What actually happened was the robot would limit cycle at a fairly low frequency. The dead band now is downstream of the integrator which integrates a finite error until a signal large enough to overcome static friction is accumulated and off the robot goes settling on the other side of the reference until it gets sent back again. This was really entertaining to watch and it never failed to catch spectators by surprise.

Attempts to cure this were to increase the integrator gain, clamp its output, and place a small deadband upstream of the integrator. The result was improved but the control signal was discontinuous and the performance was no better than the proportional system. In fact it was almost identical. This was the only method where the control was implemented digitally. The Intel 310 computer

was programmed in C but still was only updating at 100 hz for one control. This may be fast enough for the final 7 hz bandwidth but the electronics necessary to get 6 reference signals and 3 command signals in and out of the computer are more complex than the analog controllers which were already built. It is not apparent to this author that digitally implemented linear controls are worth the effort other than for their obvious sex appeal.

A more ingenious attempt was to control the tension in the cable directly by closing an inner loop with a force feedback signal from a strain gage load cell mounted along the cable. This devise was later used in the active spine and it is described in chapter 5. An outer loop which closed on position was then wrapped around the force loop. The intent of this loop was to bypass the deadband and it worked with some success. That it worked at all was a miracle to me. Again the performance was almost identical to the proportional loop and the control signal was virtually identical to the altered LQR loop. Later work with the active spine control showed that a tachometer could have improved this loop performance considerably. This method could be used in future force controls.

Active Spine Control

In the active spine as described in chapters 2 & 5, the spine force is actively controlled with a closed loop force control. Force controls are not as simple to design as position or rate loops. There are many difficulties in measuring force, the most notable is that when natural frequencies are excited the dynamic stress introduced by

the vibrations gets into the force measurement. Some of these natural frequencies may be due to mass and spring elements in the force measuring devise. For the test robot measuring cable tension with a 'C' clamp load cell is reasonable as long as the wire is not vibrating. It became necessary to provide damping in the form of electric tape between the spine and 'C' to protect against this transverse wire vibration, fig 5.8.

A force control loop with strain gage feedback is really a position loop where the position is proportional to the relative displacement of the ends of the load cell since the strain gage ultimately measures surface displacement due to bending stress. For this case the position of the winch body is also proportional to the cable tension. The control analysis developed above for the position loops applies to the force loop except of course the masses and gains are different. The same servo amplifier open loop gain was used as in the cable controls. In this case there are two motors being driven by one servo amplifier. The motors are wired in parallel with no special provision for current sharing. The torque to current relationship for the two motor combination is the same as in the single motor. When the force loop was operated under purely proportional control it oscillated wildly as predicted by the linear analysis for the cable loops. Some form of damping is needed.

For damping the signal which is needed is dF/dt but there is no way to measure it. The force signal could possibly be differentiated but this may be difficult in practicality since force is already a rather jumpy signal. The cable velocity is always in the same direction as dF/dt

except there are cases of steady state slewing where there is a velocity without a change of force. In these cases the velocity feedback limits slew rate causing sluggish performance but it does not drive the system unstable. There are no points when the velocity appears as positive feedback to the force loop. The tachometer gain was tuned on line to acceptably balance out the stability and slew problems. Unfortunately there is not alot of room for adjustment. A stable system becomes sluggish with only a slight increase of tachometer feedback. This situation may be curable with a high pass filter which will block the DC velocity signal.

The system as designed worked better than expected. The bandwidth is much higher than the cable control's bandwidth as shown in the performance section. The high bandwidth is due to lower mass and larger position to voltage gains. This higher bandwidth allowed the force control to exert the commanded force on the spine even when it was moving during endpoint transients. The higher bandwidth did add to the general hum of the system sometimes exciting the transverse string frequencies of the cables. Other than occasional cables vibration there is no notable difference in operating with the active or passive spines.

Chapter7
PERFORMANCE

Hardware

The motors are no more than sufficient for the test robot. With a 25 lbf spine force the motors can continuously run the unloaded robot during fairly strenuous transients. The motors are capable of positioning the robot with a 1 lbm load over the entire workspace but prolonged transient testing must include periodic rests when the motors become hot. The robot with a 2 lbm load overloaded the motors for spine angles greater than 45 degrees. A larger gear ratio could have been chosen since the slew rate is faster than the test robot needs. The frictional losses are difficult to contend with and will impede any advanced control techniques. The friction adds so much uncertainty that any analysis more sophisticated than my humble first pass is (1) meaningless if it does not include modeling of the nonlinearities and (2) worth far more than the motors if it does.

The tandem motors on the spine worked surprisingly well even though no provisions were made for load sharing. Predictions of two motors fighting each other were unfounded. Instabilities can occur when only one of the motors is powered and it must carry the other dead motor and the spine load. It seems that the system can not stand the additional friction deadband.

Overloading the manipulator with either excessive spine force, excessive load, or running it into the wall can result in overpowering the cable winches. Once the cable

winches are pulled away from their references the large open loop gain will demand a very large current. Without the current limiters in the servo amplifiers the motors will quickly burn out. The current limiters and large open loop gain cause the amplifier outputs to saturate for much of the transient operation. In a linear sense this saturation stabilizes the system by effectively lowering the gain.

The cable winding on the winches is workable but not optimal. The cable behaves well if it starts out tightly wound. During sudden motions the tracking springs absorb momentary slack very effectively. Small snarls and over-wraps can usually be cured by extending and contracting the manipulator. Drum grooving, sophisticated lead screws, followers, or keepers may be necessary on a real space robot to insure faultless cable winding.

The flag blocks worked perfectly. The keepers kept the cable from getting jammed between the pulley and the flanges. The spring lead always picked the block up and led the cable onto the pulley.

The potentiometers have enough resolution but their 100KΩ resistance was too high. The potentiometer is a voltage divider which appears in parallel to any downstream electronics. To maintain the pot's linearity this downstream impedance should be much higher than the potentiometer's impedance . Unfortunately the downstream impedances were the 20KΩ input resistors to op amps in the servo amplifier. The insertion of buffers with 1MΩ input impedance between the potentiometers and the servo amplifiers restored the linearity to 95%. A better

solution would be 1kΩ potentiometers and 1MΩ buffers; this combination would yield a linearity of 99.9%.

The lab for the test robot is next to the AC power service for the entire building and across the hall from an elevator motor. Noise in the electronics is a pervasive problem, the motors have a slight 60 Hz hum and the robot will waver impressively upon elevator start-up. Shielding and single point grounding helped alot but did not totally cure the problem. The electronics should be buffered with differential amplifiers for common mode rejection of the AC noise which is on both the ground and the high side of the signals.

Step Response

Step responses give a good indication of a control system's stability, and transient capacity. The test robot was subjected to step inputs in the Xe direction for all combinations of the following conditions: 70 or 50 inch spine lengths; and unloaded or with a 2 lbm load, fig 7.2, 7.3, 10.2,and 10.3.

The cable length L1, and angles θ1 and θ1e were measured with a variety of potentiometers attached to the robot and wall, fig 7.1. The cable length L1 was measured at the feedback potentiometer. The angle θ1 was measured at the base by a potentiometer mounted on the θ1 joint of the gimbal. To gage the flexing in the spine cylinder the angle θ1 was also measured at the end of the pneumatic cylinder. This angle and θ1e at the endpoint were measured by running light strings horizontally from the robot around

3 inch diameter pulleys that are attached to potentiometers mounted on the wall. The strings then go to long elastic bands which are deadheaded at the floor. The pulleys which are made from 1/8 in plexiglass, are very light. This relatively low mass measuring system is adequate for measuring the response of the robot especially at the 70 inch spine extension where the frequencies are low. At the 70 inch spine length the error is estimated to be 5%. This error increases to 15% for the 50 inch spine length. These horizontal displacements can be transformed to radians by dividing by the spine length. Little error is introduced by approximating the arc length by the chord length since the sine function for a small angle is approximately the same as the angle. At .1 rad or 5.7 degrees this approximation is within 99.8% accurate.

The step responses show that the cable controls perform as designed. The unloaded cable controls have no overshoot and 60% rise times in the .13 sec range corresponding to the 1 hz bandwidth of the prefiltered input signals. The 70 inch loaded spine shows a slower .2 sec. rise time and a slight overshoot. This rise time corresponds to a .8 Hz bandwidth. This sluggishness is attributed to current limiting in the servo amplifier. The endpoint especially in the 70 inch spine lengths oscillates well beyond where the cable length would constrain it if the spine and cable system were truly rigid. These overshoots are in the 20% to 35% range at 70 inch spine lengths and much smaller for the shorter spine lengths. Analyzing these oscillations is the subject of Chapters 9 and 10.

Trajectory Tracking

The robot's capability to track trajectories is shown in fig 7.9 and 7.10. These trajectories include circles, spirals, and boxes. The photographs are time exposures of the robot performing the trajectories with a pen light attached to the endpoint. The camera was approximately 10 feet away from the robot gimbal.

The circular and spiral transients were accomplished with a computer program which calculates a circular trajectory centered at the endpoint position as commanded by the XYZe command potentiometers, fig 5.9. The radius of the circle and frequency of rotation were input from two additional command potentiometers. The flat spirals were made by starting with a small circle and slowly expanding it. The longitudinal spirals were made by keeping the radius constant and slowly changing the Xe command, fig 7.8. Both types of transients started and ended with the robot retracing the same circle several times to show the repeatability of the robot. All of the circles were drawn slowly at .1 Hz or 10 sec per revolution. The inner and outer diameters of the large flat spiral in fig 7.8 are respectively 27 inches and 3 inches. The elliptical appearance of the outer circle is due to foreshortening and calibration errors of unknown origin. The repeatability of the robot is very good for these slow transients as seen by either the inner or outer circles. Note that small aberrations in the circle are even repeated. The longitudinal spiral is 27 inches in diameter and 50 inches long. The circular cross section appears increasingly elliptical due to the effects of perspective.

The box transients include the following four combinations: unloaded slow, unloaded fast, loaded slow, and loaded fast. The boxes are 4 feet by 4 feet by 2 feet with the two foot dimension in the Z direction. This is about the largest box which can be fit into the workspace. The load is the design load 1 lbm. The transients are recorded with time exposure photography of a pen light at the endpoint. The trajectories are created by manually turning the XYZe command potentiometers in sequence up to prearranged stops. Some of the edges have to be retraced to get the full box. These edges serve as a good indication of the repeatability of the robot under dynamic tracking. The slow trajectories are 5 sec for the long sides or approximately .8 feet per second. The fast transients are 2 sec for the long sides or 2 feet per sec. The horizontal edges are slightly arced downwards due to an undetermined cause, presumably potentiometer calibration or as a result of not including the flag blocks in the kinematics. The wiggling edges are due to the endpoint oscillation in the tangential direction as expected from design intent and previously seen in the step responses. Not shown are the errors in the cable loops, but as seen in the step responses these errors are very small and the oscillations are due almost entirely to flexibility in the cables and rod. The slow unloaded and loaded cases show tracking within .5 inch of the desired trajectory and very good repeatability. The loaded case is slightly worse than the unloaded case. The fast transients show degraded but still admirable performance. The unloaded case tracks within 1 inch while the loaded case is within 2 inches.

Active Spine

In general the position loops are very robust while the force loops are a bit finicky due to the dynamic nature of the force measurement. The spine is very intolerant of any friction or vibration at the spine motor pivots and force transducer. In spite of these obstacles and a somewhat ad hoc design approach the active spine worked very well.

Step response in the Ze and Xe directions show the similarities in the response of active and passive spines. Step response in the Ze direction at a spine force of 25 lbf for both the active and passive case are shown in fig 7.4 and 7.5. Again the .13 sec rise times are indicative of the prefiltering imposed bandwidth of 1 Hz. There is no overshooting in either case. The active spine force maintains the 25 lbf spine force smoothly during steady state and within ±4 lbf or 16% during the transient. Note that the sense of the force feedback signal in fig 7.5 is negative, downwards for increasing force. The tracking error shows that the choice of tachometer damping for the force loop is reasonable but could use improvement. During slewing the spine tachometer is trying to slow down the spine winch. This sluggishness causes the spine force to momentarily rise during retraction and lower during extension. If the DC component of the tachometer feedback were filtered out, this response could be improved during constant velocity slewing.

The response of the force loop alone can be seen from a 15 lbf step in force command, fig 7.6. This loop has a 0 to 100 % rise time in the .02 sec range with a 5% overshoot, fig 7.4. This rise time corresponds to a 30 Hz

bandwidth. The high bandwidth in comparison to the position loops is attributable to no prefiltering of the command signal, lower mass, and higher gain.

A step in the Xe direction for the unloaded active spine shows a short spine force disturbance of 2 lbf during the transient fig 7.7.. Again note that the sense of the force signal is negative, downward for increasing force. This disturbance is smaller than that in the Ze transients since the spine has moved very little in the radial direction. The cable position loop and endpoint behavior are identical to the passive spine transients.

With care a satisfactory cable driven active spine is feasible that will: (1) give equal performance to the passive spine where the reference command is not changed and (2) give superior performance where the reference signal is modulated to optimize power consumption and transient performance.

Chapter 8
POWER CONSUMPTION AND COMPLIANCE

General

Aerospace robotic applications have inherent power and flexibility limitations due to the high cost of lifting objects into outer space. There is a limited quantity of power available aboard a space craft and this power is generally rationed amongst the potential users. The present space shuttle manipulator's drive system is limited to 535 watts or .7 hp. When you consider the 30000 lbm payload and the incredibly high gear ratios in the drive system this doesn't seem like much power. For comparison to move the 1 lbm design load around the test robot cable drives use about 16 watts. The unique construction of the parallel robot presents some concerns about power consumption. The cable motors must always counteract the outward force of the spine and whatever load is present. It almost seems that we are paying for the power twice, once pushing out and once pulling in. The serial robot by comparison seems to exert more force in the direction of the load and less on purely internal forces. Analytic techniques employing principal transforms which have been developed for serial manipulators can be applied to the parallel case with some additional modifications [6]. For unobvious reasons the same analytic techniques are used to analyze compliance or flexibility. As it turns out compliance is sort of the antithesis of power consumption. The directions in which the manipulator is most power efficient are the directions of least compliance.

POWER

Principal Transform Analysis

The space shuttle manipulator uses DC brushless geared motors while the test robot uses DC brushed geared motors. The expressions for motor power consumption are the same in both cases. The motor torque equation 5.2 can be restated as

$$\tau m = Kt\ Gr\ Ne\ I \quad . \tag{8.1}$$

where: τm = output shaft motor torque
Kt = motor torque constant, .406 in lbf/amp
Gr = gear ratio, 11.5
Ne = overall efficiency, .81
I = motor current

The power dissipation of these electric motors at stall are I squared R losses in the windings where R is the winding resistance. Combining this expression for the losses with eq 8.1 yields ,

$$Pd = I^2 R = (Tl / Kw)^2 \quad . \tag{8.2}$$

where: Pd = power dissipated in motor at stall
R = winding resistance, 4.69Ω
Rw = winch radius, .5 in
Tl = cable tension
Kw = overall winch torque constant
$Kt\ Gr\ Ne / (\sqrt{R}\ Rw)$, 3.49 lbf/(watts$\cdot^{.5}$)

The total power dissipated Pt in the manipulator is the sum of the power dissipated in the motors and the spine Ps,

$$Pt = \Sigma Pdi + Ps . \quad (8.3)$$

This can be restated in terms of cable tension as,

$$Pt = \underline{Tl}^{T} \begin{bmatrix} 1/kw^2 & 0 & 0 \\ 0 & 1/Kw^2 & 0 \\ 0 & 0 & 1/Kw^2 \end{bmatrix} \underline{Tl} + Ps \quad (8.4)$$

This equation can be further transformed by the equation of static equilibrium, eq 4.3 where cable tension $\underline{Tl}$ is a function of external load $\underline{Fe}$, and spine force $\underline{Fs}$.

$$Pt - Ps = \frac{1}{Kw^2} (\underline{Fe} - \underline{Fs})^{T} \, \underline{LC} \, (\underline{Fe} - \underline{Fs}) . \quad (8.5)$$

where: $\underline{LC} = \underline{J\Sigma}^{*} \, \underline{J\Sigma}^{*T}$

The power consumed by the motors is a function of the load, spine force, motor characteristics, and kinematics. The spine can either increase or decrease the motor power consumption depending on the relative direction of the load and spine force. Since LC is positive definite as long as the Jacobian is not singular eq 8.5 is in the quadratic form and can be analyzed using a Principal Transformation. The magnitude and direction of the force difference ($\underline{Fe}$-$\underline{Fs}$) is described by families of ellipsoids for constant motor power [6]. The directions of max/min force difference lie along the principal axes of the ellipsoids which coincide with the eigenvectors of LC. The magnitude of the max/min

force difference correspond to the length of the major and minor axes and are inversely proportional to the square root of the corresponding eigenvalues,

$$|\underline{Fe} - \underline{Fs}|(min/max) = Kw \frac{\sqrt{(Pt - Ps)}}{\sqrt{EigLC(max/min)}} . \qquad (8.6)$$

where: EigLC = eigenvalues of $\underline{LC}$

Interpretation of the Ellipsoids

Grouping the spine force with the external force makes this expression and the resulting ellipsoids difficult to understand. If there were no spine and the cables were links like ballscrews or hydraulic cylinders which could support compressive loading, eq 8.6 would make sense. It would say that for a given endpoint position and fixed input power the manipulator can exert forces whose magnitude and direction can be described by an ellipsoid. The orientation and proportions, of the ellipsoid are indicative of the manipulators capacity to effectively use power in different directions. This solid link manipulator can be used as a means of comparison for the cable driven manipulator.

Definition of Power Effectiveness

A dimensionless form of eq 8.6 will be more useful though, where the power and force can be grouped together to yield an effectiveness between force potential for a given motor power and effective force applied to the

environment. Again the extremities of this relationship are described by ellipsoids which in turn can be defined by by the eigenvectors and eigenvalues of LC.

$$\frac{|Fe - Fs|(min/max)}{Kw \sqrt{(Pt - Ps)}} = \frac{1}{\sqrt{EigLC(max/min)}} \quad . \qquad (8.7)$$

The denominator is the total force the winches could produce for a given power while the numerator is the force which the winches do produce in the directions defined by the eigenvectors. This ratio is defined as the power effectiveness and represents how well the manipulator is utilizing power in relation to the very best it could do. As stated previously, this is difficult to interpret in the cable case where the spine force must be subtracted as a vector from the force the robot exerts on the environment. The relationship does describe the link case very well where there is no spine. The ellipsoids of the link case will serve as a good comparison for the cable case showing the effect of the cables and spine.

Force Separated Power Analysis, Cable Case

Unfortunately the two forces Fe and Fs cannot be be separated into a form which can be analyzed using a Principal Transformation. To derive a meaningful force/power expression for the cable robot it is necessary to eliminate some of the variables. From Chapter 4 there is a relationship between the external force and the minimum spine force necessary to maintain tension in the

cables, eq 4.5. The external force vector $\underline{Fe}$ can be resolved into a magnitude Fe and direction $\underline{Fed}$. Eq 4.5 can be arranged in the form of,

$$Fs = Fe\ Rf\ . \qquad (8.8)$$

where: Rf is a constant scalar for a given configuration and load direction.

This equation states that for a given endpoint position and load direction the magnitude of the minimum spine force which will maintain tension in the cables is proportional to the magnitude of the load. This would be the case of the very best active spine.

Eq 8.5 can be arranged into the the same power effectiveness form as used for the link case, eq 8.7

$$Fe/Kw\sqrt{Pt} = 1 / \sqrt{ABC} \qquad (8.9)$$

where: $ABC = \underline{Fed}^T\ \underline{LC}\ \underline{Fed} - 2\ Rf\ \underline{Fed}^T\ \underline{LC}\ \underline{Fsd} + (Rf^2)\ \underline{Fsd}^T\ \underline{LC}\ \underline{Fsd} + (Rf\ Km / Ks)^2$

Ks = spine torque constant somewhat arbitrarily defined as 3 Kw to match all three cable winches.

As in the link case we now have a dimensionless expression for how well the cable manipulator transforms power into force applied to the environment. The term on the right contains the directionality of the environmental force and the position of the endpoint. This equation can be solved for various loads and endpoint positions and then compared to the ellipsoids of the link case, eq 8.7. It is

important to restate that this equation is only valid for the active spine which exerts the minimum force necessary to maintain tension in the cables and where the power to drive the spine is part of the total power consumption.

Power Results

The power effectiveness ellipsoids for the link case and results from eq 8.9 for the cable case, are plotted in fig 8.1 for spine lengths of 20 to 80 inches; spine angles up to 60 degrees; base radius of 12 inches; base angle of 0 degrees ; and in zero gravity. Not surprisingly both manipulators are most effective in the radial direction and relatively ineffective in the tangential directions. In the radial direction both cases are equally effective while in the tangential directions the cable case is always less effective than the link case.

The effectiveness is roughly symmetrical in the four tangential directions, two tangential direction $\pm i\beta$ are shown, refer to fig 2.1 for the definition of the directions. The ellipsoids by definition are symmetric across the principal axes but the cable driven robot's response is not. The asymmetry shown is due to the position of the cable winches. For tension in the positive Xb direction winch I lies on the Xb axis while in the negative Xb direction tension is supplied by winches 2 and 3 which are located at ±120 degrees. As stated before the cable case is always less effective than the link case in the tangential directions. This is because the cable case must share power with the spine which always points in the radial direction.

The effectiveness in the radial direction is approximately constant over the workspace , decreasing slightly for short spine lengths . The effectiveness in the $\underline{i}\beta$ tangential direction decreases with increasing spine length and spine angle. In the $\underline{i}\alpha$ direction which is not shown in fig 8.1, the effectiveness also decreases with increasing spine length but is unaffected by spine angle. In the retracting radial direction the two cases are the same while in the extending radial direction the cable case appears better than the link case. Actually the force exerted outward in the radial direction for the cable case is due almost entirely to the spine and its torque constant Ks. The value of Ks was chosen arbitrarily to match effectiveness in the radial direction at large extensions.

From fig 8.1 the parallel manipulators seem weak in the tangential direction for large spine lengths. This must be put in the context of what are the overall geometric constraints of the problem and how might other geometries react to these constraints. A suitable model for the tangential loadings is a simple beam which balances a tangential load at one end with a moment and force at the other end. The moment which is directly proportional to both the force and beam length is supplied by an electric motor similar to the ones described earlier. The effectiveness for these tangential forces are dependent on the inverse of the length,

$$F / (Km \sqrt{Pd}) = 1 / L . \qquad (8.10)$$

It is apparent that the geometry will constrain the effectiveness to be inversely proportional to the spine length for both the serial or the parallel manipulators.

The ellipsoids are deceiving; what appears to be a weakness in the tangential is actually disproportionate strength in the radial direction which is relatively insensitive to length .

Power Consumption in a Constant Force Passive Spine

It is important to point out that the effectivenesses shown in fig 8.1 for the cable-manipulator are at the minimum spine force which will maintain cable tension which might be applied by the ideal active spine. The effect of a constant force passive spine on power consumption will decrease the manipulator's effectiveness in all directions. Additionally the radial outward direction will now be limited to this constant force.

A sense of the power consequences due to the spine force can be gained by letting the load force go to zero in eq 8.6 and solving for the total power dissipated,

$$Pt = . (Eig\ Fs^2)/(Km^2) + Ps . \qquad (8.11)$$

This can be further simplified by: assuming that the spine force is supplied by three motors identical to the cable motors which will supply 1/3 of the spine force each; and recognizing that for very long spines the eigenvalue corresponding to the radial direction for all spine angles is approaching 1/3,

$$Pt = 2/3\ (Fs^2)/(Km^2) . \qquad (8.12)$$

For an unloaded manipulator subjected to a constant spine force the total power consumption at the very best is twice

that of just the spine alone. This looks like paying for the power once to push it out and once to pull it back. For short spine lengths the power consumption due to the constant force spine gets larger as the eigenvectors of LC get large. The effectiveness drops since power consumption in the cable winches increases as the cables point less and less in the direction of the spine.

COMPLIANCE

Compliance and stiffness are inverse descriptions of each other. The force necessary to deflect an elastic material is proportional to the deflection where the proportional constant K is called the stiffness. On the other hand, the deflection is proportional to the force where the proportional constant C is called the compliance. The stiffness K is the inverse of the compliance C. A very stiff material is not very compliant and visa versa.

Manipulator stiffness or compliance at the endpoint due to external static loading is a function of the geometry, actuator, joint, and link stiffnesses. For the parallel cable manipulator the only link is the spine (as defined in Ch 3), whose bending deflections do not appear at the endpoint. Likewise, the deflections of the joints which were defined along the spine do not appear at the endpoint. The deflections of the actuator which include the closed position loops, mechanical drives and cables do appear at the endpoint. For the test robot the cables are much more compliant than the drives or position loops and their

stiffnesses will dominate the equations of this section. In the serial robots actuator, joint and link deflections appear at the endpoint. Typically the serial links are much stiffer than the joints except in space applications where the links become long and compliant.

Principal Transform Analysis

Principal transform techniques similar to those used in the power analysis can be applied to compliance analysis [2] The cable and actuator deflections can be reflected to cable lengths and related to a cable tension by,

$$\underline{Tl} = \underline{Ka}\ \delta\underline{L} \quad . \tag{8.14}$$

where: $\underline{Ka}$ = A diagonal matrix of the actuator stiffnesses which in this case is dominated by the relatively compliant cables.

The cable deflection can be reflected to endpoint deflection with the Jacobian between cable space and end space, eq 3.8. The cable tensions can be related to load and spine force by the equation of static equilibrium , eq 4.3. When these relations are combined with eq 8.14 the expression of endpoint deflection as a function of load and spine force is

$$\delta\underline{Xe} = \underline{J}^{e}\ \underline{Ka}^{-1}\ \underline{J}^{e\,T}\ (\underline{Fe} - \underline{Fs}) \tag{8.15}$$

The magnitude of the deflection is of interest which is proportional to the Euclidian norm or inner product of $\delta\underline{Xe}$. Since the actuators are identical the stiffnesses Ka can be pulled out as a scalar. The norm of endpoint is,

$$|\delta \underline{Xe}|^2 = (1/K^2)\ (\underline{Fe} - \underline{Fs})^T\ \underline{LC}^2\ (\underline{Fe} - \underline{Fs}). \qquad (8.16)$$

where: $\underline{LC} = \underline{J}_{\underline{X}}^{-1}\ \underline{J}_{\underline{\Theta}}^{-T}$

This looks suspiciously like the equation for power consumption and it is apparent that the same principal transform techniques apply except we are dealing with $\underline{LC}^2$ instead of $\underline{LC}$. If $\underline{LC}$ is positive definite then $\underline{LC}^2$ is also positive definite. The eigenvectors of $\underline{LC}^2$ are identical to the eigenvectors of $\underline{LC}$ while the eigenvalues of $\underline{LC}^2$ are equal to the square of the eigenvalues of $\underline{LC}$.

Definition of Relative Endpoint Compliance

Similar to the power analysis a dimensionless measure of relative stiffness at the endpoint can be defined as the actuator stiffness Ka divided by the endpoint stiffness. The endpoint stiffness is defined as the magnitude of force applied at the endpoint divided by the magnitude of the endpoint deflection, both in the same direction. The relative endpoint compliance is then simply the inverse of the relative endpoint stiffness. Again using the Principal Transformation as in the power analysis, the max/min relative endpoint compliance are in the direction of the eigenvectors of $\underline{LC}$ and of the magnitude of the max/min eigenvalues of $\underline{LC}$,

$$\frac{Ka\ |\delta \underline{Xe}|(max/min)}{|\underline{Fe} - \underline{Fs}|} = Eig\underline{LC}(max/min)\ . \qquad (8.17)$$

Interpretation of the Ellipsoids

For a given endpoint position the manipulator compliance in different directions as compared to the compliance of a single cable can be described by an ellipsoid. These relative compliances are a dimensionless comparison between the actual compliances in different directions and a bench mark compliance defined above as the compliance of a single cable. The orientation and proportions, of the ellipsoid are indicative of the manipulators tendency to deflect when subjected to loads from different directions. In directions with large relative compliance the manipulator is less stiff than in directions with small relative compliance. The combination of the spine force and load force is not as confusing as it was in the power analysis since the spine force points only in the radial direction where the parallel manipulator is stiffest. The spine force then produces relatively little deflection in the radial direction and no deflection in the tangential direction..

Compliance Results

Ellipsoids for the relative endpoint compliance in the $\underline{i}R$ and $\underline{i}\beta$ directions have been drawn for a zero base angle, base radius of 12 inches, spine lengths from 20 to 80 inches, and spine angles of 0 to 60 degrees, fig 8.2. These ellipsoids show the opposite orientation as the ones in power analysis, which is no surprise since the magnitudes are related by the inverse of the square roots of the eigenvalues of $\underline{LC}$. These ellipsoids show that the manipulator is much stiffer in the radial direction than

the tangential direction. The radial stiffness is fairly constant over the workspace . The tangential stiffness in the $\underline{i}\beta$ direction decreases linearly with increasing spine length and quadratically with increasing spine angle, fig 8.3. The manipulator is stiffer in the $\underline{i}\alpha$ direction (which is not shown) than in the $\underline{i}\beta$ direction. The $\underline{i}\alpha$ stiffness decreases with spine length but is unaffected by spine angle since the relative cable angles in this direction do not change greatly with spine angle.

An analog to spine power consumption exists for the flexibility analysis. The compliance of the manipulator depends on the spine force. For the vertical position the endpoint compliance stiffness was measured for spine forces 10, 20 ,and 30 lbf, this is compared with the theoretical eigenvalue prediction, fig 8.4. As the spine force is increased the manipulator becomes markedly stiffer. If the cables were replaced by solid links the manipulator stiffness would not be sensitive to a spine force inside the linear stress-strain range. Typical strain stiffening occurs in structures where a deflection constraint in one direction changes the stress pattern of a different form of loading. For example a pinned beam under large bending deflection will exhibit greater bending stiffness than a simply supported beam. For the parallel robot since the strands in the cable are twisted, initially the deflection is due to bending. As the strands straighten out and become constrained by contact the deflection becomes increasingly due to axial strain in the strands. This results in a nonlinear longitudinal cable stiffness at moderate cable tensions. At the higher loadings it will approach the solid link case. This presents an interesting

relationship, the endpoint stiffness depends on spine force but not spine flexibility. The parallel cable robot endpoint stiffness can be adjusted with spine force [1]. This advantage doesn't come for free, though, since the power analysis has shown that the system pays twice in power consumption for excessive spine force.

Chapter 9
DYNAMIC EQUATIONS WITH FLEXIBLE ELEMENTS

General

The question yet unanswered is whether cable actuated parallel robots offer any advantage over conventional serial robotics when the manipulators are long, light, and flexible. The current Space Shuttle serial robot arm is reported to be very flexible. This flexibility has necessitated running at very low speeds. Experimenting with the 3 DOF test robot shows that even though the cables are being controlled without overshoot, flexibility in the robot causes the endpoint to oscillate. The major sources of flexibility are in the rod and the cable drives. Recent research has investigated robotic modes using finite element analysis [7]. This thesis will use a simpler approach, a four spring and five mass linear model at a vertical operating point for various spine lengths.. Justification of this model comes from observation that the dynamic behavior of the end point is not particularly sensitive to the spine angle. Sinusoidal excitation of the unloaded test robot shows that there are two vibratory modes of immediate interest, fig 9.1. Both of these modes use the first bending mode of the rod. In the lowest modes there are nodes at the endpoint and the pivot. The next highest modes have one node at the pivot. The frequencies of these modes are in TABLE 9.1

TABLE 9.1

Experimental Parallel Modal Frequencies

Spine Length inches	Mode 1 Hz	Mode 2 Hz
80	2.6	7.1
70	3.4	11.6
60	4.4	16.6

These frequencies are low enough to be excited by the closed loop bandwidth as seen in the endpoint behavior during transients.

The dynamic equations for the parallel manipulator were derived in four steps: (1) non linear rigid spine, (2) linear spine dynamics, (3) non linear flexible equations which incorporate the spine dynamics, and (4) linear flexible dynamics. Additionally dynamics were derived for a dynamically similar serial robot which will be used in chapter 10 for a dynamic comparison with the parallel robot.

Non-Linear Rigid Spine Dynamics

The spine is comprised of four elements the rod, the cylinder, the gimbal, and the counterweight. The same coordinate systems as defined in the kinematic analysis will be used, fig 3.1 & 9.2. The base coordinate system has it's center at the pivot O and is stationary. The first and second coordinate systems have their origins at O

and rotate with the generalized coordinates θ1 and θ2. The third coordinate system origin is at the endpoint E and it translates with the generalized coordinate R. The cables are not present in this model. The forces applied at the endpoint are resolved into the $\underline{i\theta 1}$, $\underline{i\theta 2}$, and $\underline{iR}$ directions corresponding to the generalized forces Γ1, Γ2, and Fr.

The mass quantities of gimbal and counterweight are lumped with the cylinder. The cylinder assembly has a centroid at Lc1 from the pivot; mass Mc; and inertias Icx, Icy, and Icz with the principal directions along the second coordinate system. The rod has a centroid at Lc2 from the pivot; mass Mr; and inertias Irx, Iry, and Irz again with principal axes parallel to the second coordinate system .

The dynamic equations were derived using Lagrangian Dynamics. The system is located by a set of generalized coordinates, qi. The total kinetic energy T and potential energy U are derived in terms of the generalized coordinates. The Lagrangian £ is defined as,

$$£(\dot{q}i, qi) = T - U \ . \qquad (9.1)$$

The dynamic equations then come directly from the Lagrangian equations of motion,

$$\frac{d}{dt}\frac{\delta £}{\delta \dot{q}i} - \frac{\delta £}{\delta qi} = Qi \ . \qquad (9.2)$$

where: Qi are the generalized forces corresponding to the generalized coordinates qi.

The final equations can be put in the standard non linear form [2] of,

$$\underline{H}\,\ddot{\underline{q}} + \underline{h(q,\dot{q})} + \underline{G(q)} = \underline{Q} \,. \qquad (9.3)$$

where: $\underline{H}$ = manipulator inertia tensor
$\underline{h}$ = non linear Coriolis and Centrifugal terms
$\underline{G}$ = gravitational terms

The elements for these matrixes are in Appendix 9.1.

As discussed in chapter 6 the inertia tensor is diagonal and hence the spine is dynamically uncoupled in terms of the generalized coordinates. This is generally not the case for robots, and achieving just this result has been a goal in the direct drive robotic field [8]. The advantage of dynamic decoupling is especially useful with high performance robots; it ensures that large accelerations in one joint will not induce interactive inertial torques in the other joints. This decoupling requires driving the spine along the joints but the cable drives do not point in the directions of the joints. But as will be shown later driving the robot with flexible drives isolates the coordinates and recovers this decoupling.

The nonlinear Coriolis and centrifugal terms would not exist if the manipulator's inertia were configuration independent. On the spine the rod is the only element that changes the inertia. It would be conceivable that a moving counterweight could eliminate this dependence and all of these terms would disappear. The only hitch is that a simple counterweight could not eliminate both the

gravitational and these non linear terms simultaneously. It would have to be a two DOF counterweight. There may be some use of this in very high performance robots but definitely not here. Of course in space where there is no gravity so a simple counterweight would do the trick. The manipulator would then be completely decoupled in terms of the generalized coordinates.

The gravitational terms can be eliminated by making the terms,

$$Mc\ Lc1 + Mr\ Lc2 = 0 \quad . \tag{9.4}$$

This is what the counterbalance does at a spine extension of 20 inches. A smart counterweight could track Lc2 and counterbalance the spine over the entire workspace.

Linear Rigid Spine Dynamics

The non-linear dynamic equations are a function of the generalized coordinates and their derivatives,

$$Q = f(q, \dot{q}, \ddot{q}) \tag{9.5}$$

These equations can be linearized at an operating point using the the first order terms of a Taylor series approximation,

$$\text{dlt } Qi \approx \sum_{j=1}^{3} \frac{\delta Qi}{\delta \ddot{q}j} \text{dlt } \ddot{q}j + \frac{\delta Qi}{\delta \dot{q}j} \text{dlt } \dot{q}j + \frac{\delta Qi}{\delta qj} \text{dlt } qj \qquad (9.6)$$

where: dlt = delta, a small change around the operating point

The choice of a vertical and stationary operating point simplifies the linearization of the dynamic equations considerably. All of the gravity terms will disappear even for spine extensions which are not quite counterbalanced. This is especially nice since this generalizes the analysis to include both the actual robot and that imaginary space robot. The centrifugal and Coriolis terms will also drop out since their linear form will depend on a non-stationary operating point. The non-linear equations rather neatly collapse to,

$$\begin{aligned} \text{dlt } \Gamma 1 &= (Mc\ Lc1^2 + Mr\ Lc2^2 + Icrx)\ \text{dlt } \ddot{\theta}1 \\ \text{dlt } \Gamma 2 &= (Mc\ Lc1^2 + Mr\ Lc2^2 + Icry)\ \text{dlt } \ddot{\theta}2 \\ \text{dlt } Fr &= (Mr\ )\ \text{dlt } \ddot{R}\ . \end{aligned} \qquad (9.7)$$

At the operating point in terms of the generalized coordinates the spine looks like three uncoupled ordinary differential equations

Non-Linear Flexible Manipulator Dynamics

The full 3 DOF parallel robot has been modeled as a lumped parameter system with four spring and five mass elements, fig 9.3. The spring elements are joint

stiffnesses Ka at the three cable drives and rod bending stiffness on the spine. The mass elements are the drive inertias Im, an endpoint mass Me, and the spine mass. The endpoint mass is a combination of the load mass and some of the rod mass. Normally some of the cable mass would be included in the endpoint mass but in this case the cable mass is negligible. The spine mass and inertias are the same as before minus that rod mass which is included in the endpoint mass. This analysis uses the same coordinate system as the spine dynamics, fig 9.2.

The generalized coordinates are the original three θ1, θ2, and R; the three cable lengths L1, L2, and L3; plus endpoint coordinates θ1e, θ2e which are the angular displacements measured by a straight line from the endpoint through the origin O in the same coordinate systems as θ1 and θ2 are measured. The generalized forces now become the cable tensions TL1, TL2, and TL3.

The derivation of the non-linear dynamic equations follows the same Lagrangian format as spine dynamics. The resulting equations are, as expected, a mess; for the curious they are given in Appendix 9.2. Before moving on it is useful to point out that the manipulator still has a diagonal inertia matrix and it is still dynamically uncoupled. This would not be the case if the manipulator were modeled rigidly. In the rigid case torque can be transferred along the cables and rod, while in the flexible case force can only be transmitted by spring displacement. The non-linear centrifugal, Coriolis and gravitational terms are still present.

Linear Flexible Manipulator Dynamics

The linearization technique and operating point are the same as before. The gravity, centrifugal and Coriolis terms fall out because of the choice of operating point. The final linear equations can be expressed in second order differential matrix form,

$$\underline{M}\,\ddot{\underline{q}} + \underline{K}\,\underline{q} = \underline{Q} \quad . \tag{9.8}$$

where: $\underline{M}$ = mass matrix
$\underline{K}$ = stiffness matrix

The elements for these equations are in Appendix 9.3. These matrices can be used to form state space matrices of the form

$$\dot{\underline{X}} = \underline{AO}\,\underline{X} + \underline{BO}\,\underline{U} \quad . \tag{9.9}$$

where: $\underline{X}$ = states $\begin{bmatrix} \dot{\underline{q}} \\ \underline{q} \end{bmatrix}$

$\underline{U}$ = inputs $\begin{bmatrix} \underline{TL} \\ \underline{0} \end{bmatrix}$

$\underline{AO}$ = state equation $\begin{bmatrix} \underline{0} & -\text{inv}(\underline{M})\,\underline{K} \\ \underline{I} & \underline{0} \end{bmatrix}$. (9.10)

$\underline{BO}$ = input equation $\begin{bmatrix} \text{inv}(\underline{M})13 \\ \underline{0} \end{bmatrix}$. (9.11)

inv(M)13 = 1 to 3 columns of M inverse

These equations do not include the closed loop motor dynamics or the damping due to back emf. Additionally in reality these springs have some sort of inherent damping. The damping terms should be present for any open loop analysis. Assuming that each of the springs has a parallel damper a structural damping matrix $\underline{B}$ can be formed of identical structure to the stiffness matrix $\underline{K}$ except spring terms Ka and Kr are replaced with damping terms Ba and Br. The equivalent damping at cable length Beq can be added to the first three diagonal elements of $\underline{B}$. These elements get multiplied by cable speed and will eventually be subtracted from cable tension. The open loop robot state matrix with damping becomes,

$$\underline{A1} = \begin{bmatrix} -inv(\underline{M})\ \underline{B} & -inv(\underline{M})\ \underline{K} \\ \underline{I} & \underline{0} \end{bmatrix} . \qquad (9.12)$$

The closed loop motor dynamics can be added by including the compensator gains for proportional and velocity feedback. These gains are included in the gain matrices $\underline{Kp}$ and $\underline{Kv}$, Appendix 9.3. The final closed loop system becomes,

$$\underline{A3} = \begin{bmatrix} -inv(\underline{M})\ \underline{B} - inv(\underline{M})13\ \underline{Kv} & -inv(\underline{M})\ \underline{K} - inv(\underline{M})13\ \underline{Kp} \\ \underline{I} & \underline{0} \end{bmatrix} . \qquad (9.13)$$

$$\underline{B3} = \begin{bmatrix} inv(\underline{M})13\ \underline{Kp} \\ 0 \end{bmatrix} . \qquad (9.14)$$

Mode shapes and frequencies can be found from the eigenvalues and eigenvectors of the closed loop state equation $\underline{A3}$, fig 9.4 & table 9.2. Comparison between these

and the measured modes of table 9.1 show a good correlation especially for the a spine length of 80 inches.

TABLE 9.2

Analytic Parallel Modal Frequencies

Spine Length inches	Mode 1 Hz	Mode 2 Hz
80	2.4	7.3
70	2.7	9.5
60	3.2	10.0

Flexible Serial Robot Dynamics

An 'equivalent 'serial robot has been invented for dynamic comparison to the parallel robots, see Ch. 10. The equivalent robot has the identical spine but only 2 DOF, one rotation at the base and the rod translation. A full 3 DOF robot is not needed since the endpoint oscillations occur primarily in the tangential directions along the path of travel and these conditions can be reproduced with step response at a vertical position, see ch. 10. No actuator mass has been added to the spine which in reality would make the serial arm look worse than presented here. The endpoint mass and rod stiffness are the same. The equivalent actuator stiffness $K\theta$ is found by reflecting the cable stiffness Ka from the cable to the base rotation by the Jacobian defined between cable length and joint angle,

$$K\theta = J_{\theta}^{T} \, Ka \, J_{\theta} \, . \qquad (9.15)$$

The derivation of the non-linear and linear equations follow the same techniques used in the parallel case. The states, mass, stiffness, and damping matrices are defined in Appendix 9.4. The closed loop state equations are

$$\underline{A3s} = \begin{bmatrix} -\text{inv}(\underline{Ms})\ \underline{Bs} - \text{inv}(\underline{Ms})12\ \underline{Kvs} & -\text{inv}(\underline{Ms})\ \underline{Ks} - \text{inv}(\underline{Ms})12\ \underline{Kps} \\ \underline{I} & \underline{0} \end{bmatrix} \tag{9.13}$$

$$\underline{B3} = \begin{bmatrix} \text{inv}(\underline{M})12\ \underline{Kps} \\ 0 \end{bmatrix} . \tag{9.14}$$

When modal analysis is applied to the state equations of the equivalent serial robot very different mode shapes and frequencies are found, fig 9.5 and Table 9.3.

TABLE 9.3

Serial Analytic Modal Frequencies

Spine Length inches	Mode 1 Hz	Mode 2 Hz
80	3.1	7.7
70	4.4	8.5
60	6.2	10.0

These frequencies are generally higher than the parallel robot for the unloaded case, but are substantially lower than the parallel robot for the loaded case.

Chapter 10

COMPARISON OF PARALLEL AND SERIAL FLEXIBILITY

To compare the capabilities of the two types of robots in controlling endpoint position the linear models of chapter 9 will be calibrated against the test robot. These model's dynamic response will be compared for varying load, actuator stiffness and rod stiffness. Step responses will be used to study the dynamics since they excite the same dynamics as a more realistic ramp. A typical transient with the test robot shows the presence of structural modes in the endpoint θ1e and base angle θ1 positions during a slow traverse in the x direction, fig 10.1.

It is apparent from the Performance chapter that it is not difficult to get the test robot to control winch position with a well dampened response. Even though the winches are controlling well the endpoint is still wavering around due to flexibility in the drive system and spine. These endpoint responses are outside of the closed loop control and other than disturbance torques the closed loop has no feedback information about them. It is conceivable that a flexible robot could be built where the feedback is taken at the endpoint and the structural modes will be controlled closed loop. Conceivable but not likely with systems of appreciable bandwidths, since personal experience with 1 DOF helicopter rotor control systems has demonstrated that this is not simple when the dynamics are stationary. Robotic dynamics have the distinction of being both multidimensional and non stationary. It seems for the moment that open loop systems which minimize these structural modes are the pragmatic answer.

Data Match

The analytic and actual robot were matched in two steps. First, the measured mode shapes and frequencies were matched at a spine length of 70 inches for the unloaded case to the analytic linear model, see Chapter 9. Second, this match was fine tuned to the actual step responses by adjusting nominally calculated spring rates Ka, Kr and the structural damping terms, fig 10.2 & 10.3.

Measurement Definitions

The step responses can be characterized by the magnitudes of the oscillations of θ1 and θ1E around the spine angle calculated from the actuators displacement. The nominal step size for the simulations is 1 inch of cable length corresponding to θ1 and θ1e displacements of approximately .056 radians. The linear responses are normalized by the step size yielding percent of step size. The following terms will serve as a basis for the comparison.

1. endpoint magnitude (% overshoot) = $\frac{\text{first } \theta 1E \text{ oscillation}}{\text{spine angle step size}}$

2. base magnitude (% overshoot) = $\frac{\text{first } \theta 1 \text{ oscillation}}{\text{spine angle step size}}$

Frequency Response

Frequency responses at the nominal 70 inch spine length case offer insight into the endpoint control problem for both the parallel and serial manipulators.. In the parallel case , fig 10.4, and serial case, fig 10.5, frequency response from motor current to cable position show damped resonant peaks above 10 r/s for both the loaded and unloaded cases. When the control is added the open loop gain and damping have effectively eliminated the effect of these resonances from the actuator position loop. The closed actuator position loop is also free of resonant peaks. The resonant peaks reappear in the closed loop response to endpoint position since the flexible dynamics are outside the actuator position loops and the control cannot affect these dynamics. In both parallel and serial cases the resonance magnitudes of the loaded case are considerably larger than the unloaded case.

Step Response Results

The step responses for all combinations of unloaded, loaded, parallel and serial manipulators for varying spine length, rod stiffness and actuator stiffness are presented in fig 10.6 to 10.8. The endpoint $\theta 1e$ and base $\theta 1$ magnitudes of the oscillations from these plots have been plotted in fig 10.9 to 10.11.

As predicted from the modes: $\theta 1e$ is always less than $\theta 1$ for the parallel case; while $\theta 1e$ is always greater than $\theta 1$ for the serial case .

As the spine length is shortened the spine inertia decreases, while both the cable and rod become stiffer, fig 10.6 & 10.9. For both manipulator types and loads the endpoint and base magnitudes decrease with decreasing spine length. The endpoint magnitudes for the parallel manipulator are less than those of the serial manipulator for all spine lengths and loadings except for the unloaded case less than 60 inches. At this point the rod extension is very short and there is very little equivalent rod end mass for the serial case while the parallel case still has the spine inertia to contend with. The base magnitudes of the serial manipulator are less than those of the parallel manipulator for all spine lengths and loads.

For increasing actuator stiffness Ka the end magnitudes decrease for both manipulators and loadings, fig 10.7 & 10.10. For all cases the endpoint magnitudes for the parallel manipulator are less than those of the serial manipulator. Just the opposite occurs with the base magnitudes, the serials are smaller than the parallels for all cases. In the parallel case the endpoint magnitude can be decreased drastically by increasing the actuator stiffness whereas only a moderate improvement can be gained in the serial case. Note that just the opposite is true for base magnitudes increasing actuator stiffness will reduce the serial base magnitude drastically but only moderately for the parallel case.

For increasing spine stiffness the endpoint magnitude for the parallel manipulator increases while the serial decreases, for both loadings, fig 10.8 & 10.11. Still the endpoint magnitudes of the parallel manipulator are smaller except in the unloaded case for stiffnesses above 5Kr.

Again the base magnitudes exhibit just the opposite tendency, decreasing for the parallel and increasing for serial. Increasing spine stiffness only gives a moderate improvement in endpoint magnitude for the serial manipulator.

For all loaded cases and most unloaded cases the parallel manipulator controls endpoint position better than the serial manipulator due the cable going directly to the endpoint. This constraint forces the mode to assume a shape where the endpoint is a node, or close to it even though the first bending mode of the cantilever rod is being excited. The serial case always assumes modes where all masses are moving in the same direction, away from the desired endpoint position. The most surprising result is that the parallel manipulator's endpoint magnitude can be improved by stiffening the actuators or cables without stiffening the spine furthermore stiffening only the spine may actually make matters worse by transmitting larger disturbances to the cables. Of course we know from the existing parallel manipulator [1] that if both the cables and rod are very stiff the manipulator will be stiff. In the limit rigid cables will control the endpoint without oscillation regardless of the rod stiffness. In actuality this stiffness will be limited by the spine's capability to exert outward force and the buckling strength of the rod. This cable stiffening is very handy because in outer space applications it may be impossible to stiffen the spine but possible to rig heavier cables.

On the other hand the serials's endpoint magnitude can only be eradicated by stiffening both the actuators and the

spine. As mentioned before stiffening the spine may be impossible. Stiffening the actuators may also be very difficult since the flexibility is presumably in a very large ratio gear train. If the actuators were rigid you would still have to contend with an unsupported flexible cantilever beam.

Chapter 11
CONCLUSIONS

Robots in outer space are limited by power consumption and flexibility. The design and analysis of a simple counterbalanced 3 DOF lightweight electrically-driven parallel cable-controlled test robot has provided insight into the advantages and limitations of parallel robotics in space. The test robot has a maximum spine length of 80 inches and a maximum spine angle of 60 degrees, fig 1.3 and 2.1. This robot is powered by inexpensive brushed DC servo gearmotors and has both a pneumatic passive spine and an electric active spine. The major conclusions of the project are:

1) The kinematic equations for the 3 DOF robot are easily solvable in all directions. The 3 DOF robot can be expanded to 6 DOF by adding a platen, fig 1.1, or a wrist, fig 2.6. The expansion with the wrist will have the advantage of simple solvable kinematics.

2) Cable tension increases approximately linearly with spine length and spine angle. A passive spine force which will maintain cable tension over the entire workspace will become the major contributor to cable tension and power consumption at most moderate endpoint positions, figs 4.2 to 4.6.

3) The cable position can be controlled adequately by three uncoupled proportional-plus-derivative linear controls, where rate feedback is provided by a tachometer. Phase margins up to 90 degrees are easily attained for bandwidths up to 20 Hz, fig 6.5. Even when

the cable position loops are controlling without overshoot the endpoint oscillates due to flexible elements in the cable drives and spine.

4) Large deadbands due to static friction in the motors and spine can cause proportional cable position loops to perform very haltingly. These jitters are cured with rate feedback provided by the addition of tachometers.

5) The active test spine has response equal to the passive spine when it is controlled with a constant force reference. Furthermore the active spine has the potential for superior performance when the spine force is optimized.

6) The power consumption analysis shows that if the spine force is actively controlled to an optimal minimum then the cable controlled parallel manipulator can approach the power consumption of a parallel manipulator which has compressive and tensile links such as hydraulic cylinders instead of cables. Furthermore the total power consumption in the spine and cable drives attributable to just the spine force is at best twice the power consumption of the spine alone.

7) The parallel configuration with active spine effectively transforms power to force for small spine lengths in all directions. For long spine extensions power effectiveness in the tangential direction decreases inversely proportional to the spine length but remains relatively constant in the radial direction, fig 8.1.

8) The endpoint of the parallel robot is equally stiff in all directions for very short spine lengths . Stiffness in

the radial direction is relatively unaffected by spine length and spine angle while stiffness in tangential directions decreases with the spine length and spine angle, fig 8.2 and 8.3. Endpoint stiffness increases with spine force but this increased spine force has a high cost in terms of power consumption. The endpoint stiffness of the parallel robot is dependent on the cable and actuator stiffnesses, but is independent of the spine bending stiffness. This last point assumes that the spine can support the buckling load.

9) Dynamic tangential endpoint position oscillations are primarily caused by flexibilities in the cable drive system and the spine rod. The cables constrain the bending modes such that the magnitudes of the oscillations are decreased by 1/2 to 1/3 from what they would be with a 'dynamically equivalent' serial robot. In primary bending mode of the parallel robot the midpoint of the spine bends outward in relation to the endpoint while in the serial robot the midpoint bends inward, fig 9.4 and 9.5.

10) The dynamic tangential endpoint oscillations in the loaded lightweight parallel robot can be decreased dramatically by increasing the cable stiffness, but not by increasing the spine bending stiffness since the endpoint stiffness is independent of the spine bending stiffness. Increasing the spine bending stiffness in the parallel robot may actually increase the endpoint oscillations by transmitting larger force disturbances to the cables. In contrast the tangential oscillations in the loaded lightweight serial robot can be decreased only by increasing spine bending stiffness. Furthermore, this decrease is only a moderate improvment in comparison to the improvement easily attainable in the parallel robot.

Further Research

This work may be continued in a variety of ways. The potential utility of these robots in outer space has been demonstrated in this thesis. To continue this work a variety of robots can be built, which with careful scaling and realistic design, will further exercise these concepts.

1) The current 3 DOF robot can be expanded with an active spine which will collapse to a fraction of its fully extended length.

2) The current 3 DOF robot can be expanded to 6 DOF by adding a wrist.

3) A 3 DOF robot with 2 translational and 1 rotational DOF which operates only in a horizontal plane could demonstrate positioning very large masses in zero gravity.

4) The conclusion that parallel manipulator tangential stiffness is independent of spine bending stiffness can be demonstrated with a 3 DOF robot with a very flexible spine and very stiff cables.

5) A project which intrigues me is a very light and fast 4 DOF robot which can track and catch flies.

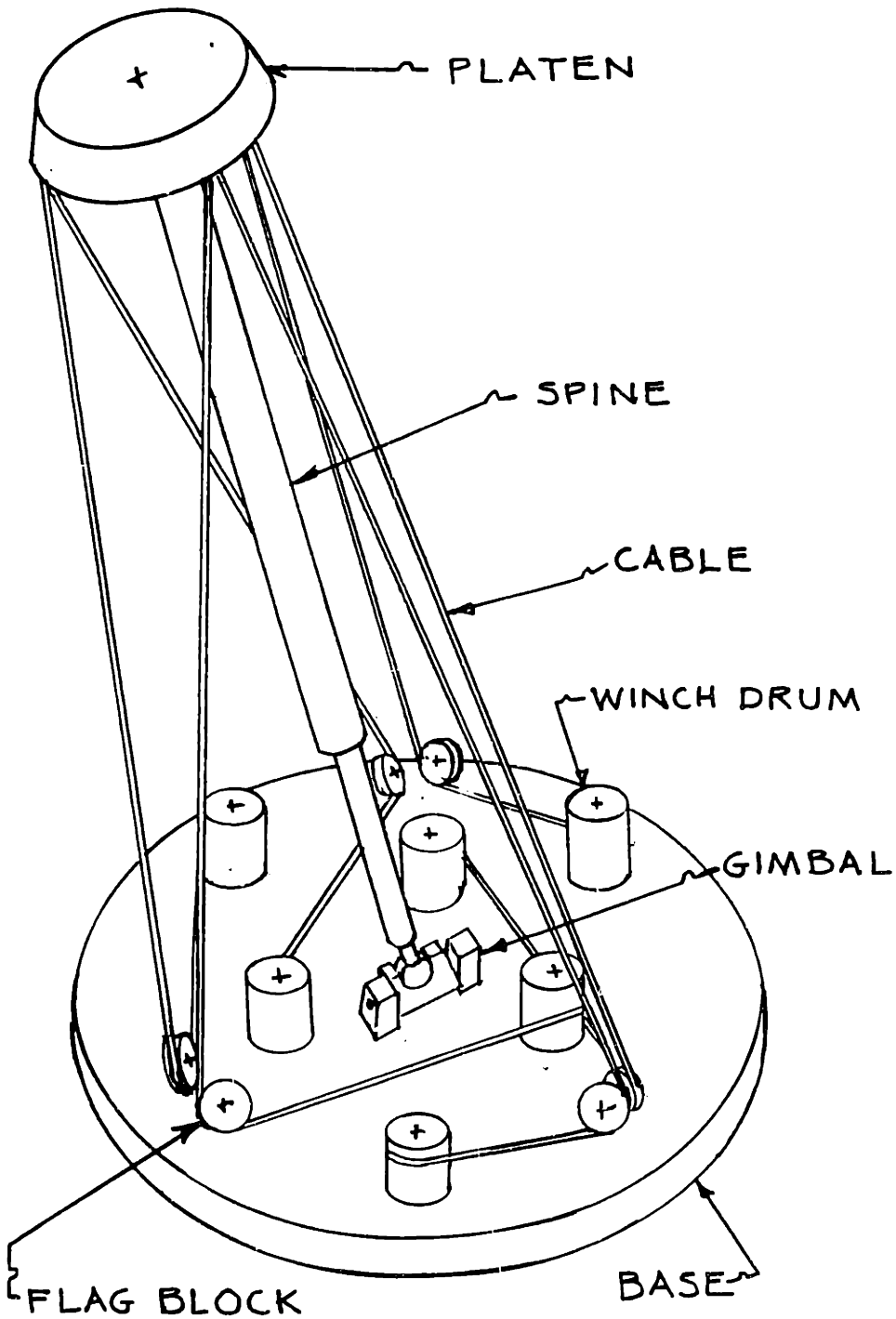

FIGURE 1.1 : 6 DOF CABLE-CONTROLLED PARALLEL ROBOT

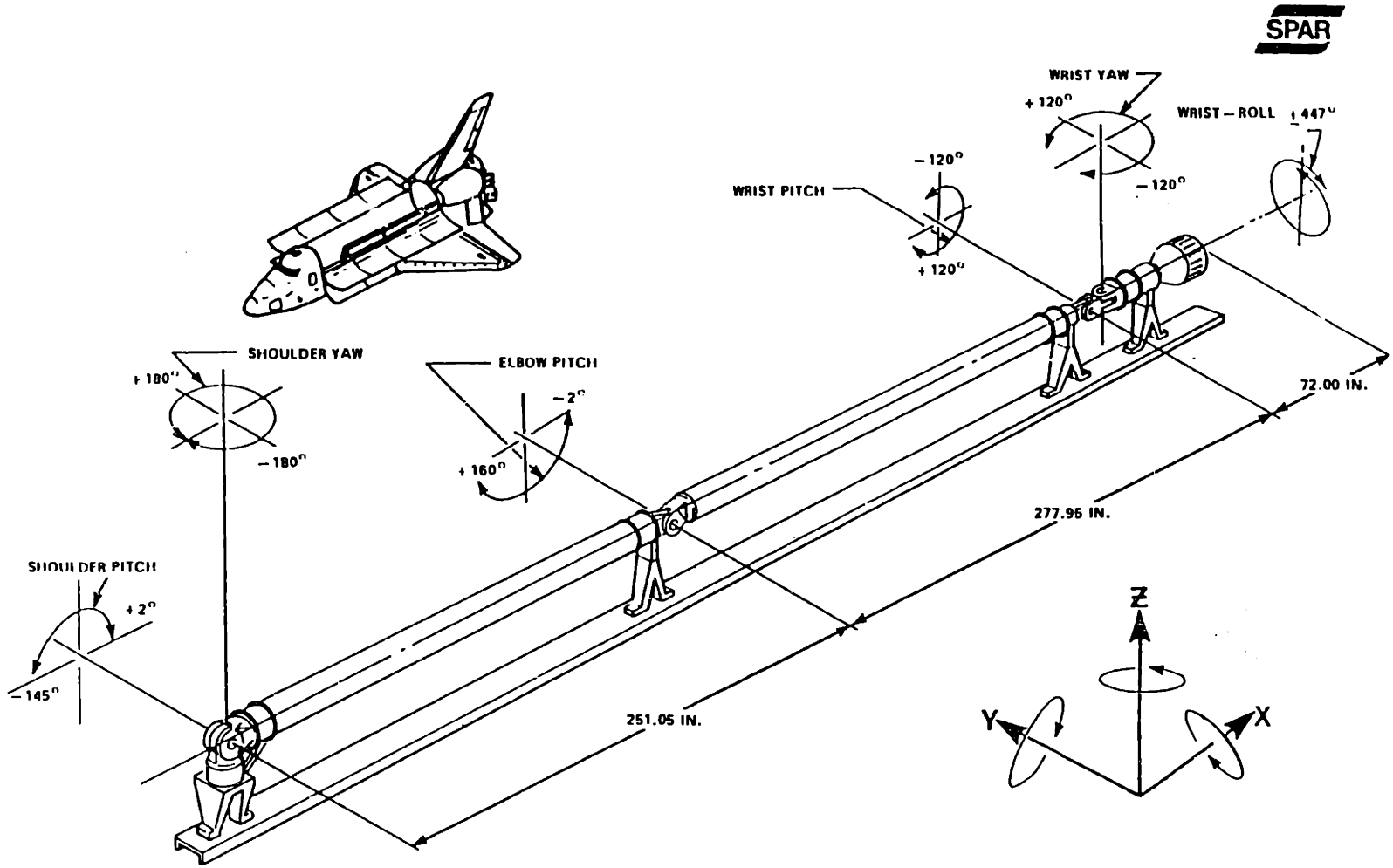

REPRINTED FROM REF [9]

FIGURE 1.2: SPACE SHUTTLE SERIAL ROBOT ARM

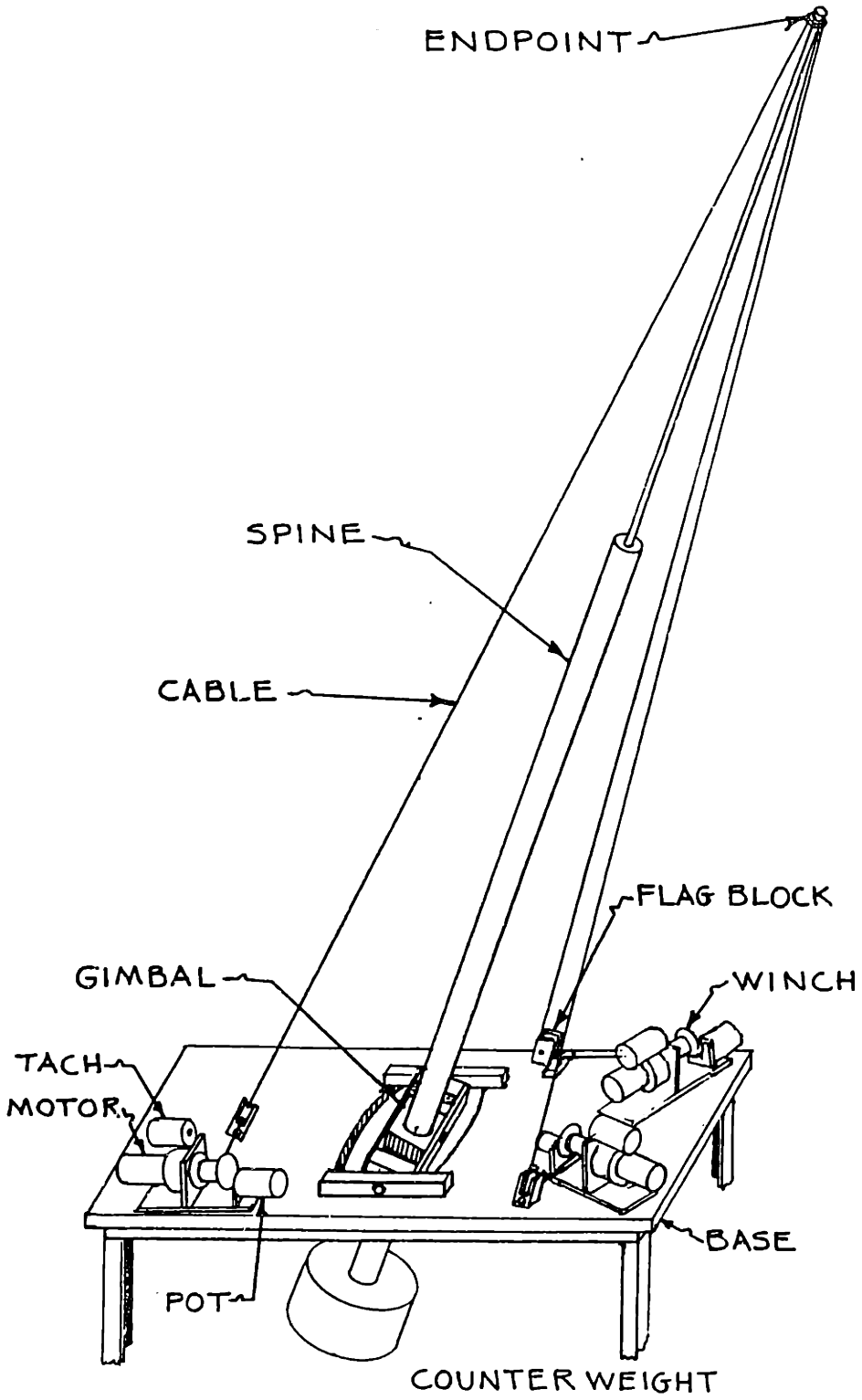

FIGURE 1.3 : THREE DOF PARALLEL TEST ROBOT

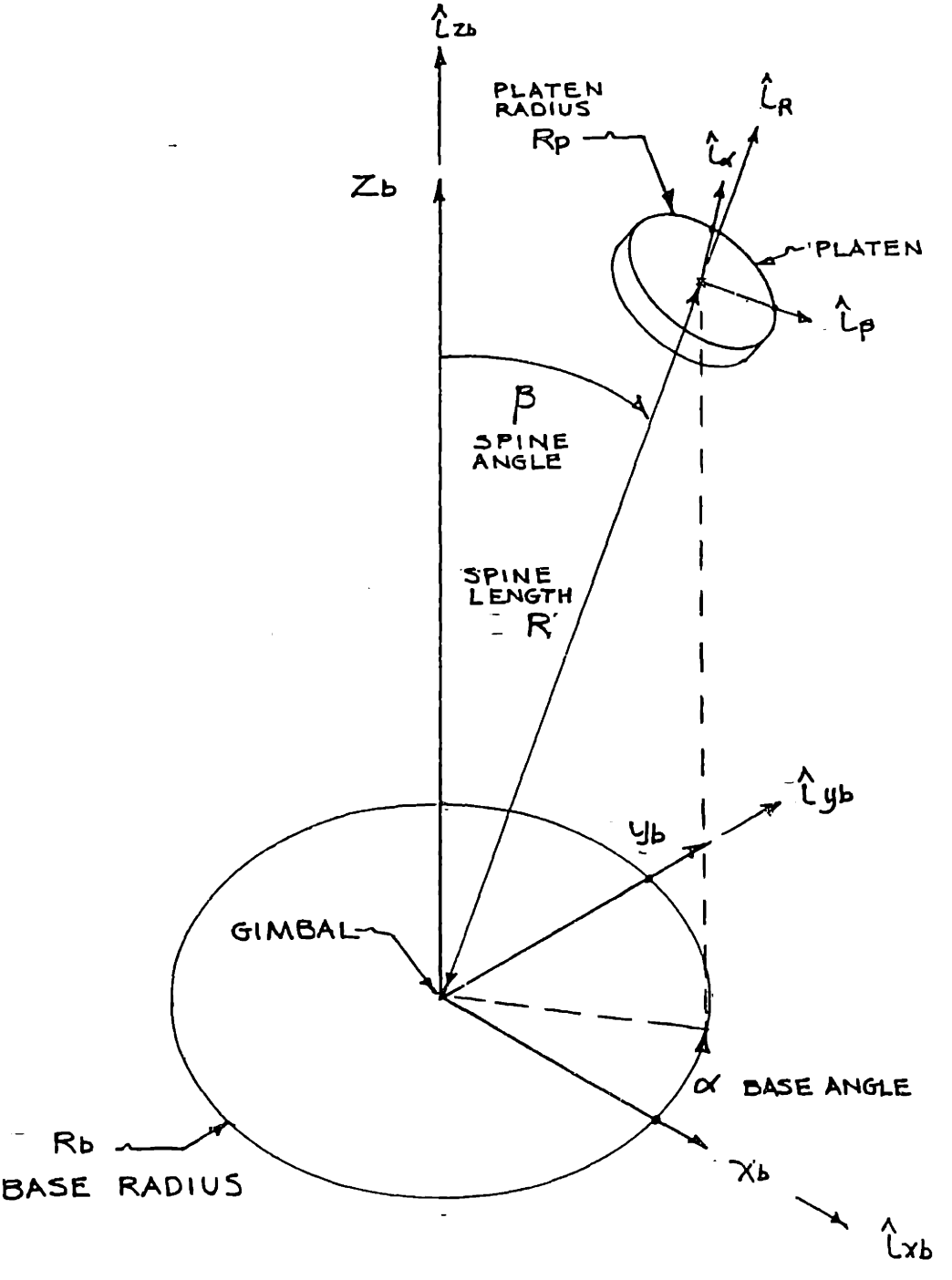

FIGURE 2.1: TERMS FOR PARALLEL ROBOTS

RESULTS FROM PRELIMINARY STATIC ANALYSIS USING THE 6DOF ROBOT OF FIG 1.1

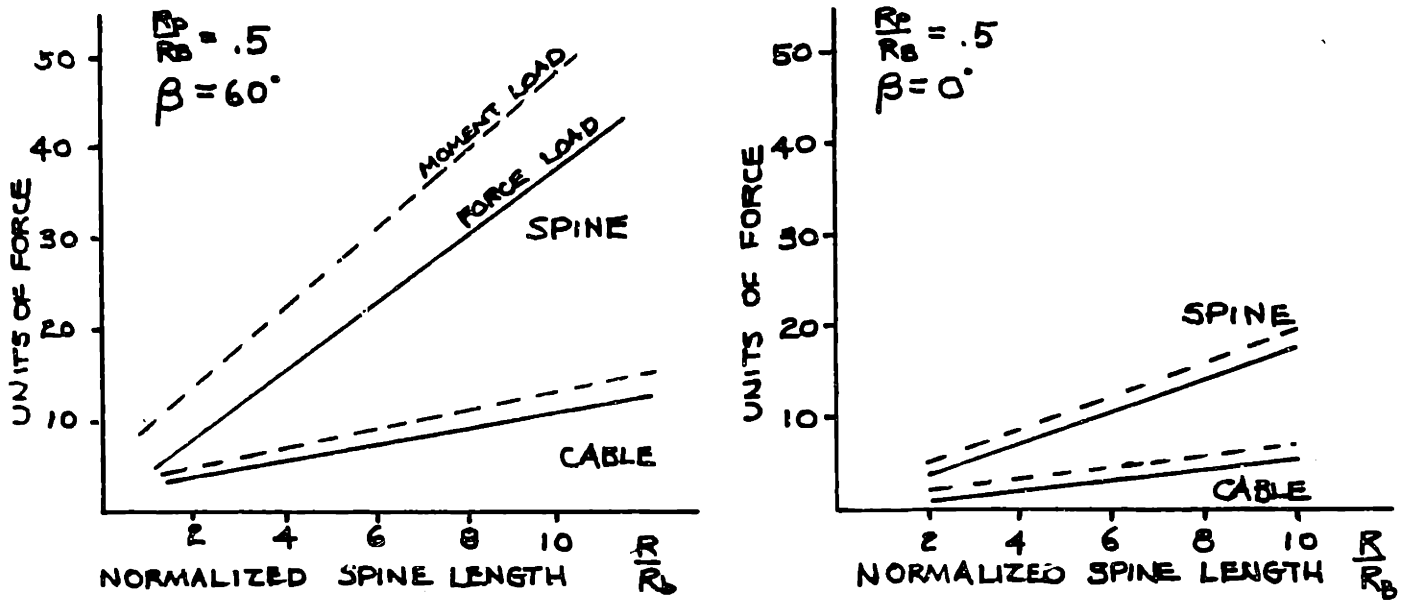

FIGURE 2.2 CABLE TENSION & SPINE FORCE VERSUS SPINE LENGTH

(DERIVED FROM [1])

RESULTS FROM PRELIMINARY STATIC ANALSIS USING THE 6DOF ROBOT OF FIG 1.1

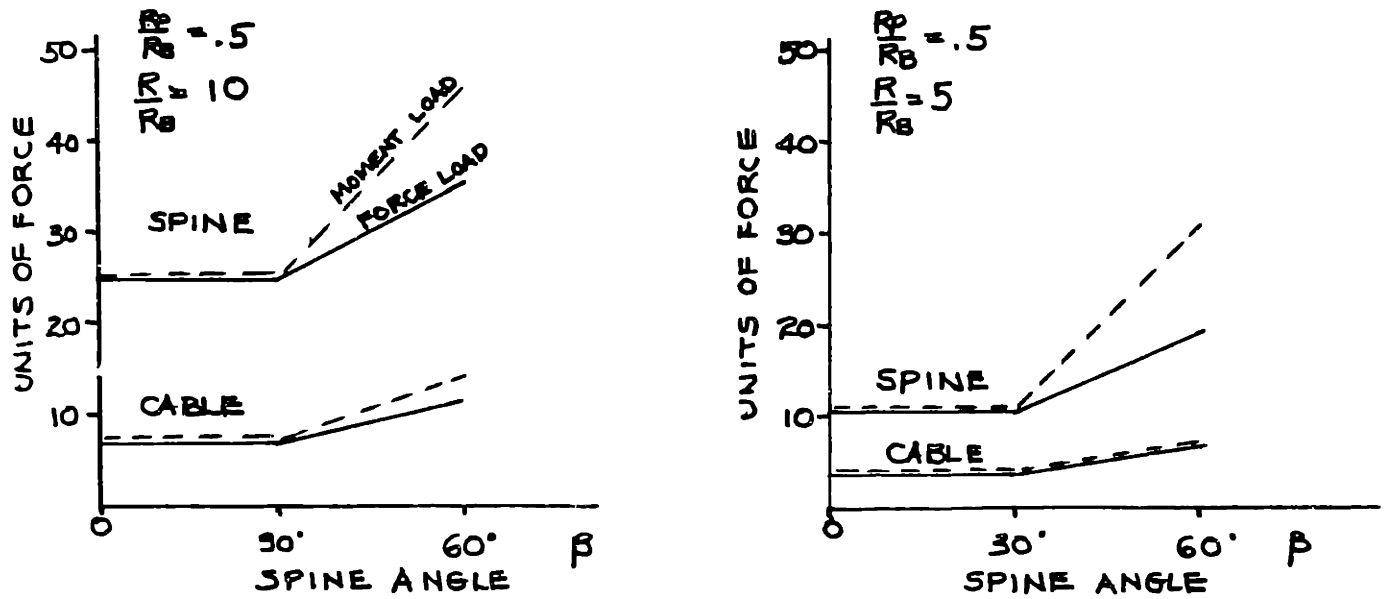

FIGURE 2.3: CABLE TENSION & SPINE FORCE VERSUS SPINE ANGLE (DERIVED FROM [1])

RESULTS FROM PRELIMINARY STATIC ANALYSIS USING THE 6DOF ROBOT OF FIG 1.1

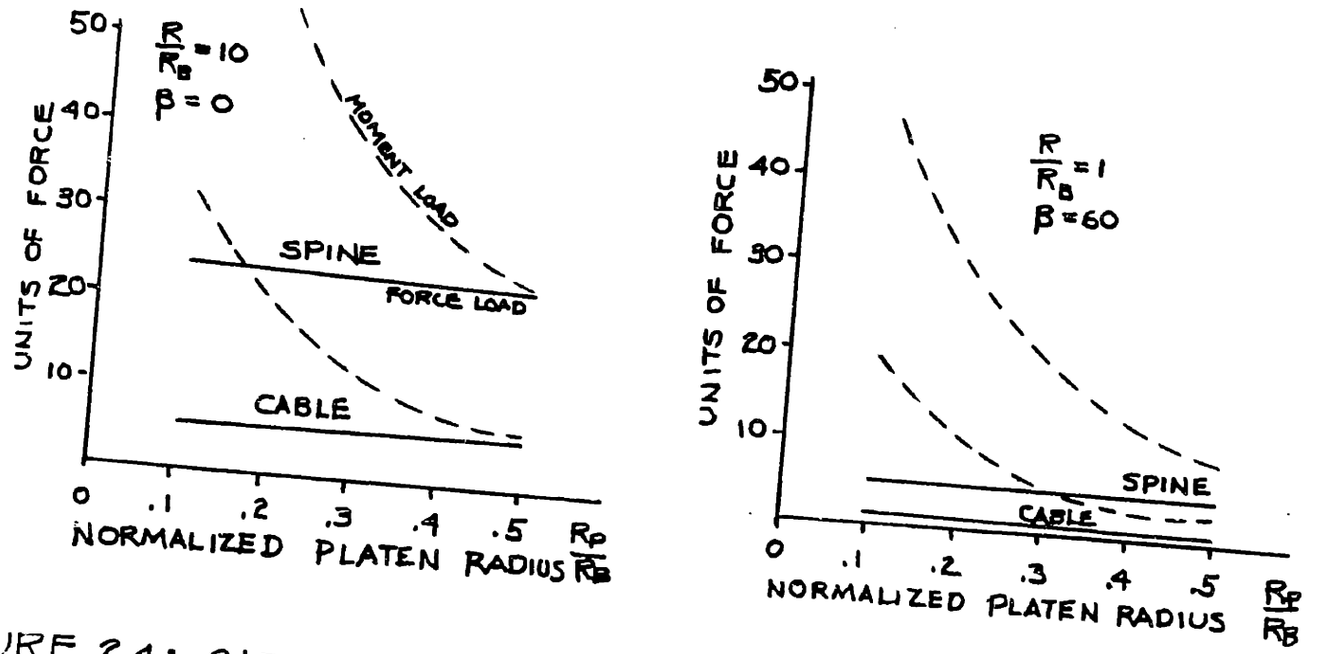

FIGURE 2.4: CABLE TENSION & SPINE FORCE VERSUS PLATEN RADIUS (DERIVED FROM [1])

RESULTS FROM PRELIMINARY STATIC ANALYSIS USING THE 6 DOF OF FIG. 1.1

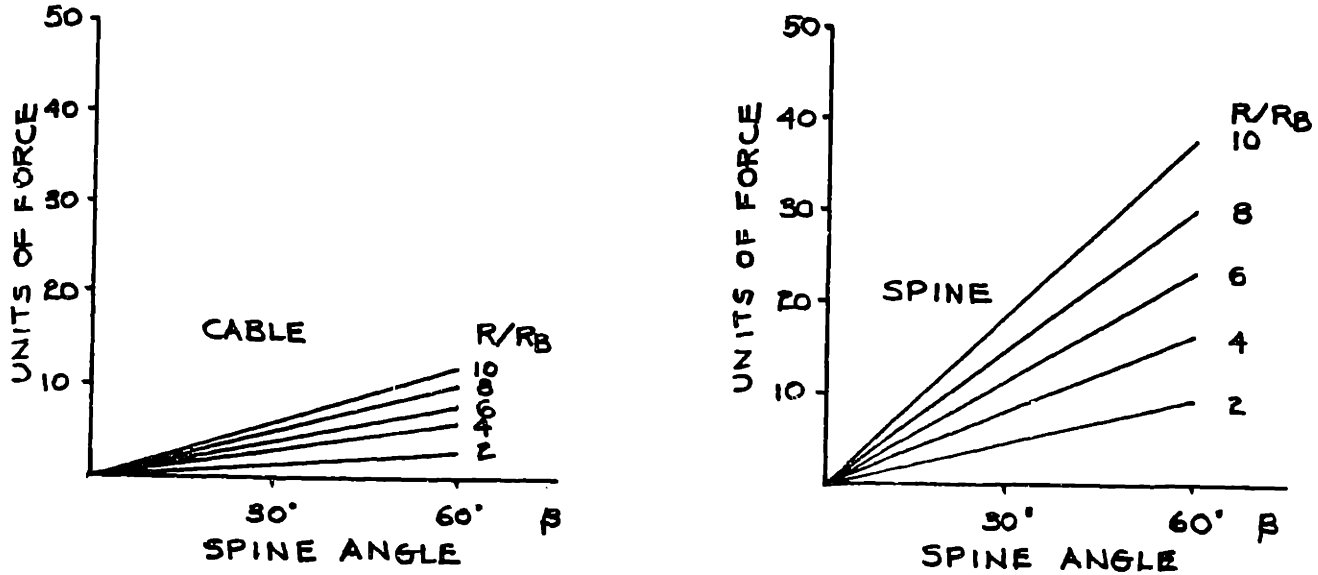

FIGURE 2.5: CABLE TENSION & SPINE FORCE FROM GRAVITY LOADING (DERIVED FROM [1])

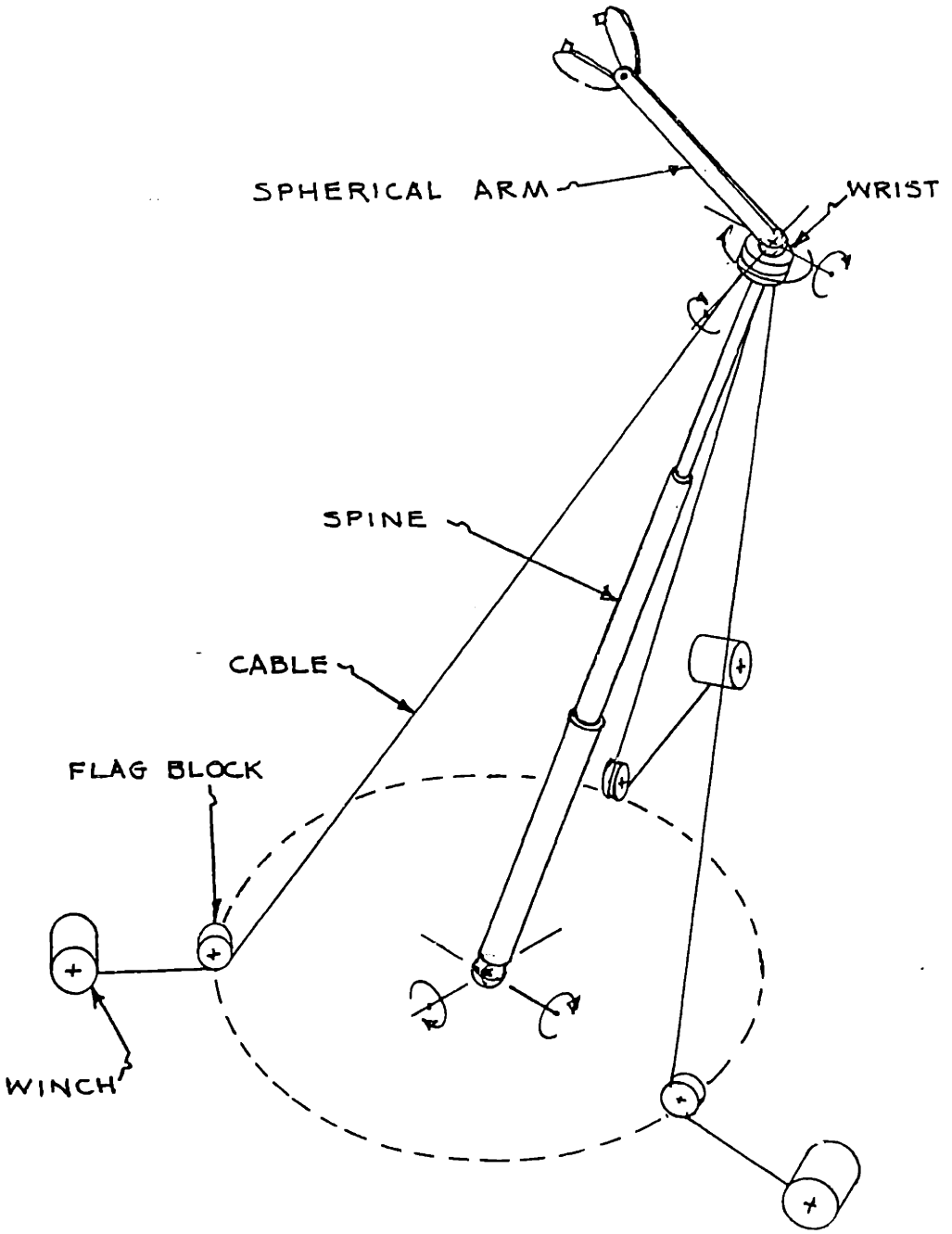

FIGURE 2.6: HYBRID 6 DOF CABLE CONTROLLED MANIPULATOR

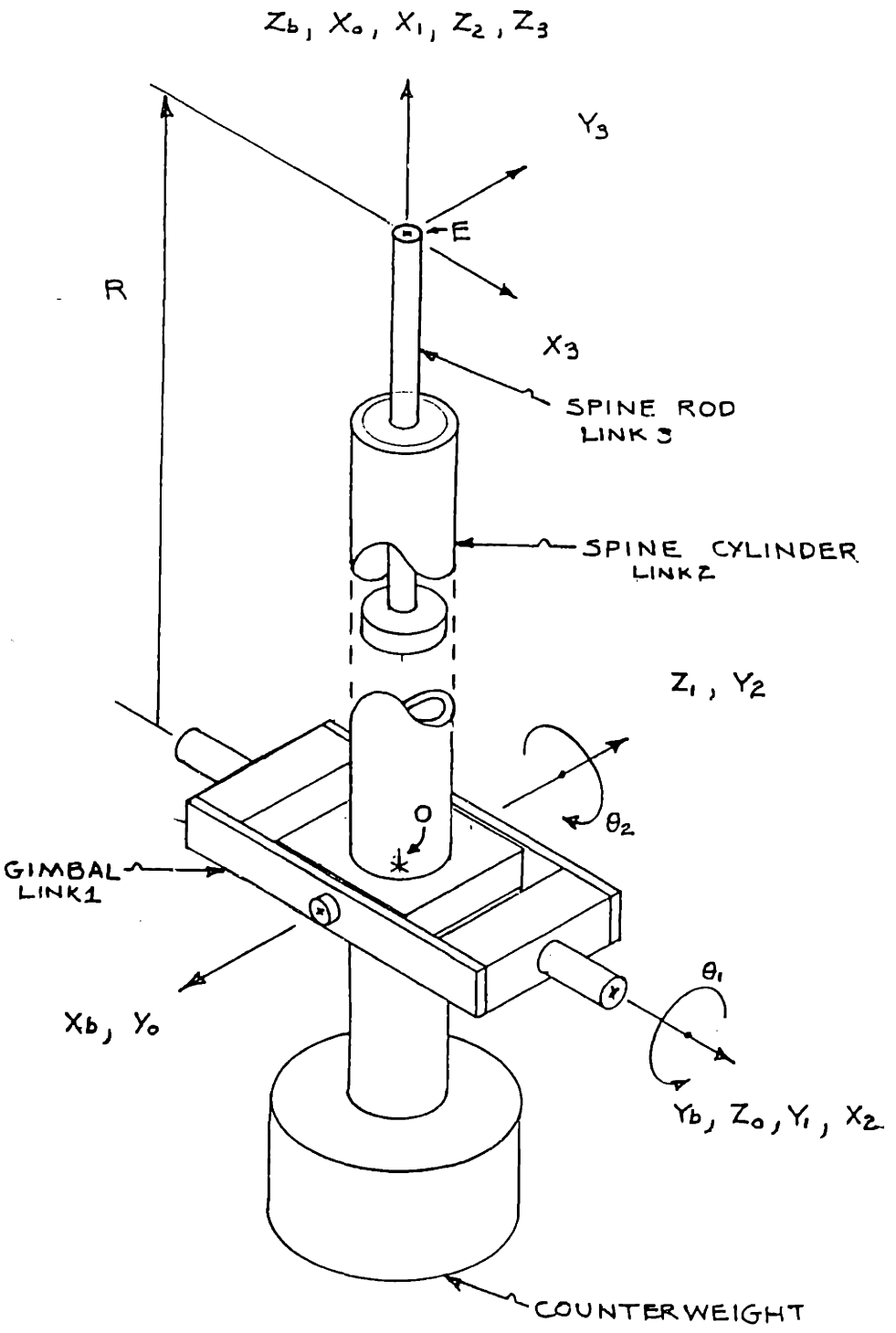

FIGURE 3.1: SPINE & GIMBAL FOR DEN-HARTENBERG NOTATION

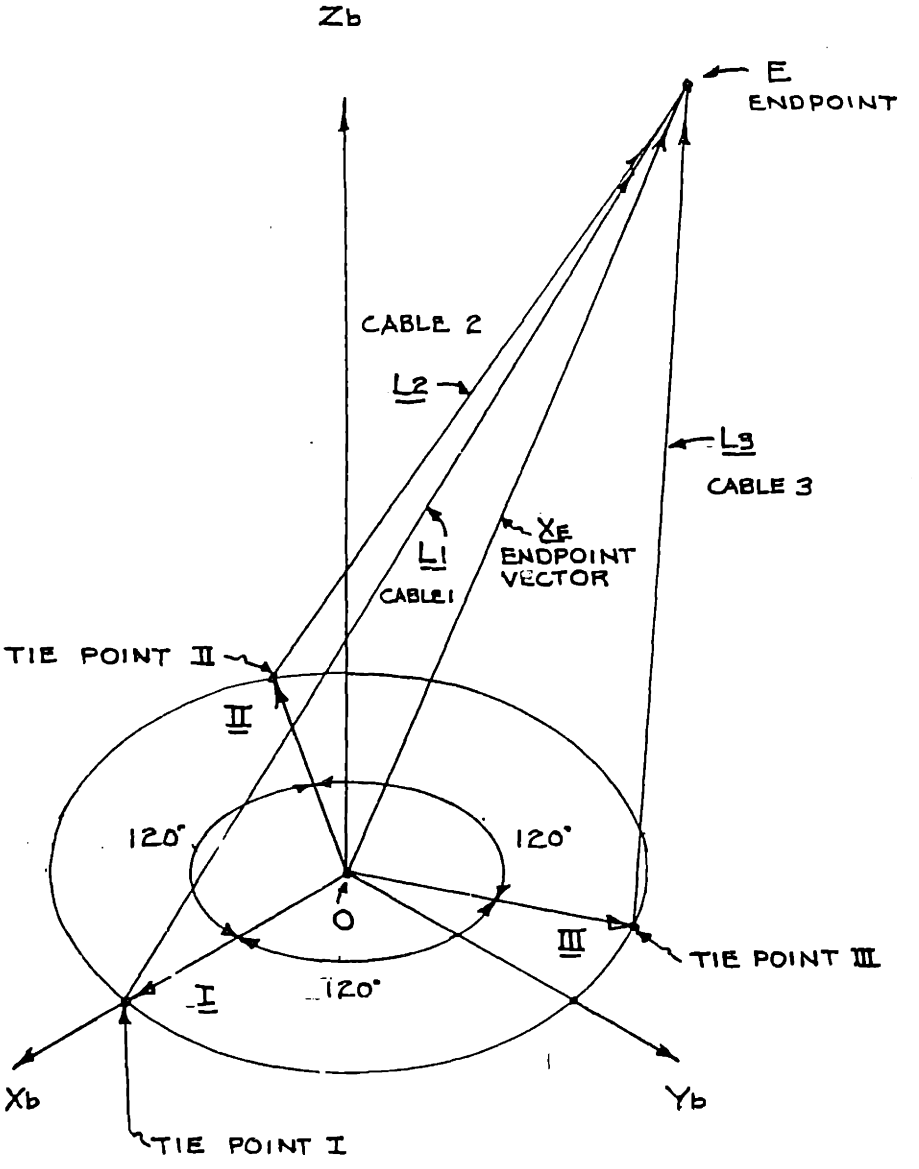

FIGURE 3.2: CABLE SPACE DEFINITONS FOR JACOBIANS

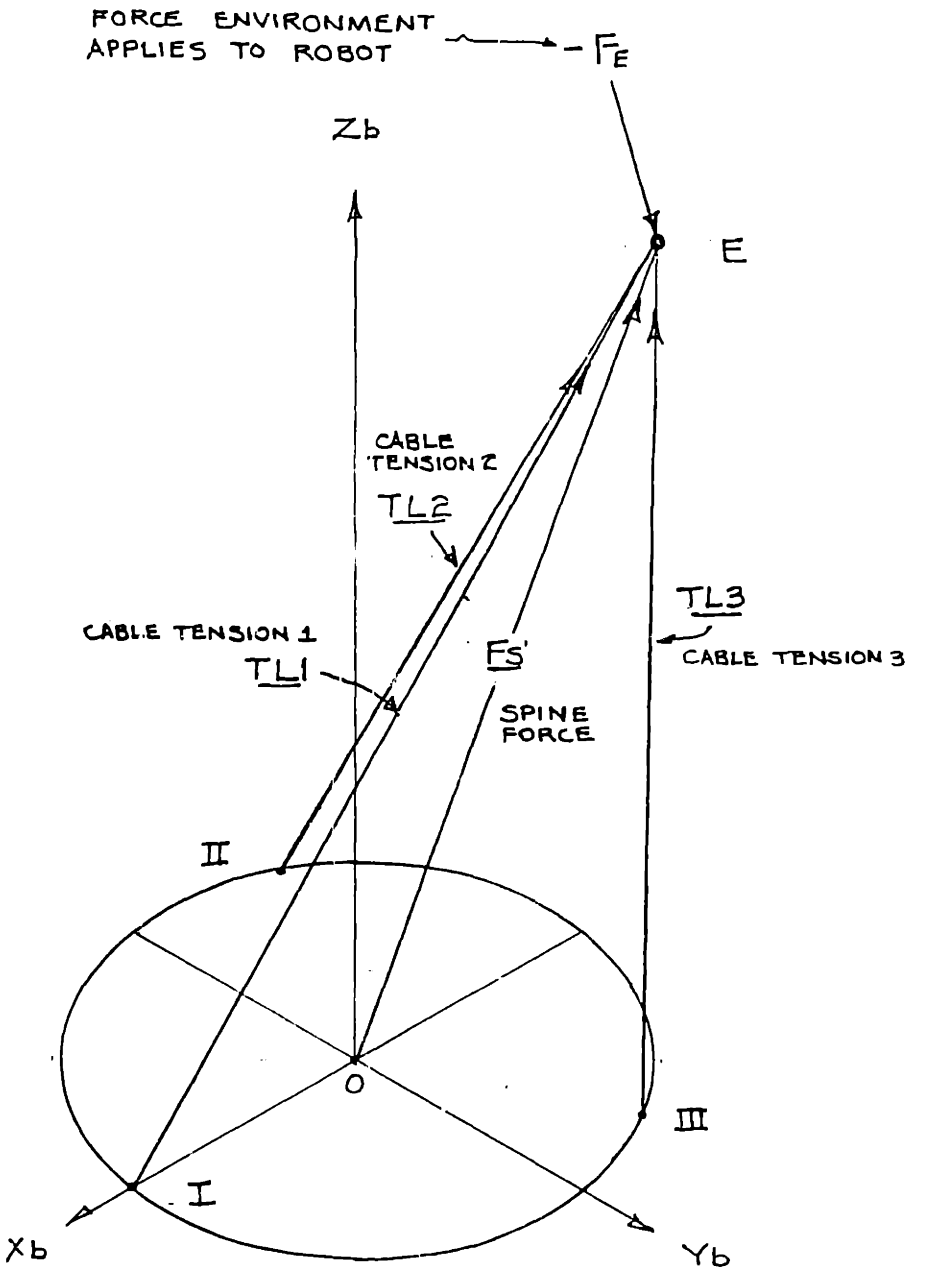

FIGURE 4.1 : FORCES ON 3 DOF MANIPULATOR FOR STATICS

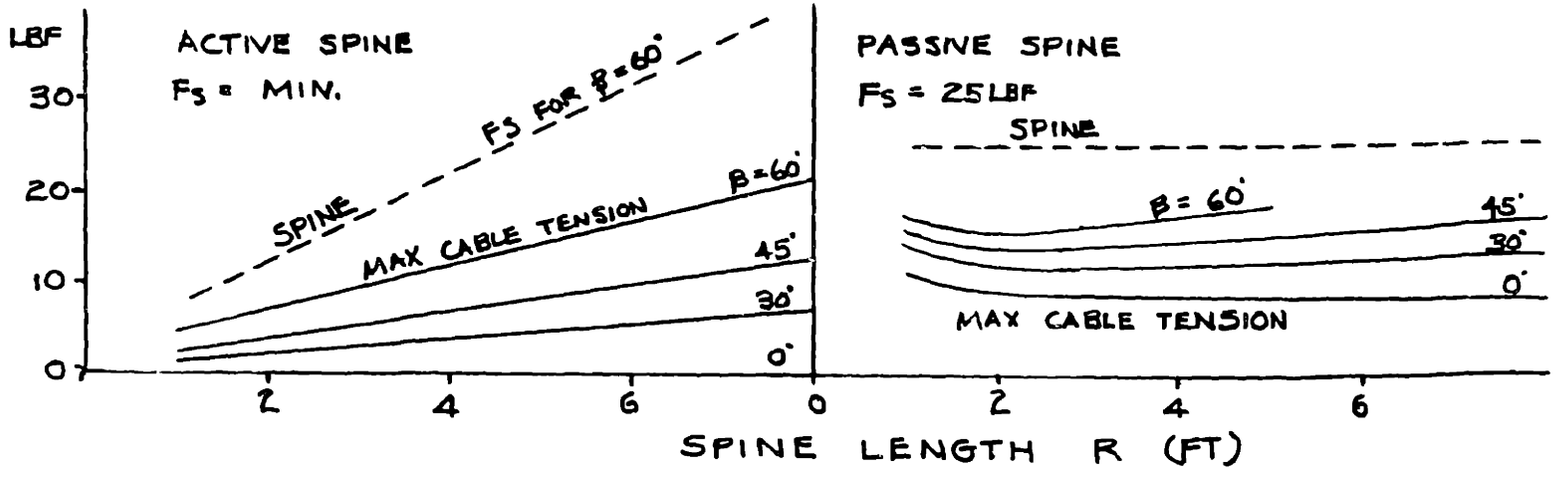

FIG. 4.2: 3 DOF STATICS, NO LOAD, NO COUNTERBALANCE

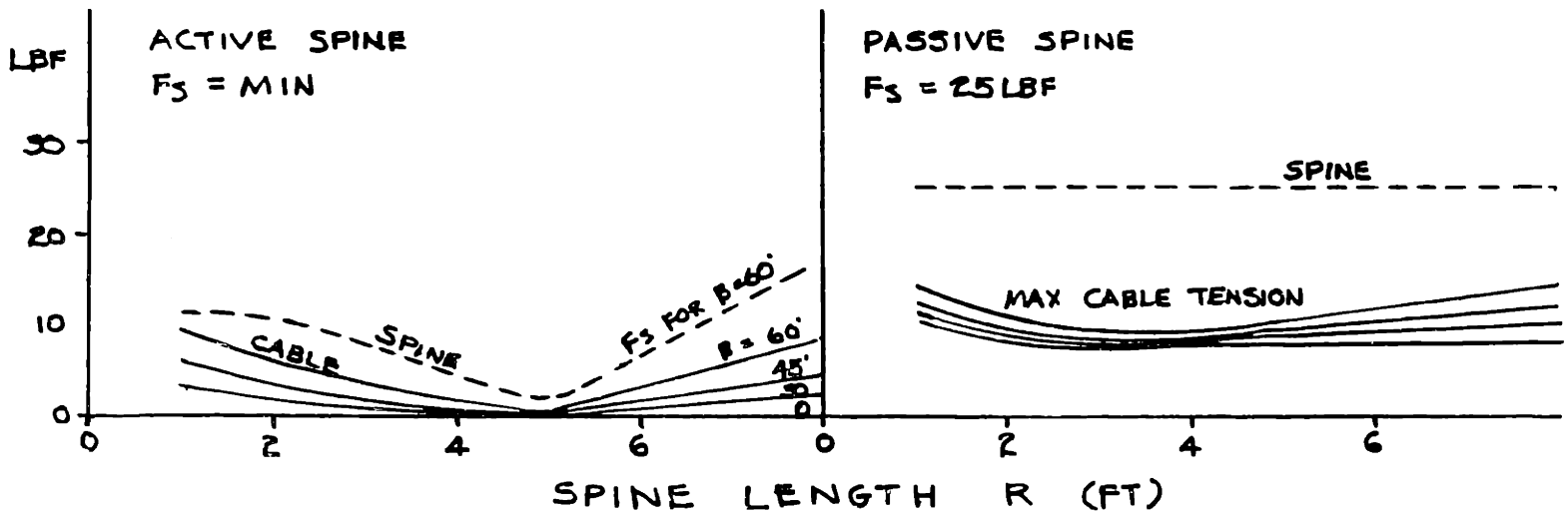

FIG. 4.3: 3DOF STATICS, NO LOAD, COUNTERBALANCED

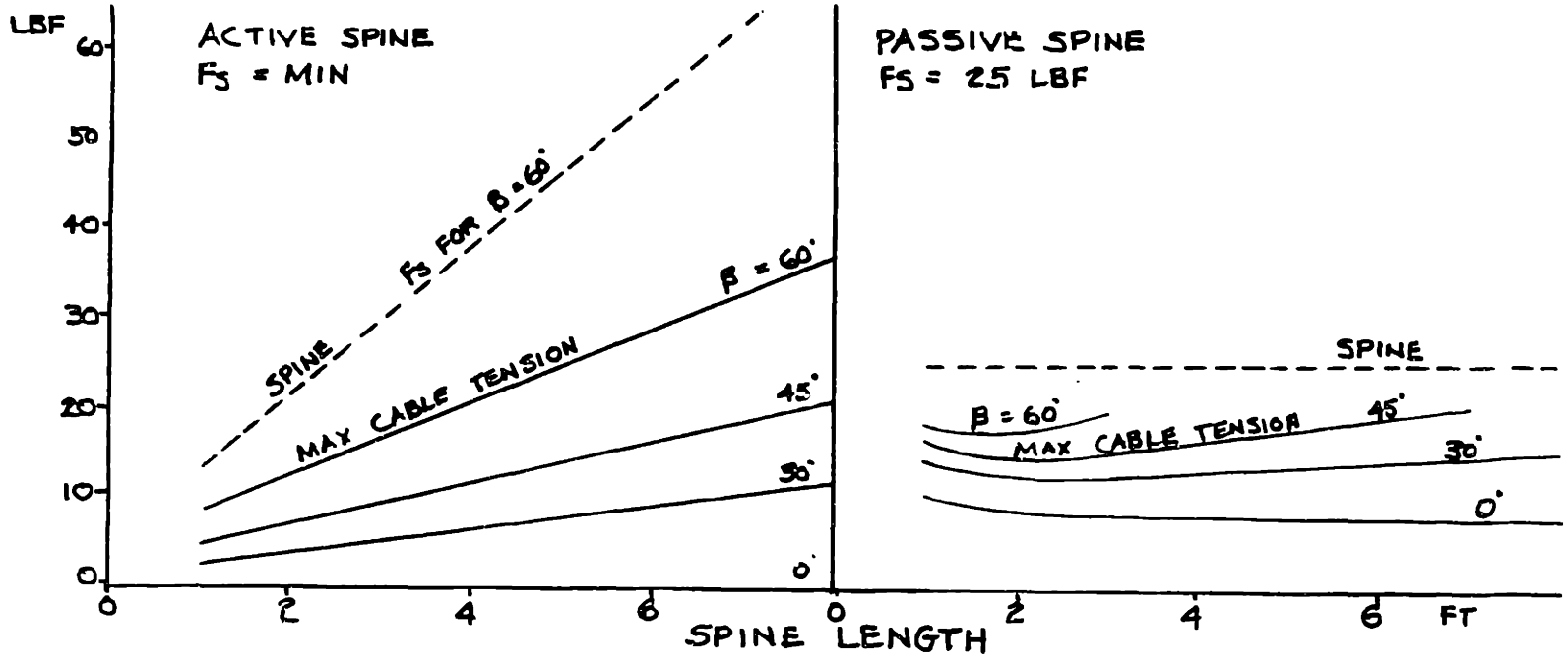

FIG. 4.4 : 3DOF STATICS LOADED NO COUNTERBALANCE

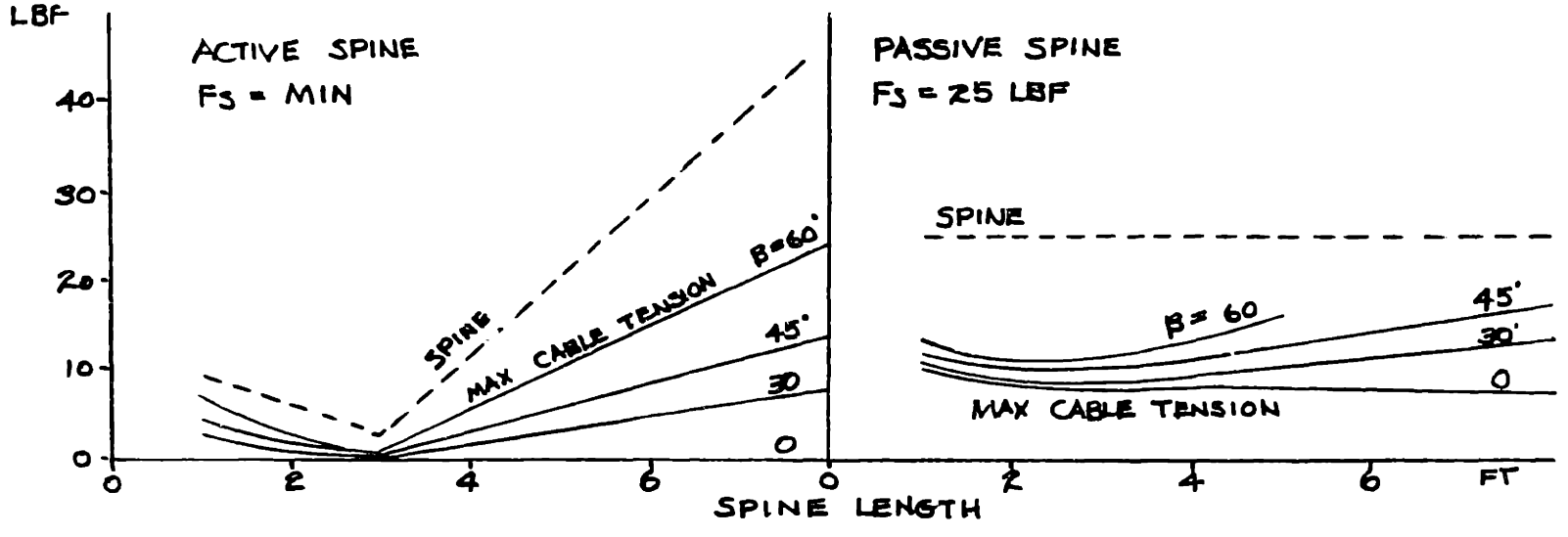

FIG. 4.5: 3 DOF STATICS LOADED COUNTERBALANCED

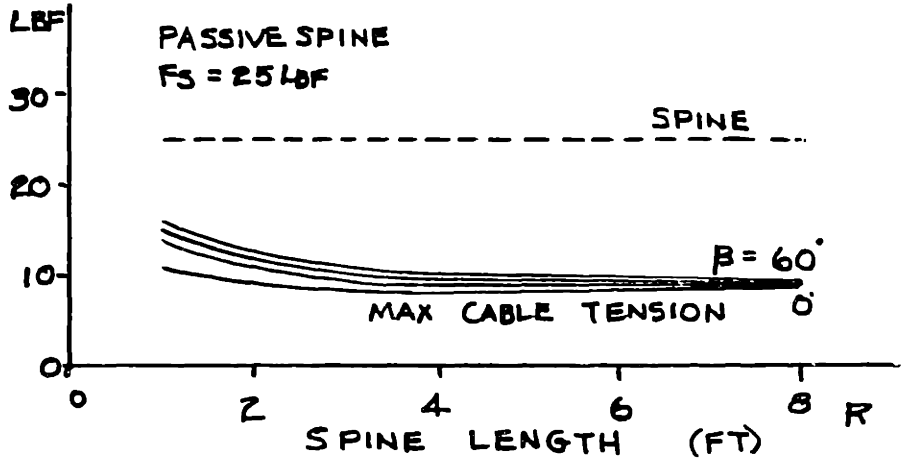

FIGURE 4.6: 3 DOF STATICS Fs = 25 NO GRAVITY

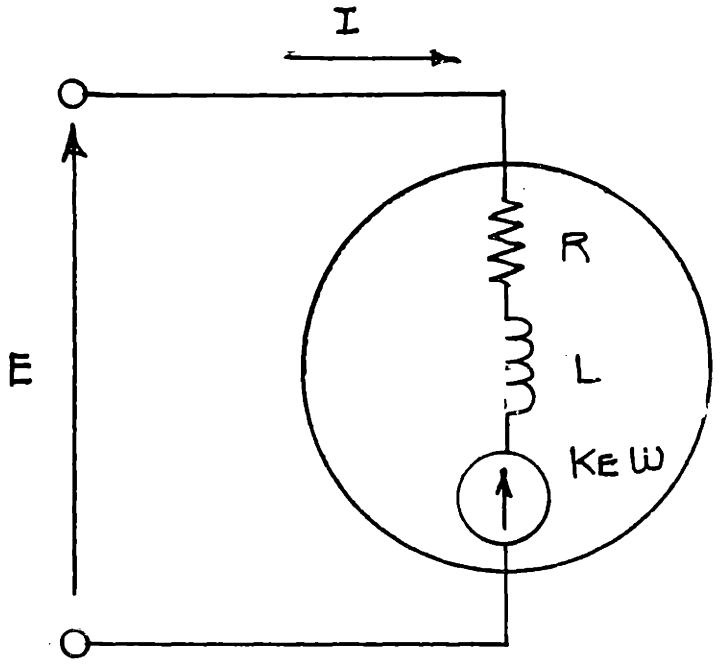

FIGURE 5.1: DC MOTOR MODEL

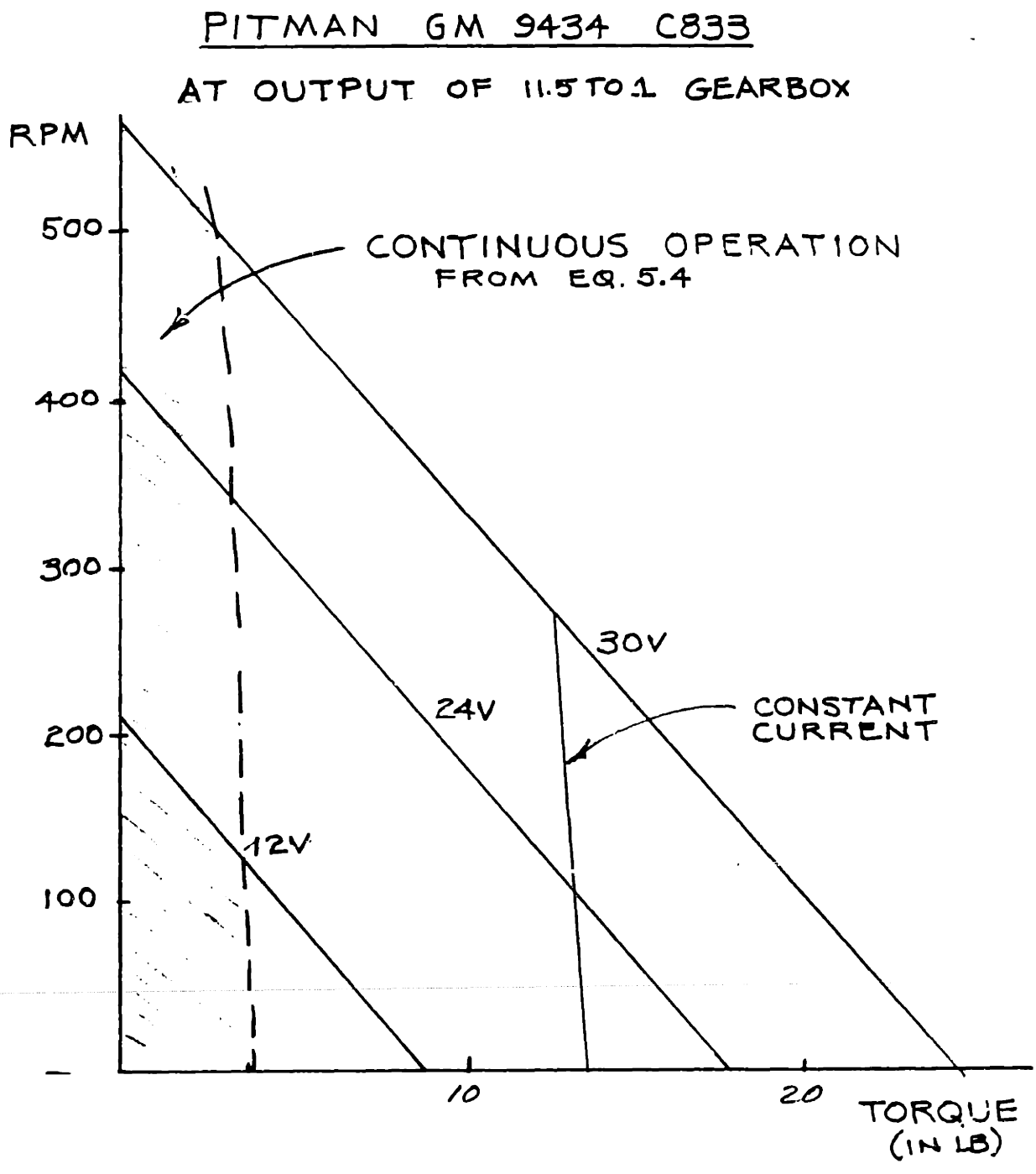

FIGURE 5.2: DC MOTOR TORQUE VS. SPEED

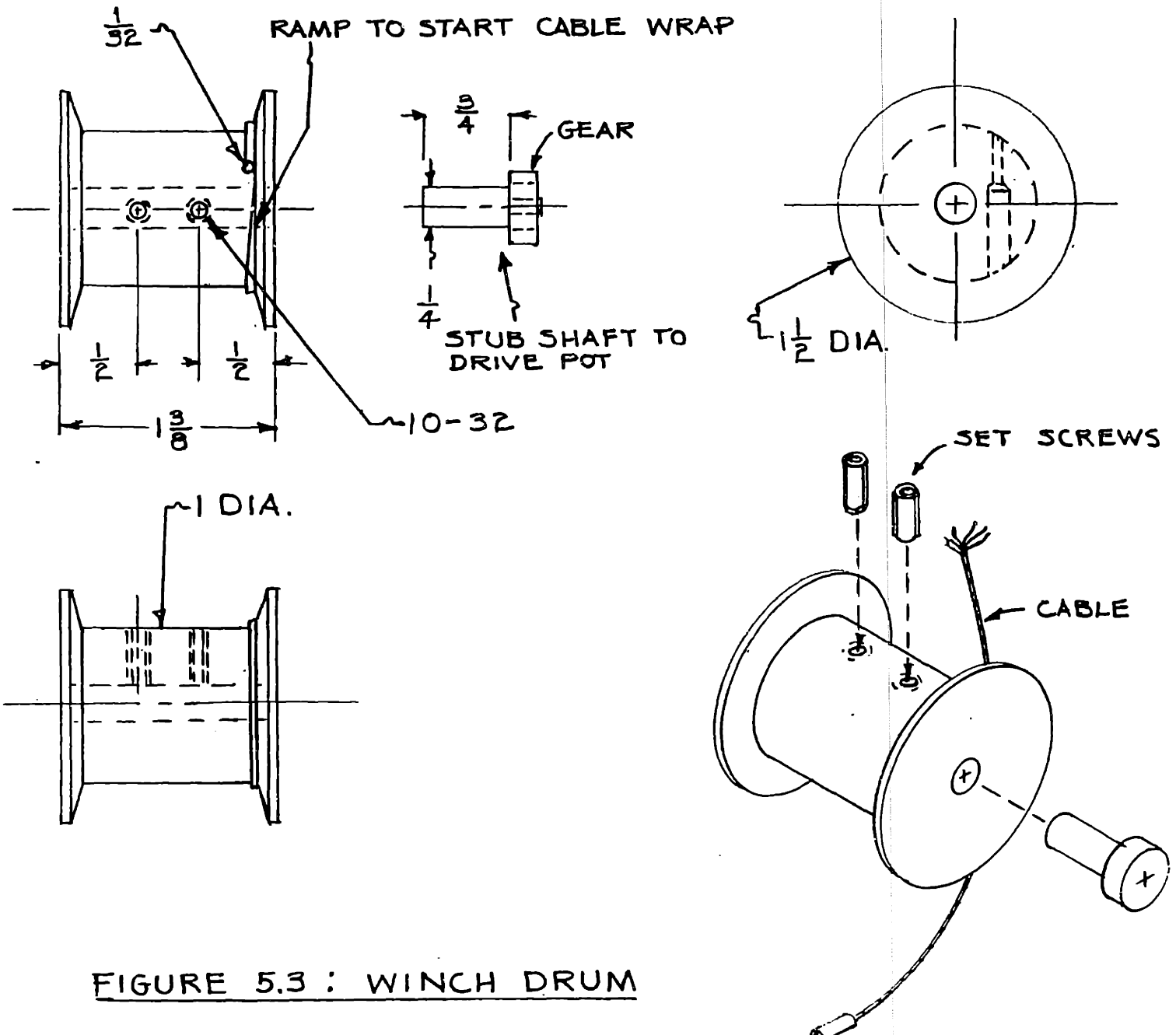

FIGURE 5.3 : WINCH DRUM

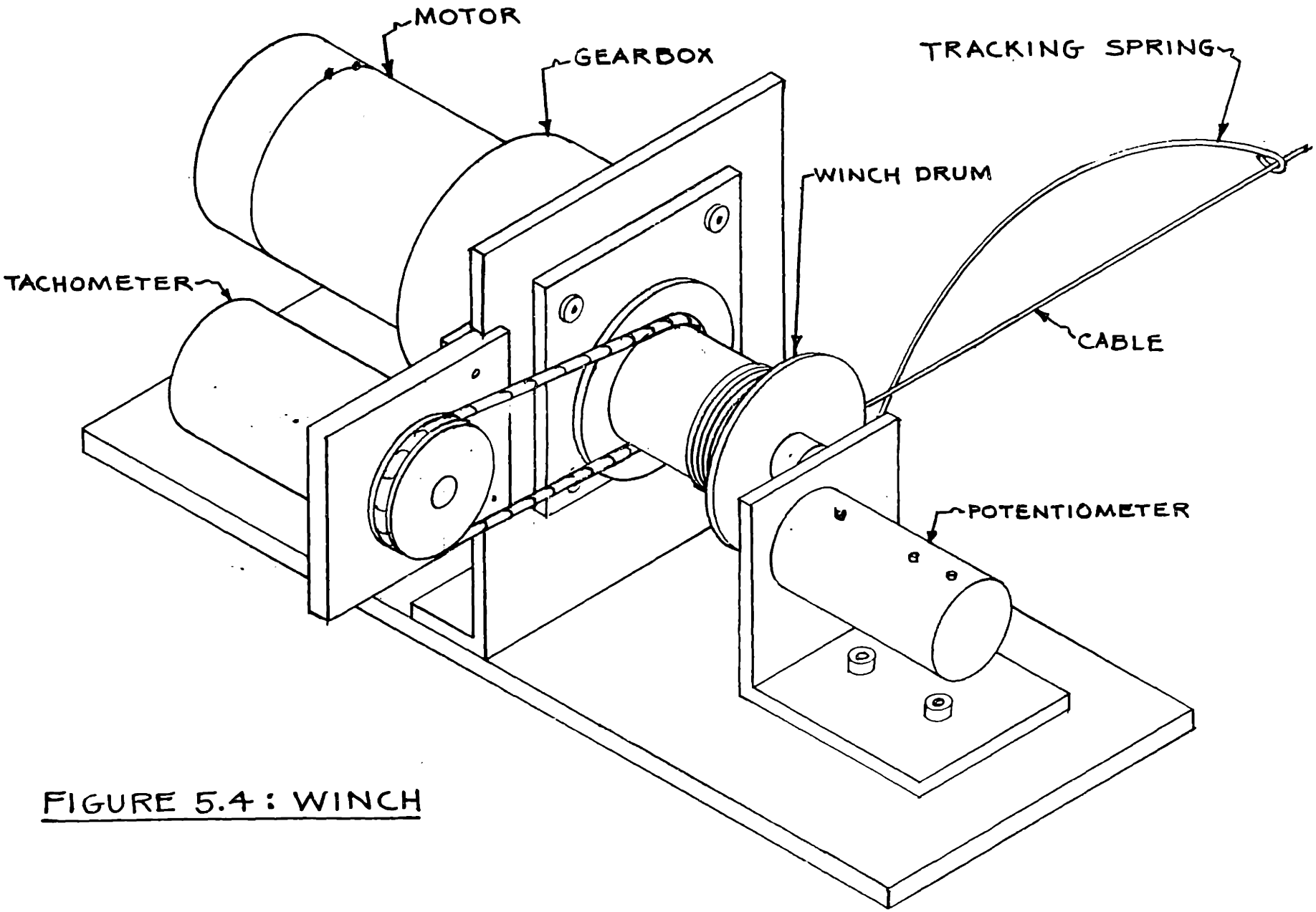

FIGURE 5.4 : WINCH

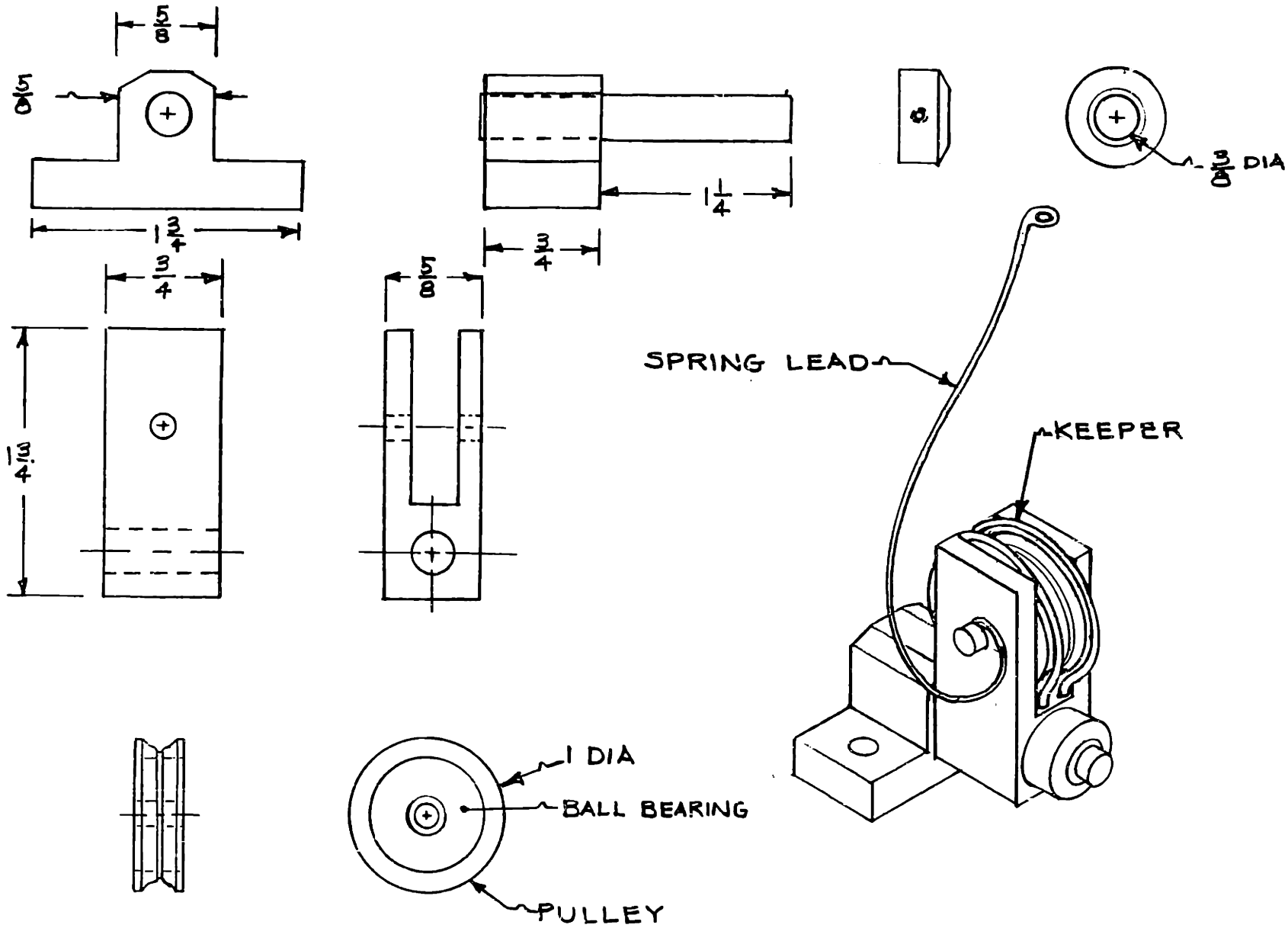

FIGURE 5.5 : FLAG BLOCK

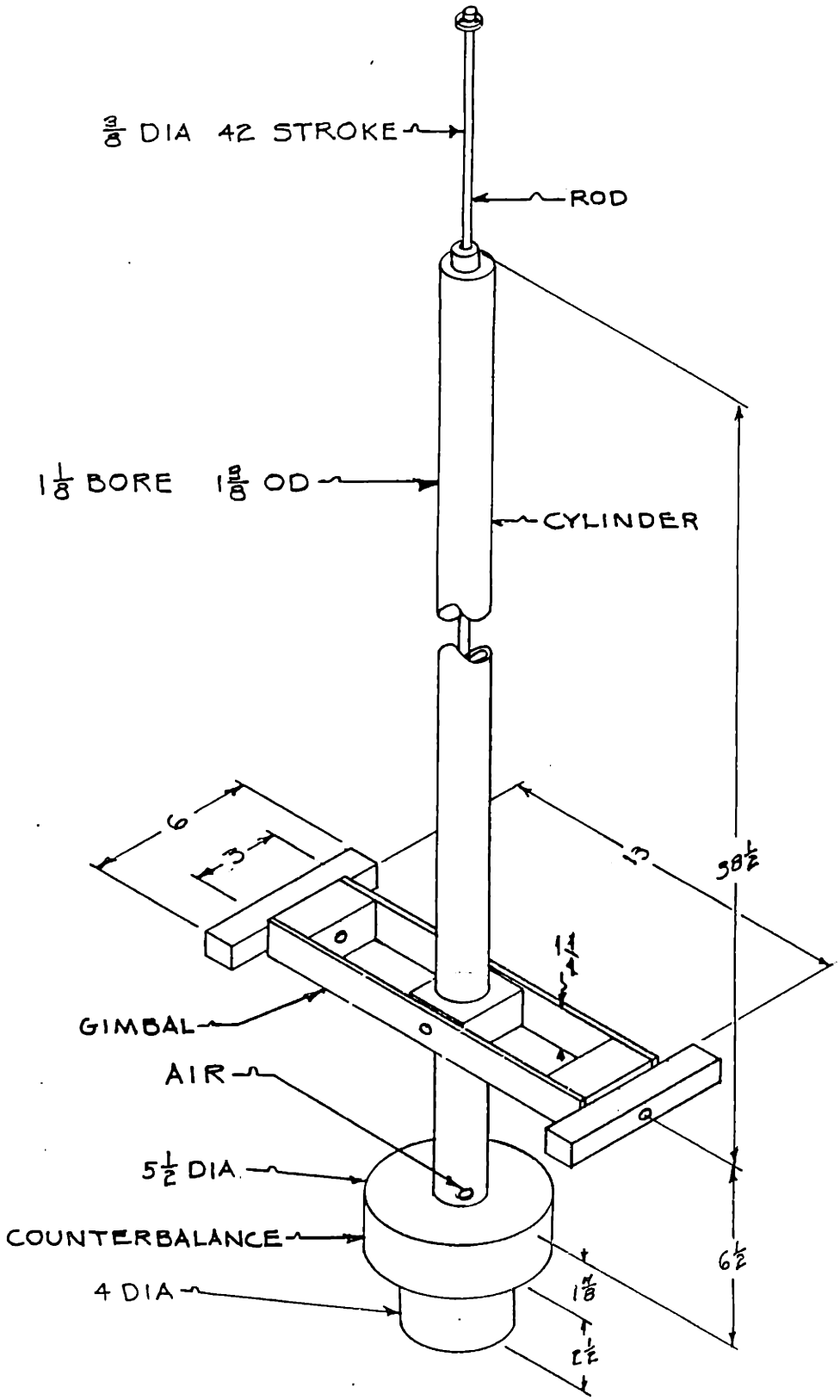

FIGURE 5.6: PNEUMATIC CYLINDER SPINE & COUNTERBALANCE

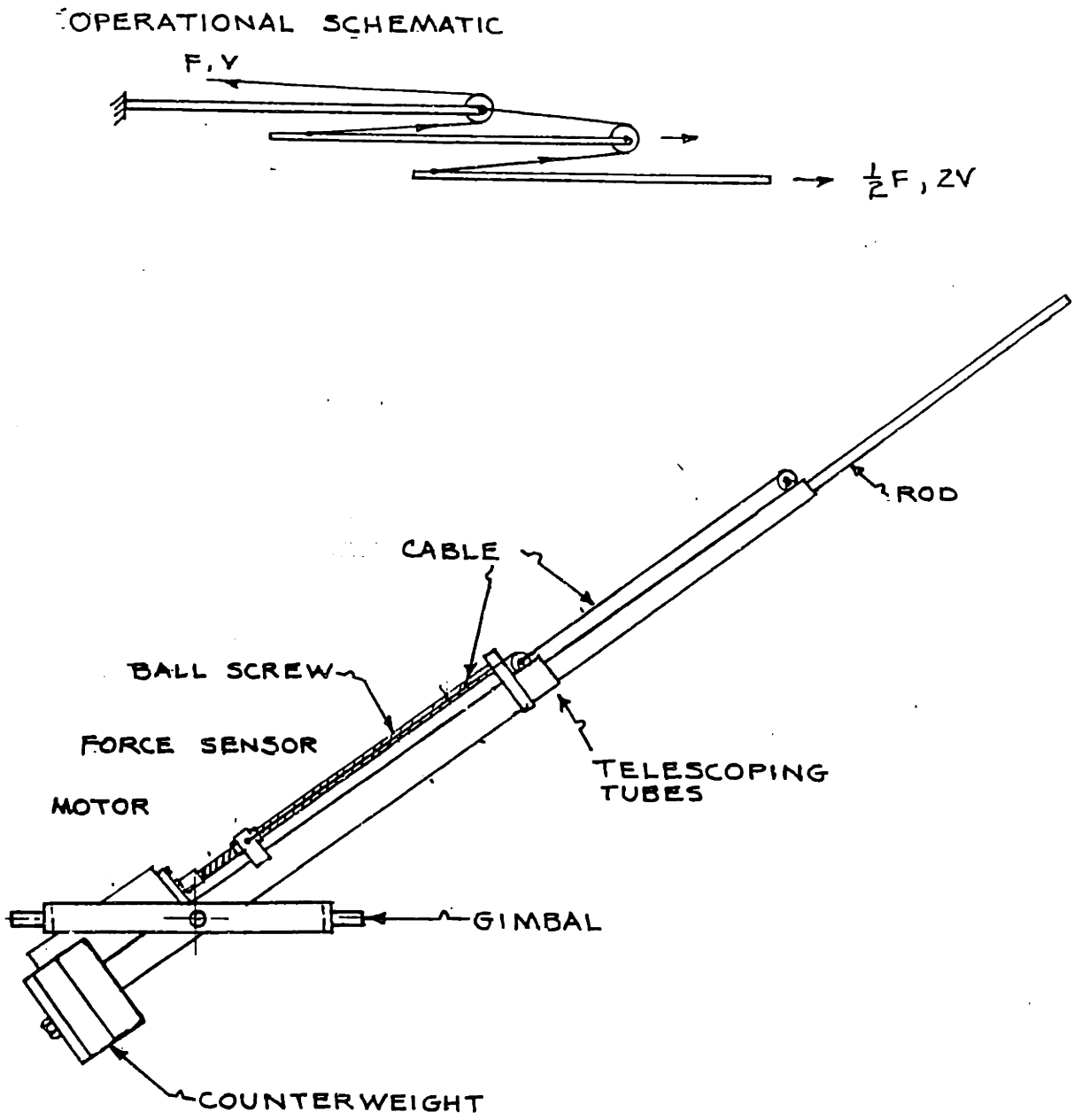

FIGURE 5.7: PROPOSED FULL ACTIVE SPINE

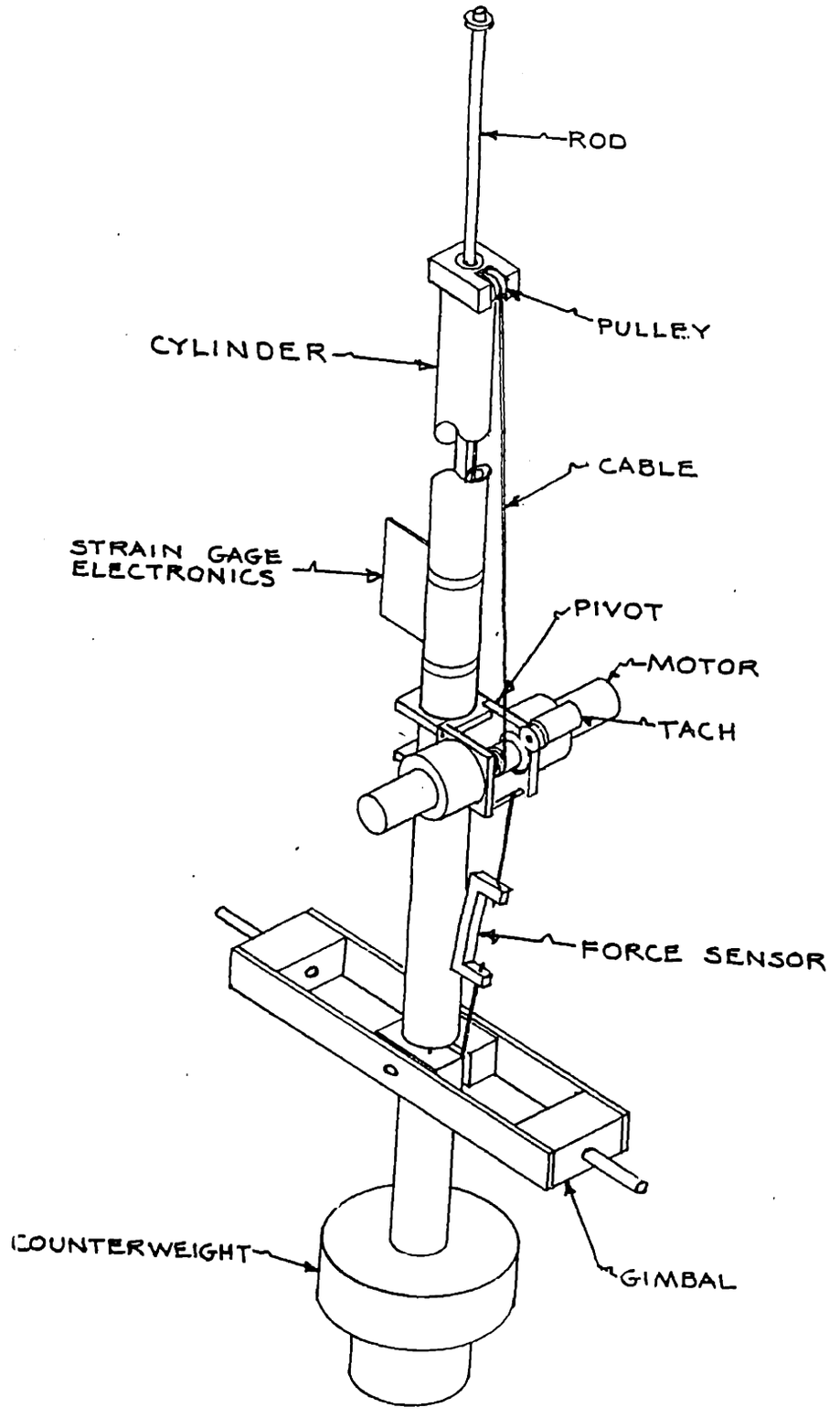

FIGURE 5.8: TEST ROBOT ACTIVE SPINE

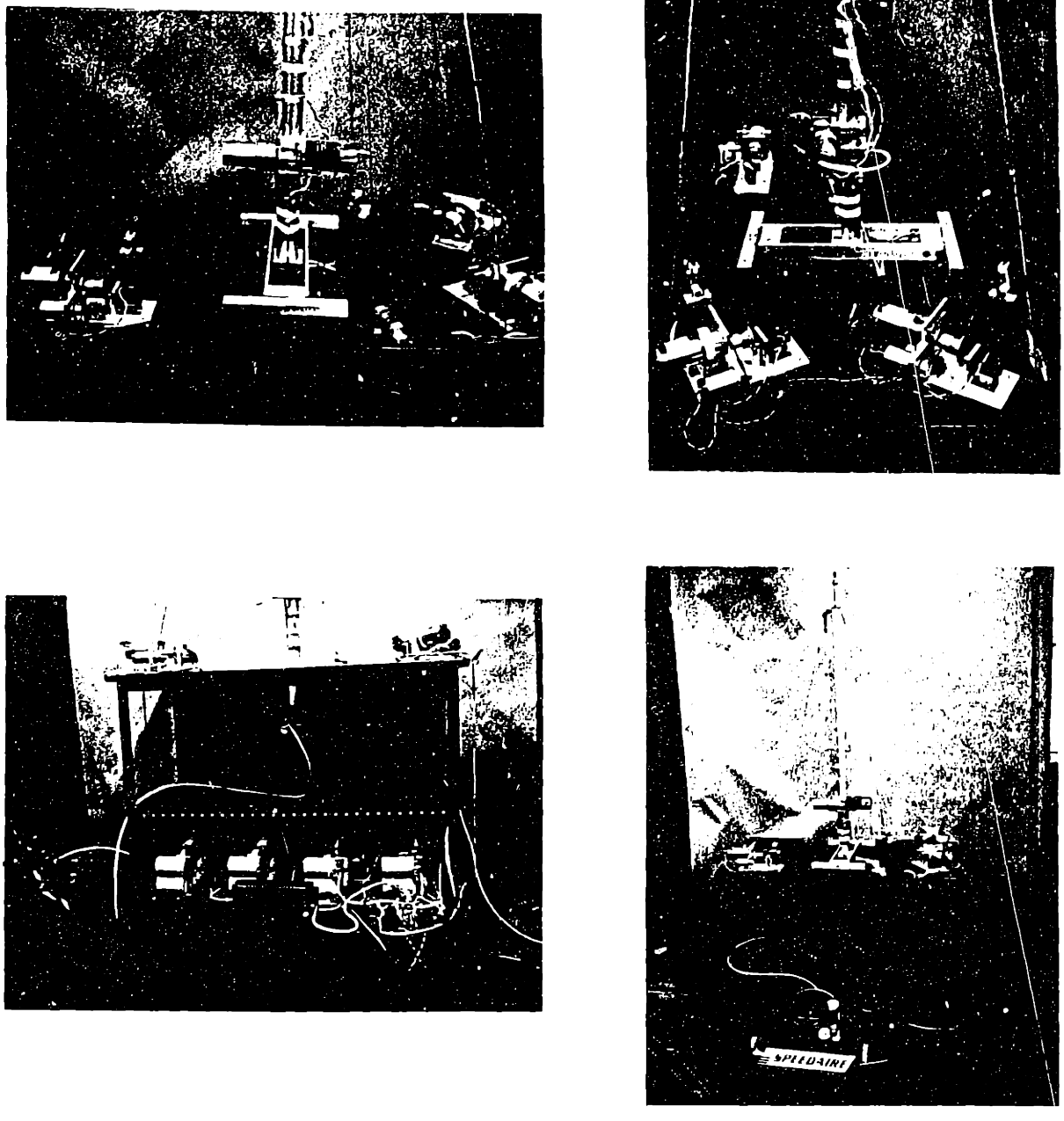

FIGURE 5.9: TABLE LAYOUT

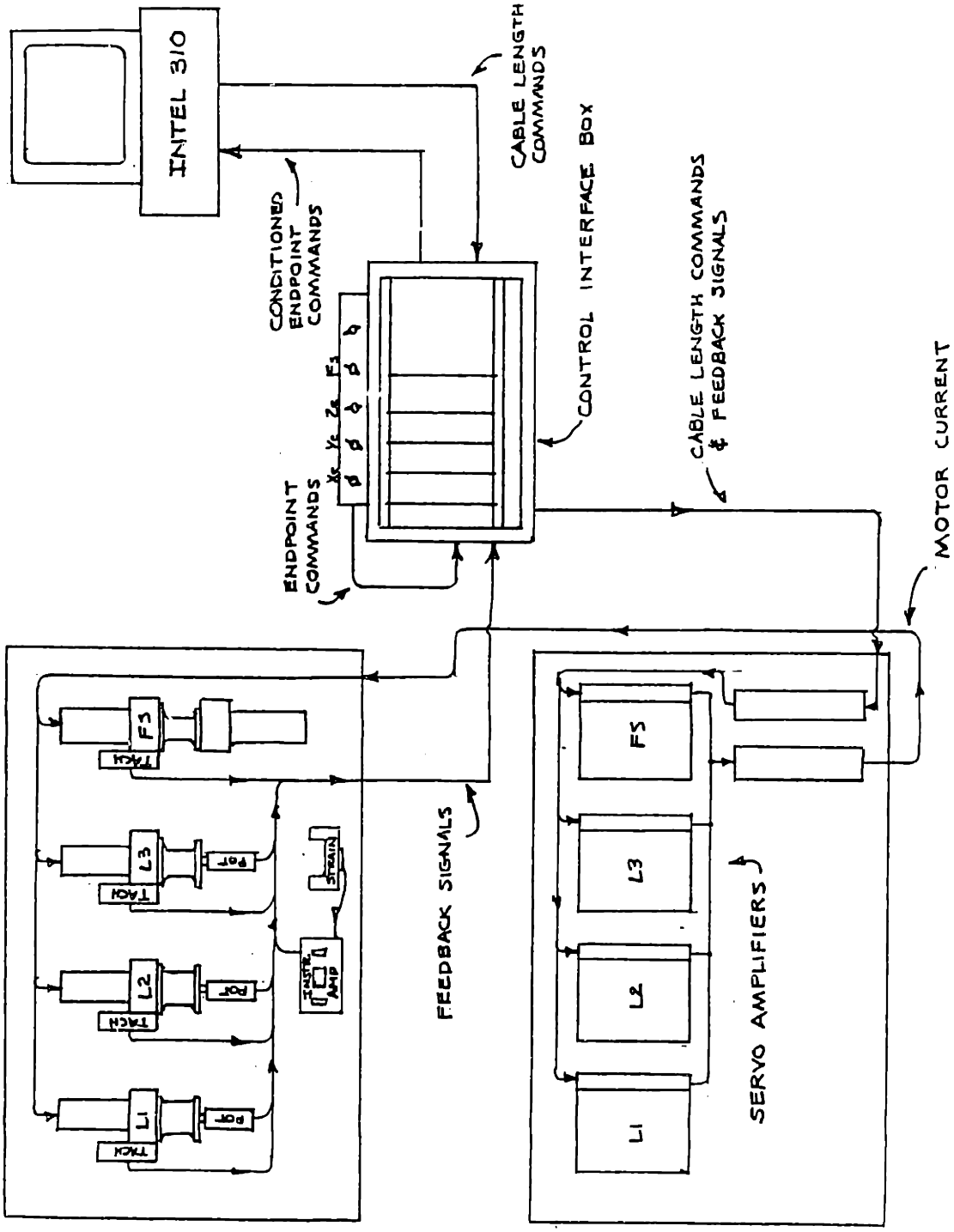

FIGURE 5.10: ELECTRONICS LAYOUT

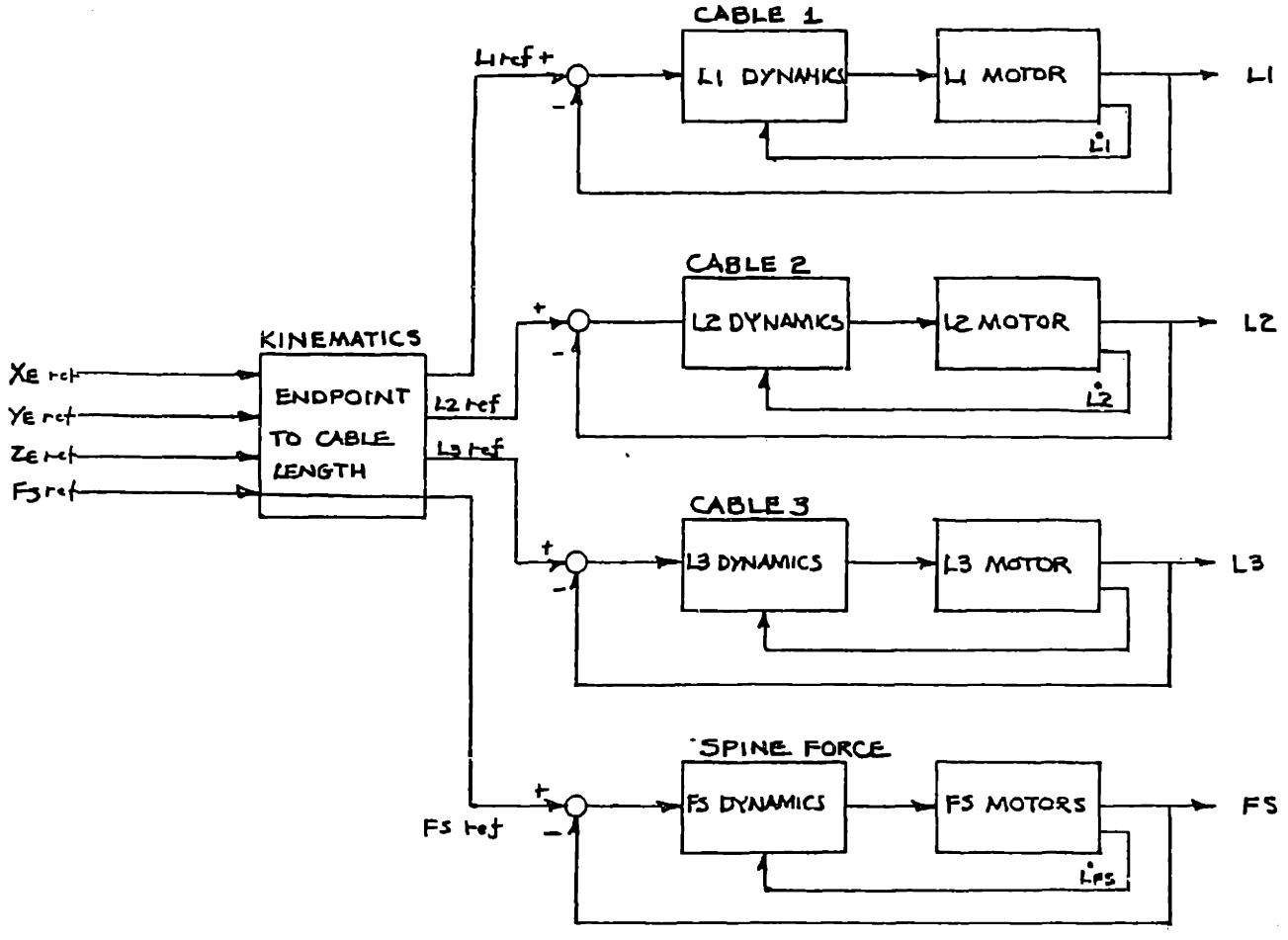

FIGURE 6.1 : CONTROL LAYOUT AND FUNCTIONAL DIAGRAM

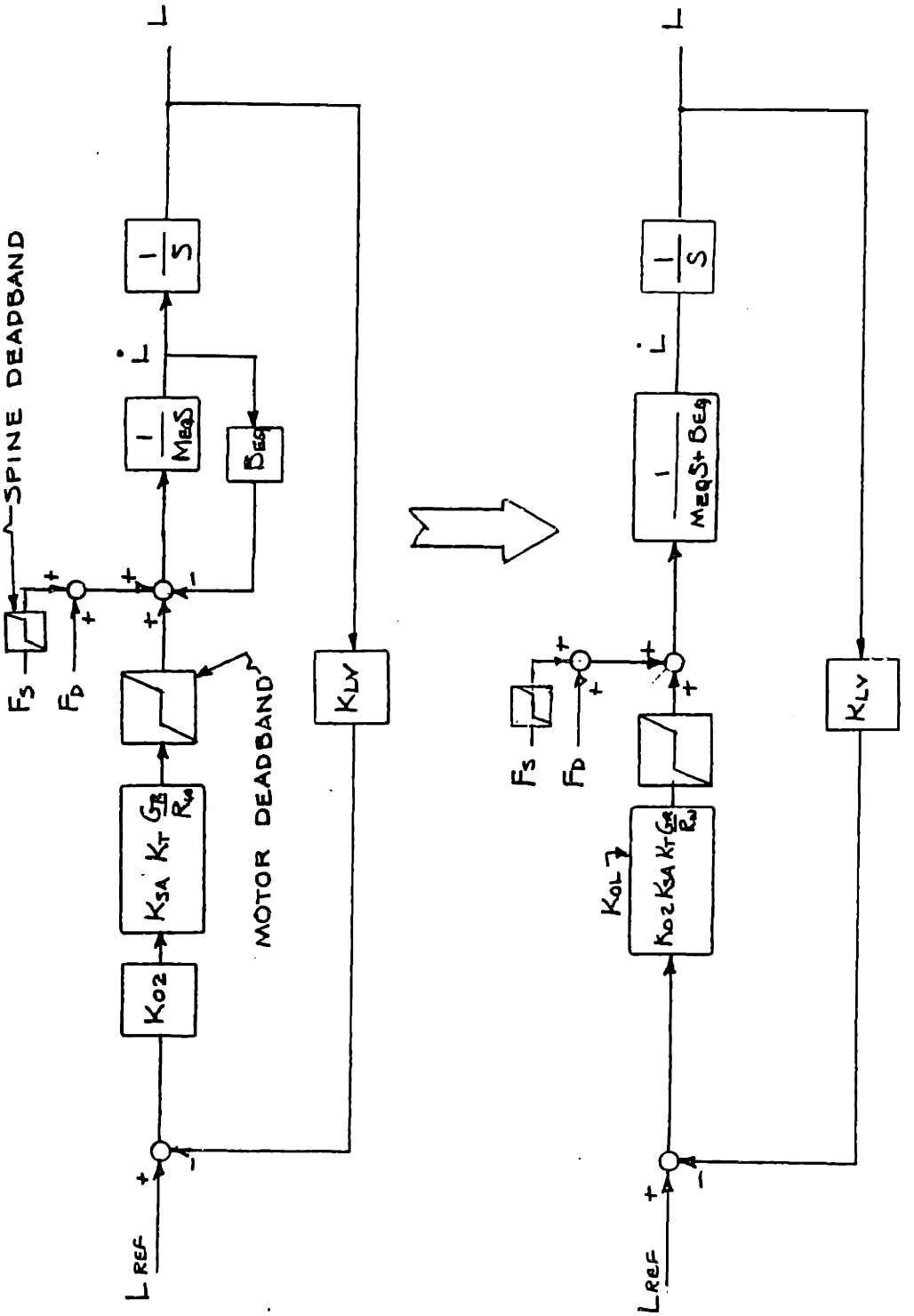

FIGURE 6.2: PROPORTIONAL CONTROL BLOCK DIAGRAM

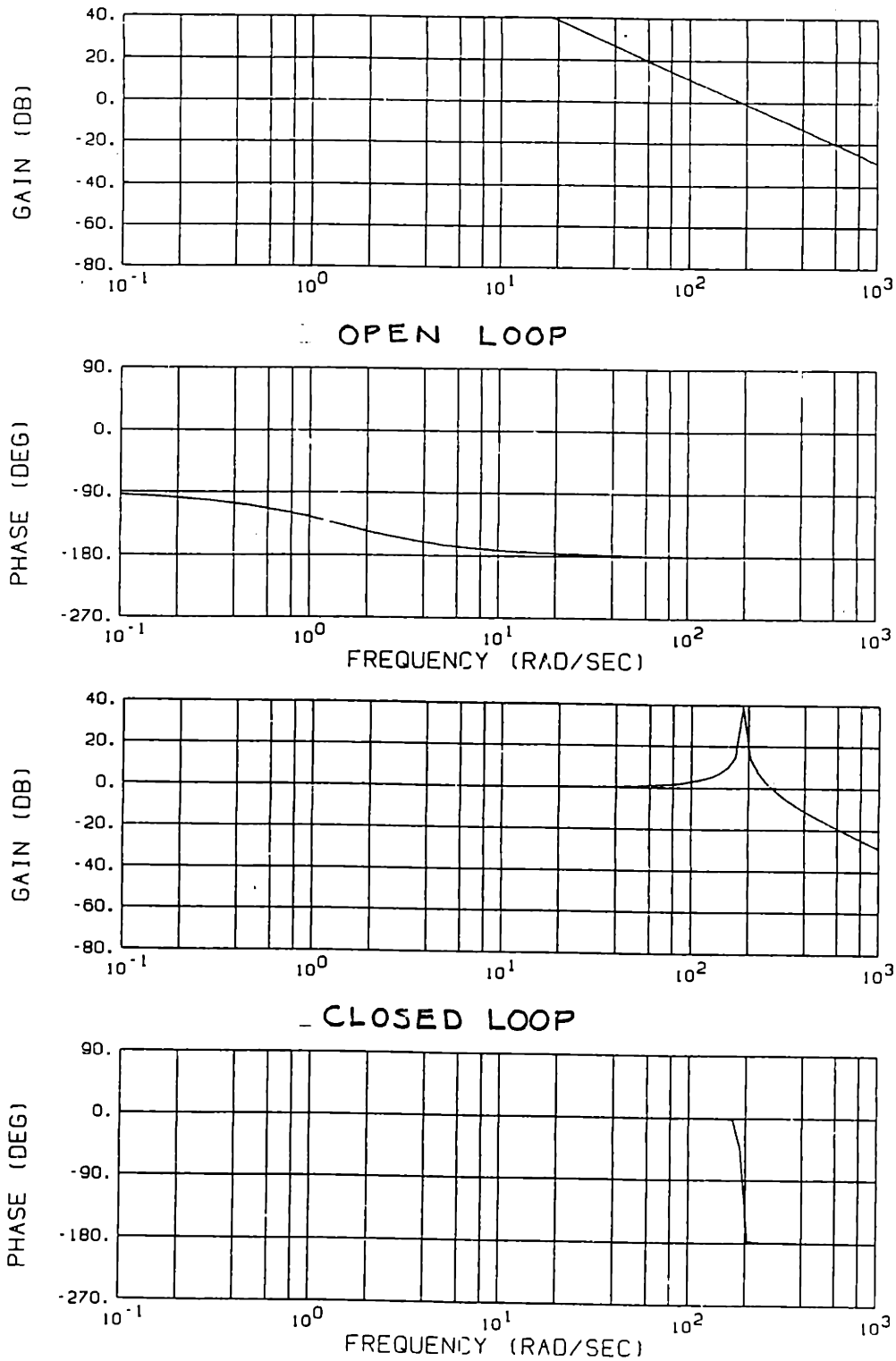

FIGURE 6.3: PROPORTIONAL CONTROL OPEN & CLOSED BODE PLOTS

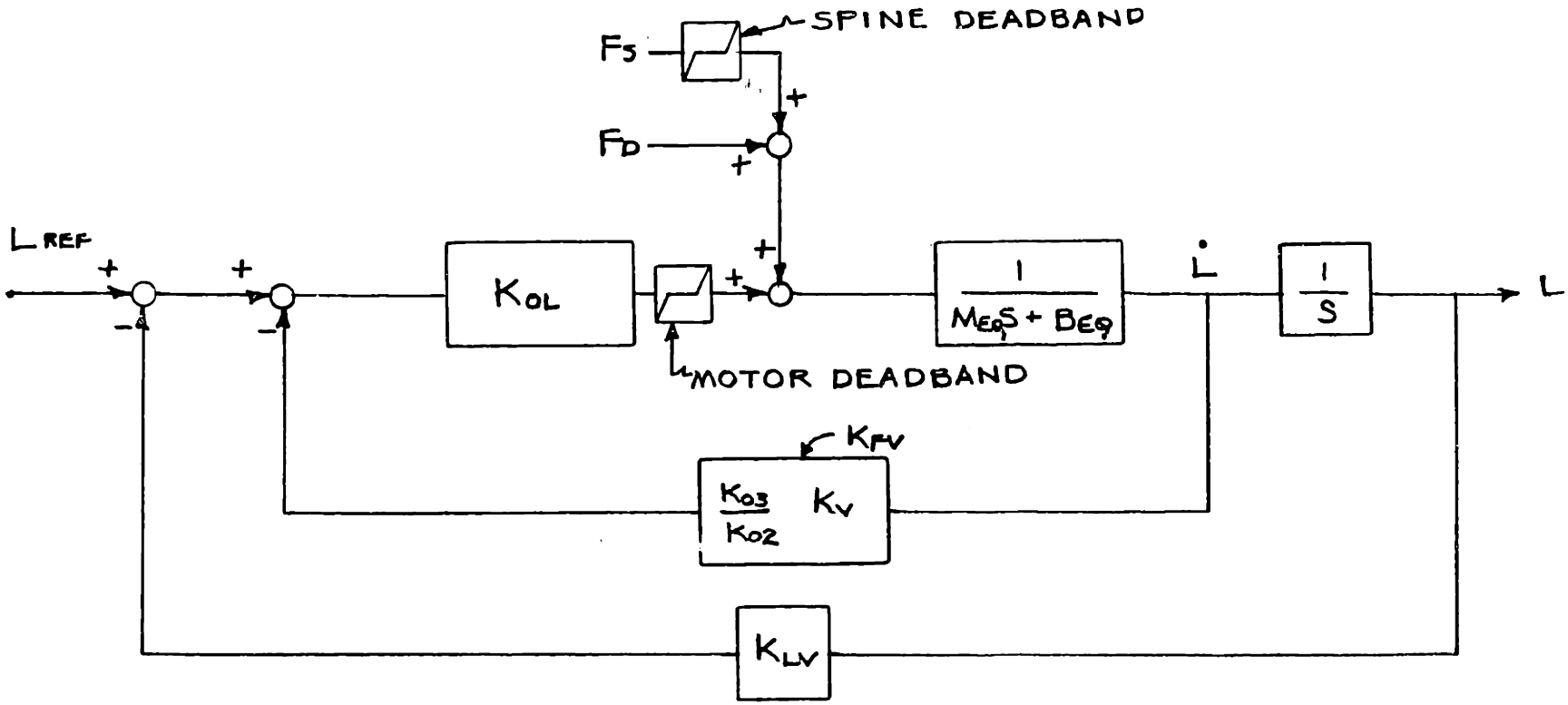

FIGURE 6.4 : PD CONTROL BLOCK DIAGRAM

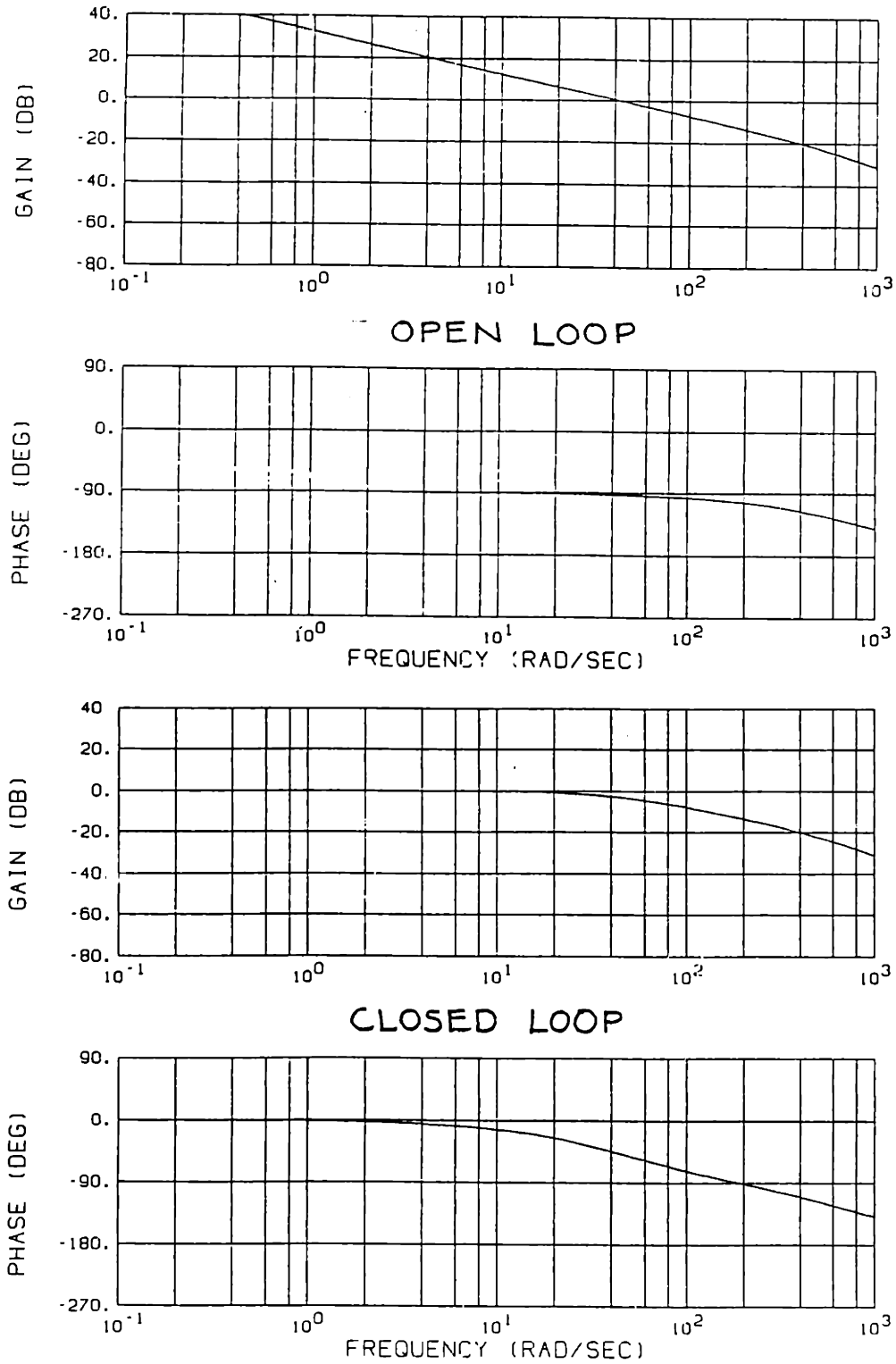

FIGURE 6.5 : PROP & DERIV. CONTROL OPEN & CLOSED BODE PLOTS

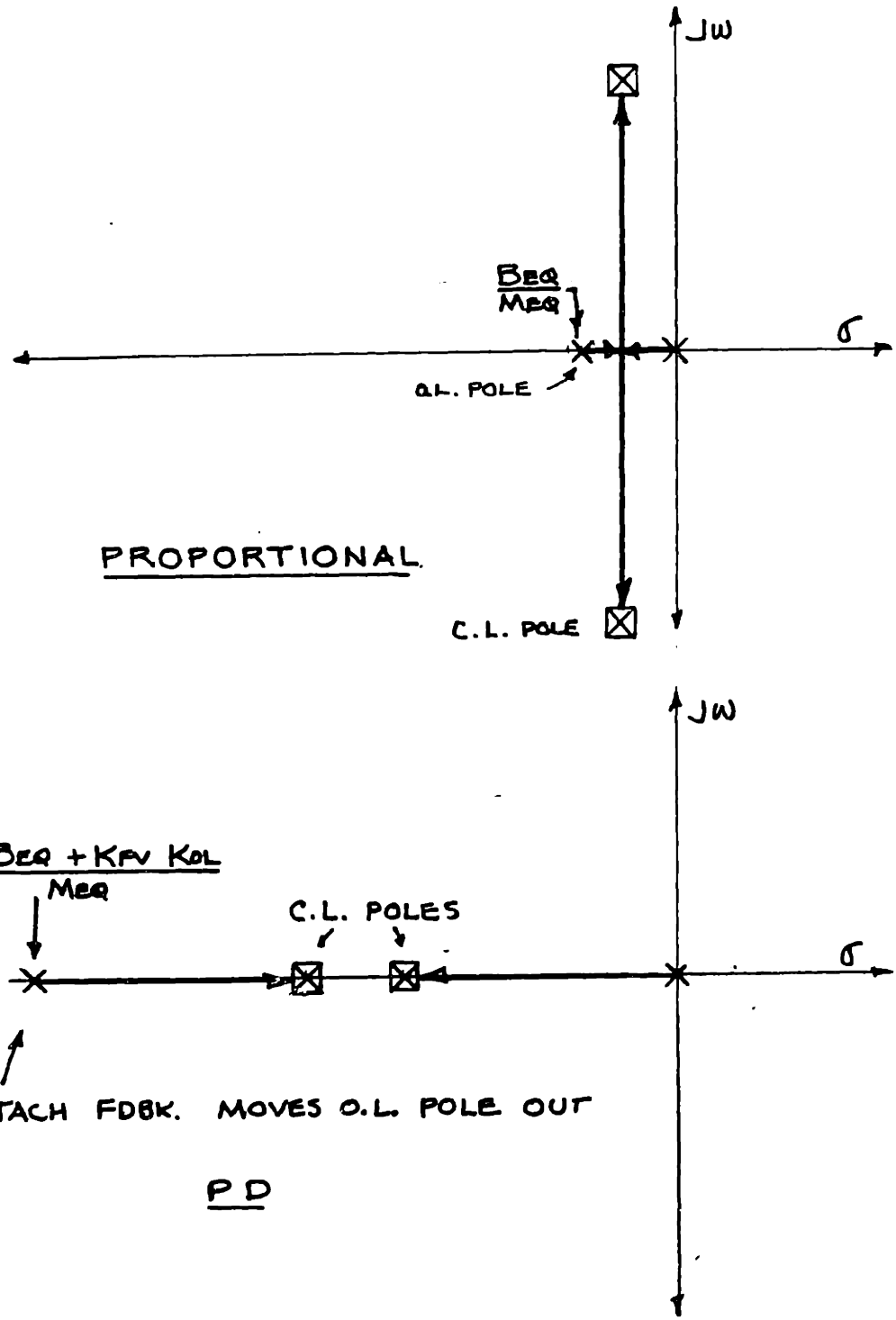

FIGURE 6.6 : ROOT LOCUS

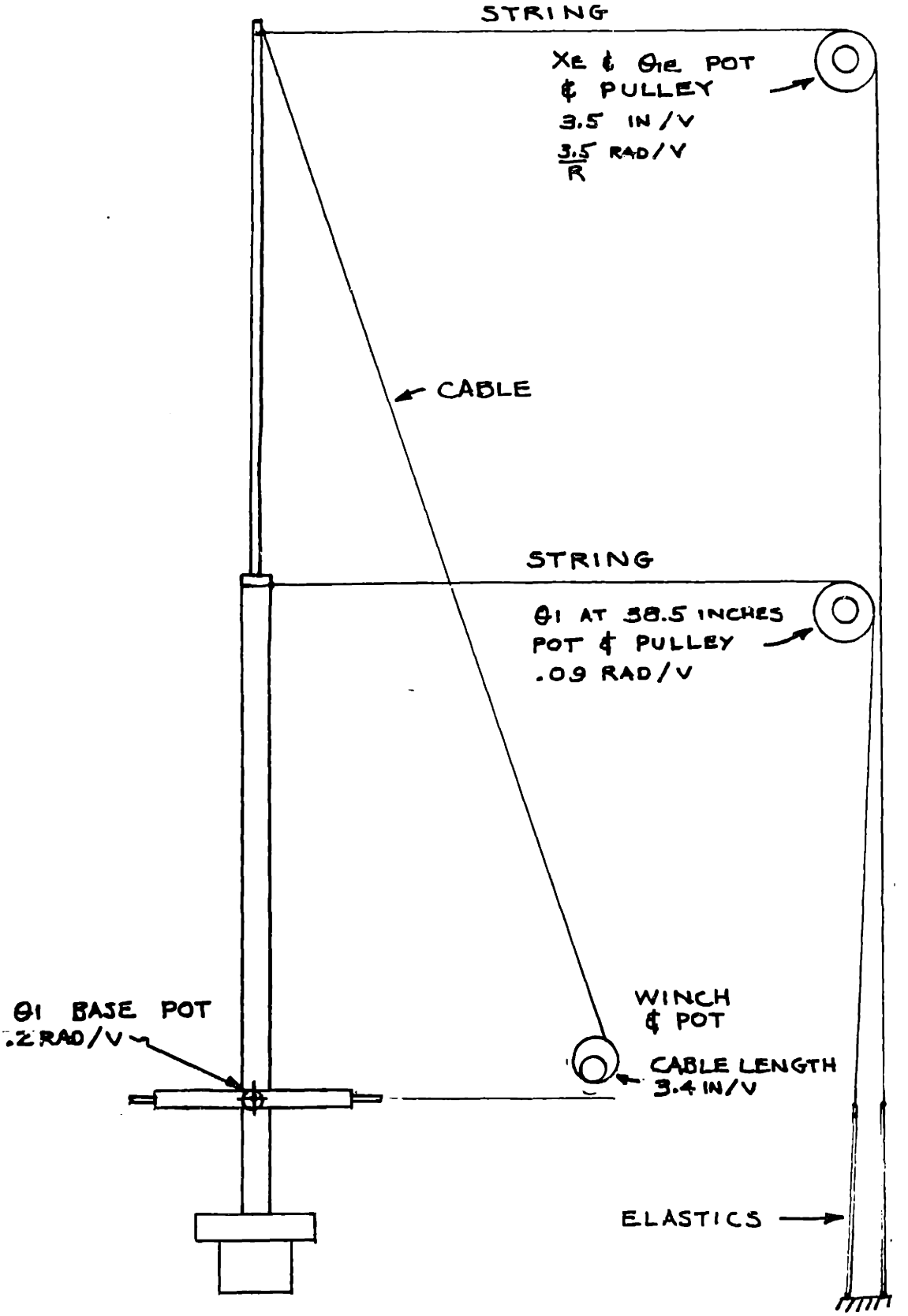

FIGURE 7.1: EXPERIMENTAL SET UP FOR STEP RESPONSE

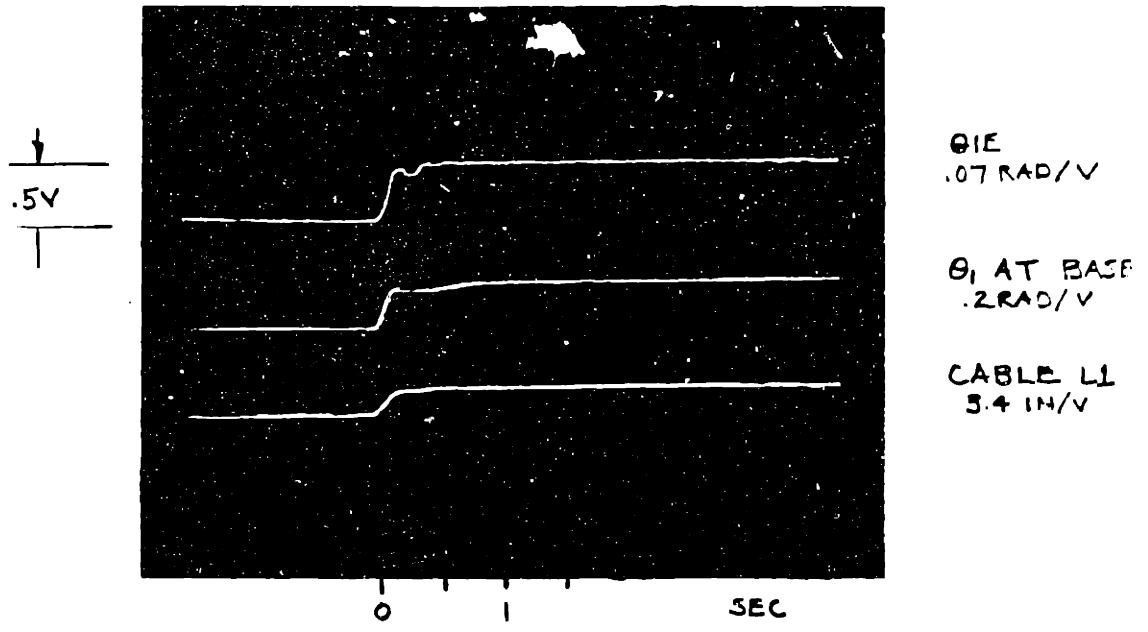

FIG 7.2: STEP RESPONSE R=50 IN., β=0, ML=0 X_E STEP

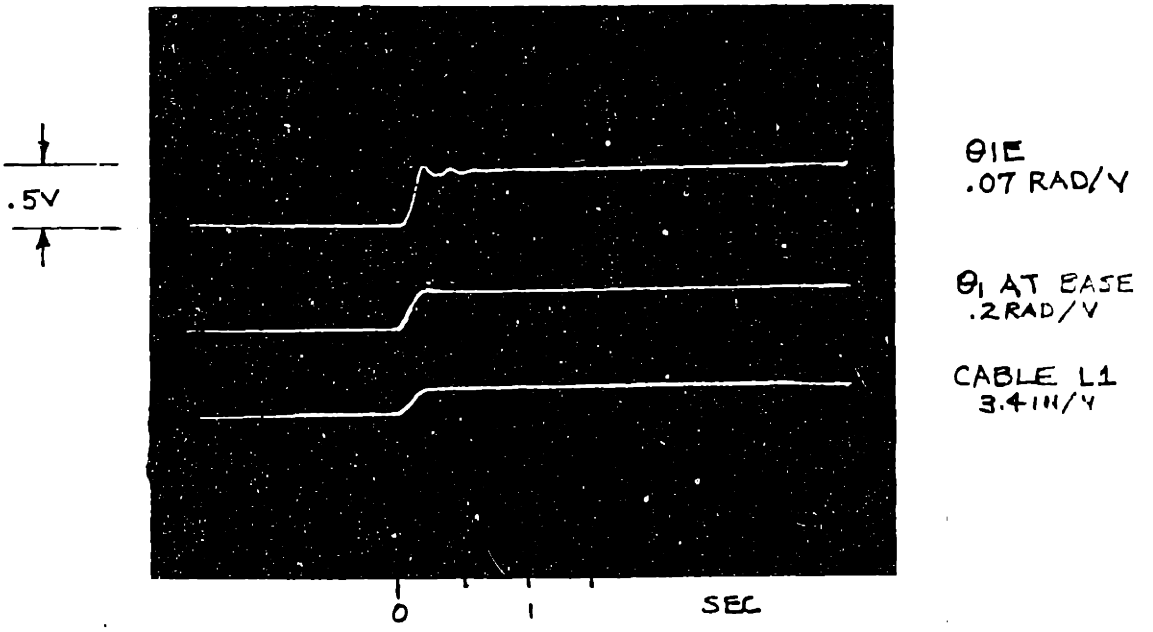

FIG 7.3: STEP RESPONSE, R=50, β=0, ML=2, X_E STEP

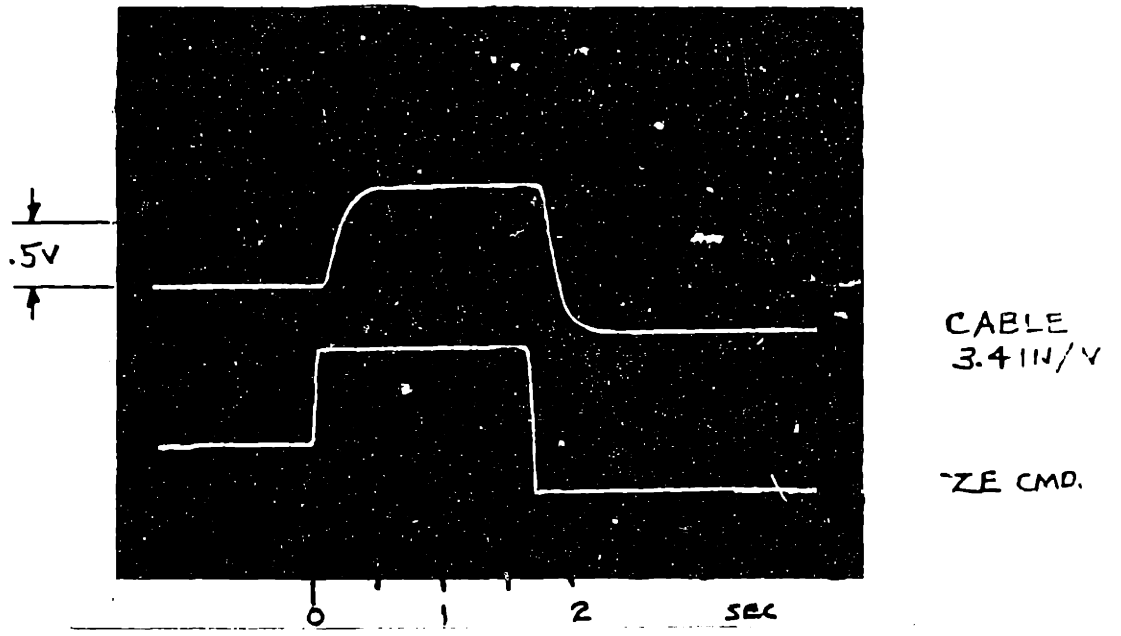

FIG 7.4: Z_E STEP PASSIVE SPINE R=60, B=0

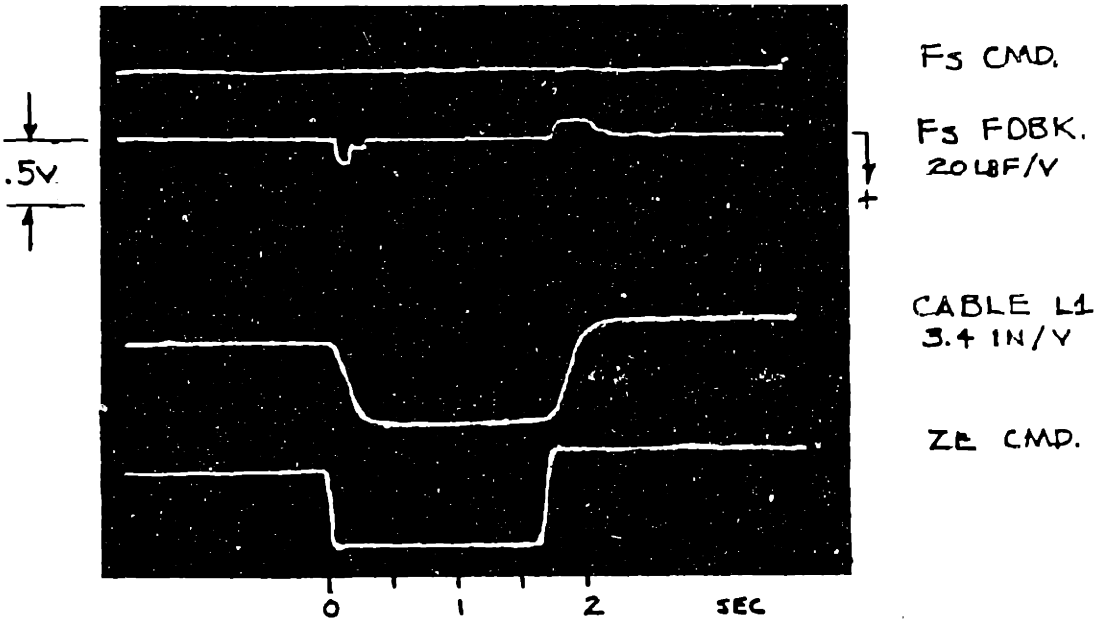

FIG 7.5: Z_E STEP ACTIVE SPINE R=60 B=0

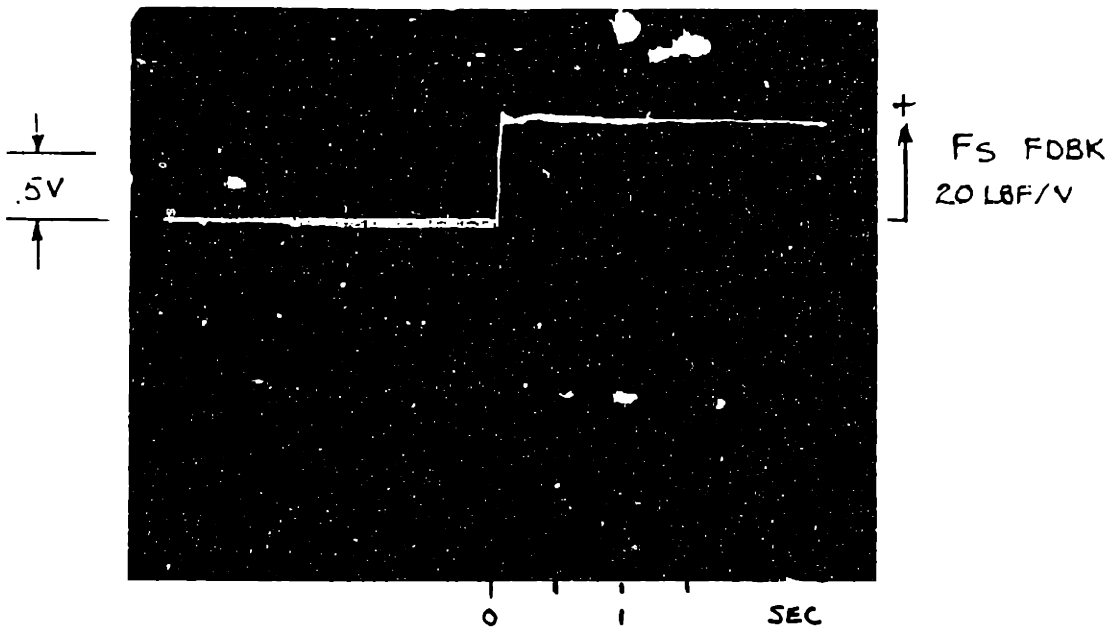

FIG 7.6: STEP IN ACTIVE SPINE FORCE

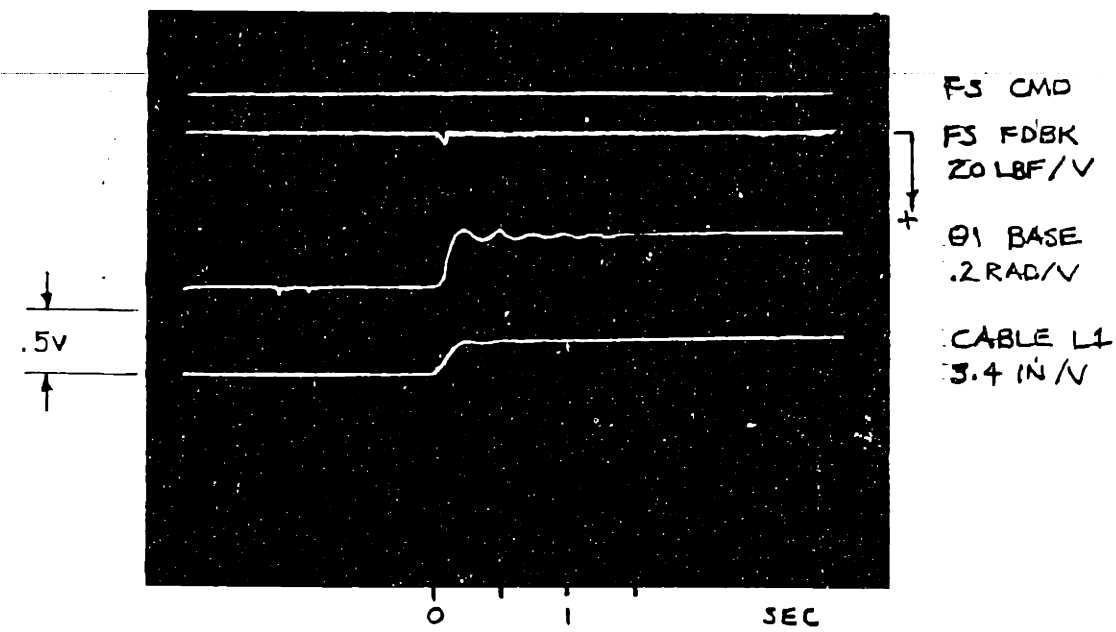

FIG 7.7: XE STEP ACTIVE SPINE R=60 β=0

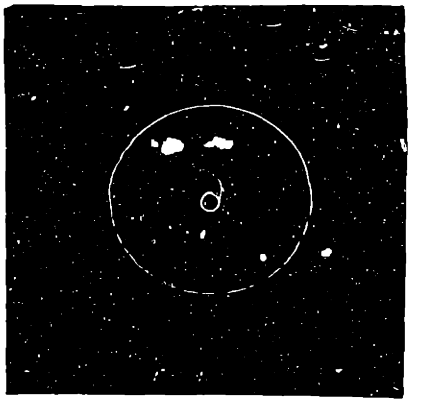

FLAT SPIRAL 27 IN. O. D.

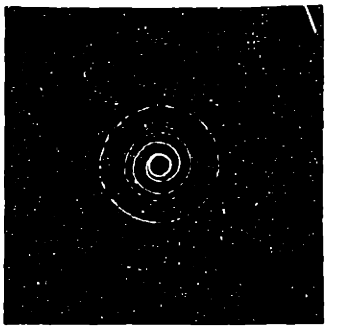

FLAT SPIRAL 16 IN. OD

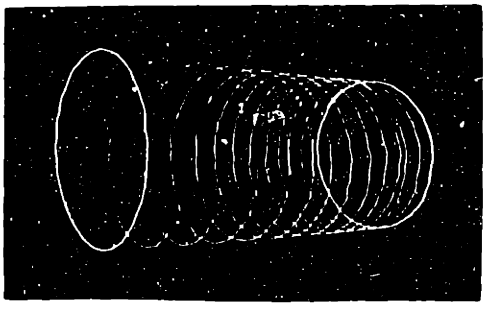

LONGITUDAL SPIRAL 27 IN DIA × 50 IN. LONG

FIGURE 7.8: CIRCULAR AND SPIRAL TRAJECTORIES

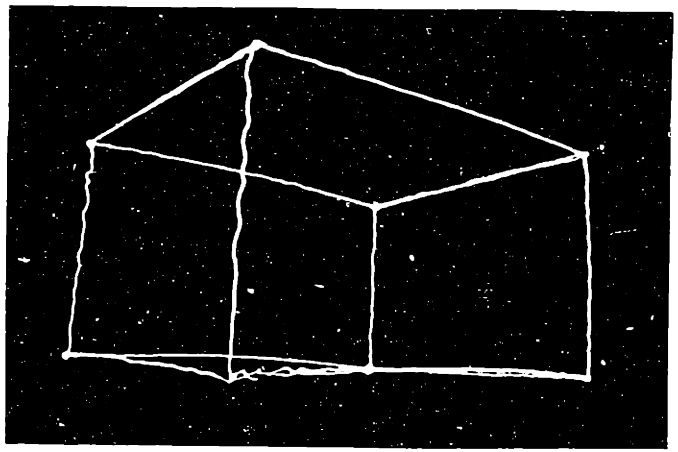

UNLOADED SLOW .8 FT/S

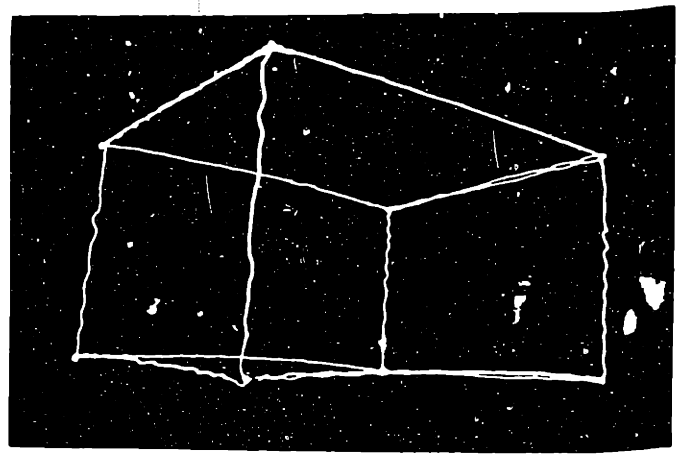

LOADED ML=1LBM SLOW .8FT/S

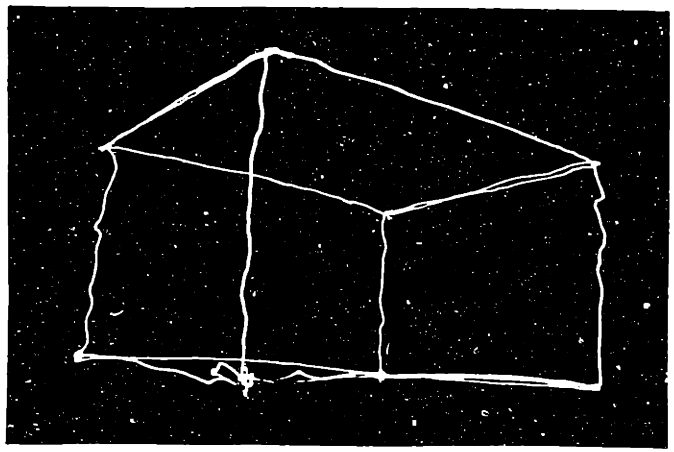

UNLOADED FAST 2FT/SEC

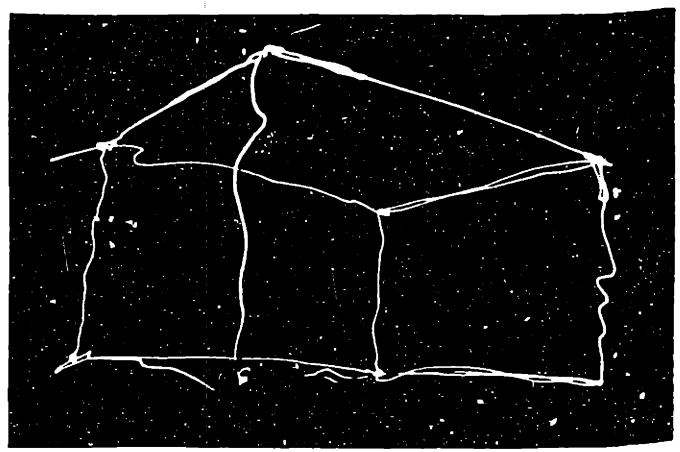

LOADED ML=1LBM FAST 2FT/S

FIGURE 7.9 XYZ BOX TRAJECTORIES

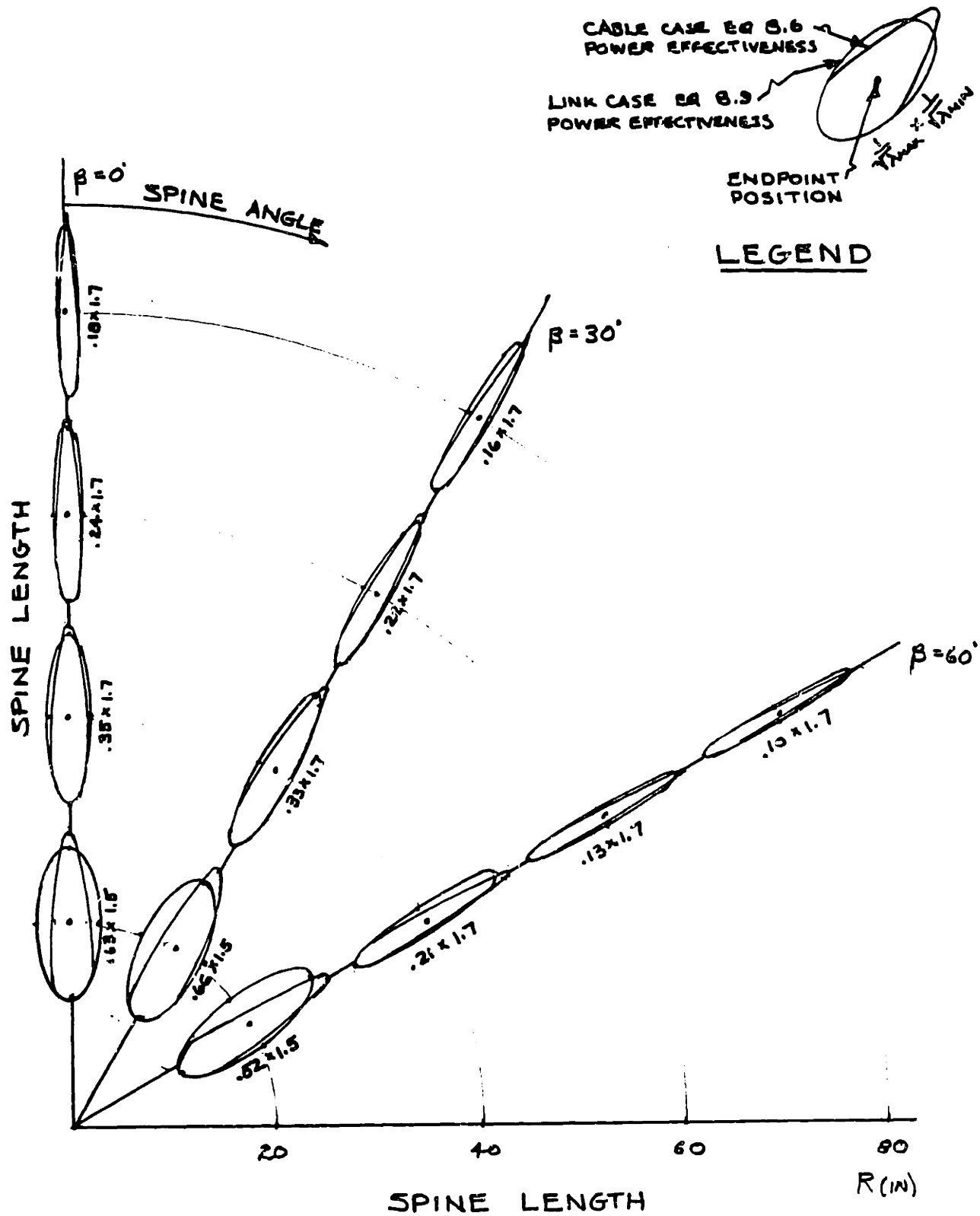

FIGURE 8.1: POWER ELLIPSOIDS

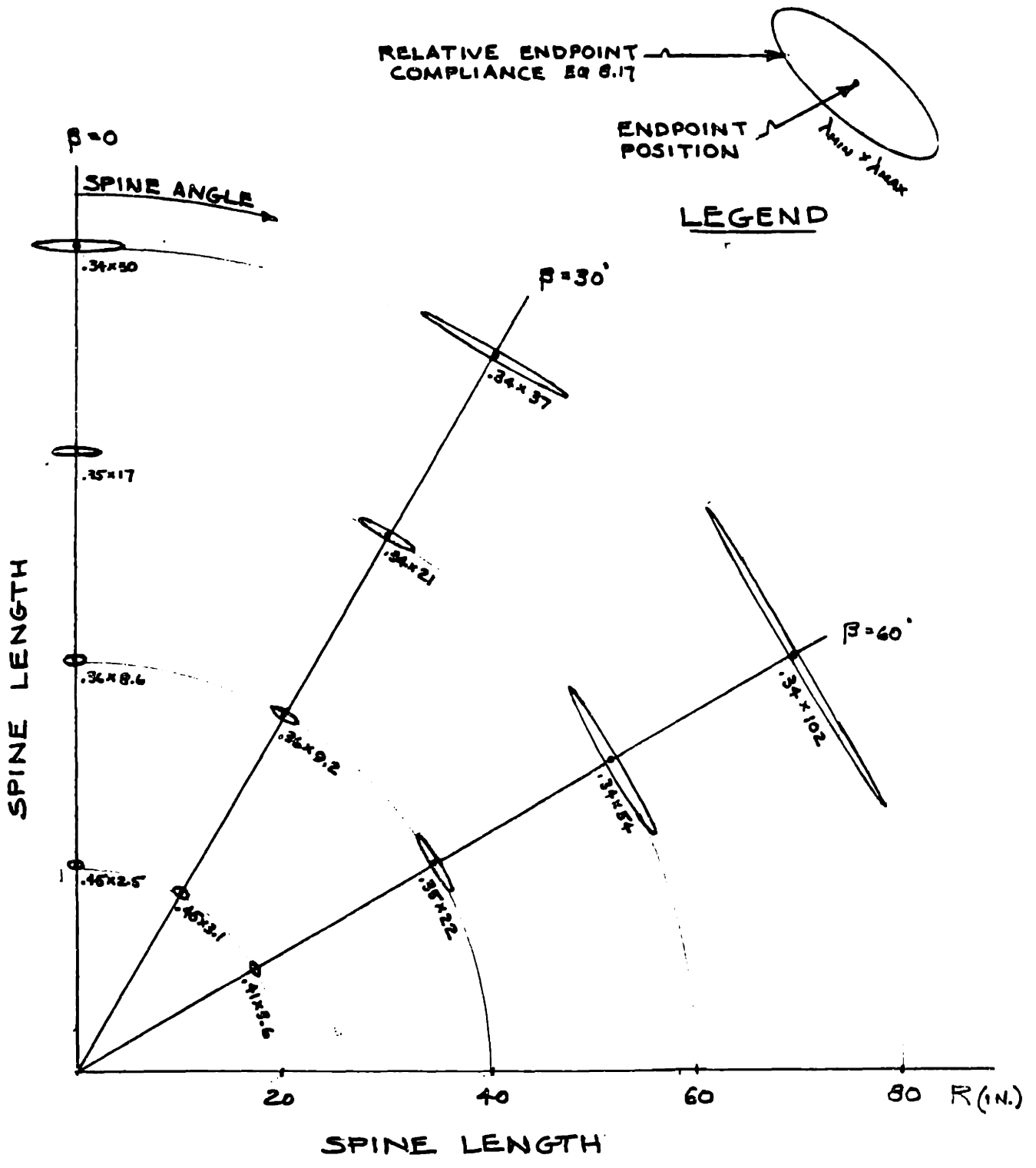

FIGURE 8.2: COMPLIANCE ELLIPSOIDS

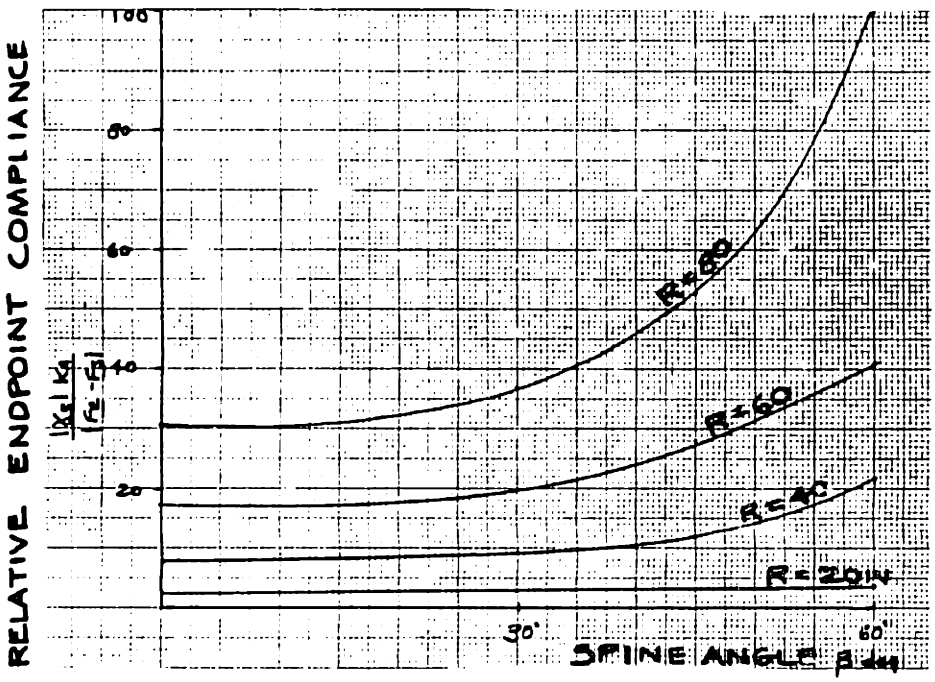

FIG. 8.3 : TANGENTIAL COMPLIANCE OVER WORSPACE

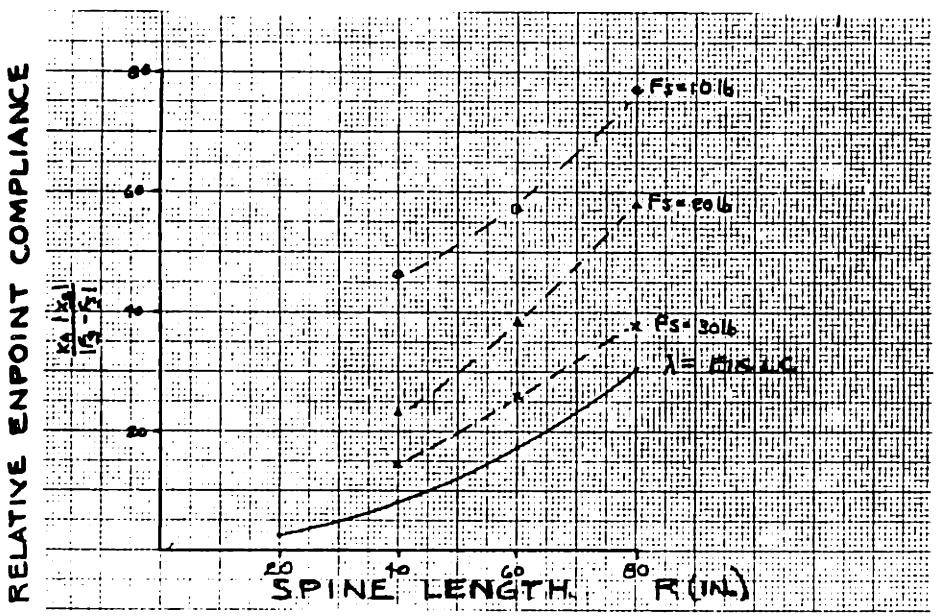

FIG. 8.4: MEASURED ENDPOINT COMPLIANCE

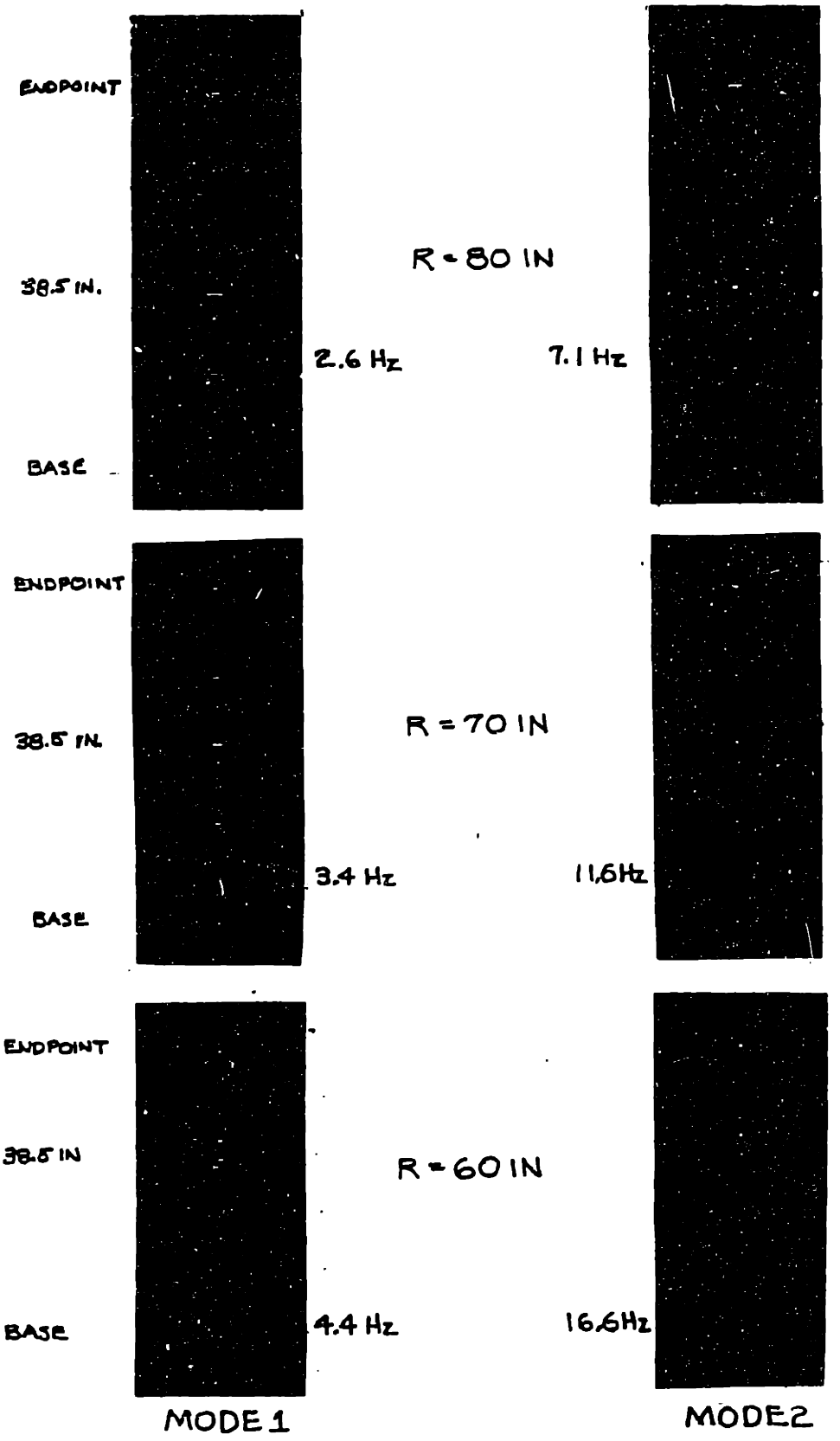

*TIME EXPOSURE OF SMALL LIGHTS ALONG SPINE WITH SINUSOIDAL EXCITATION

FIGURE 9.1: EXPERIMENAL VIBRATORY MODES

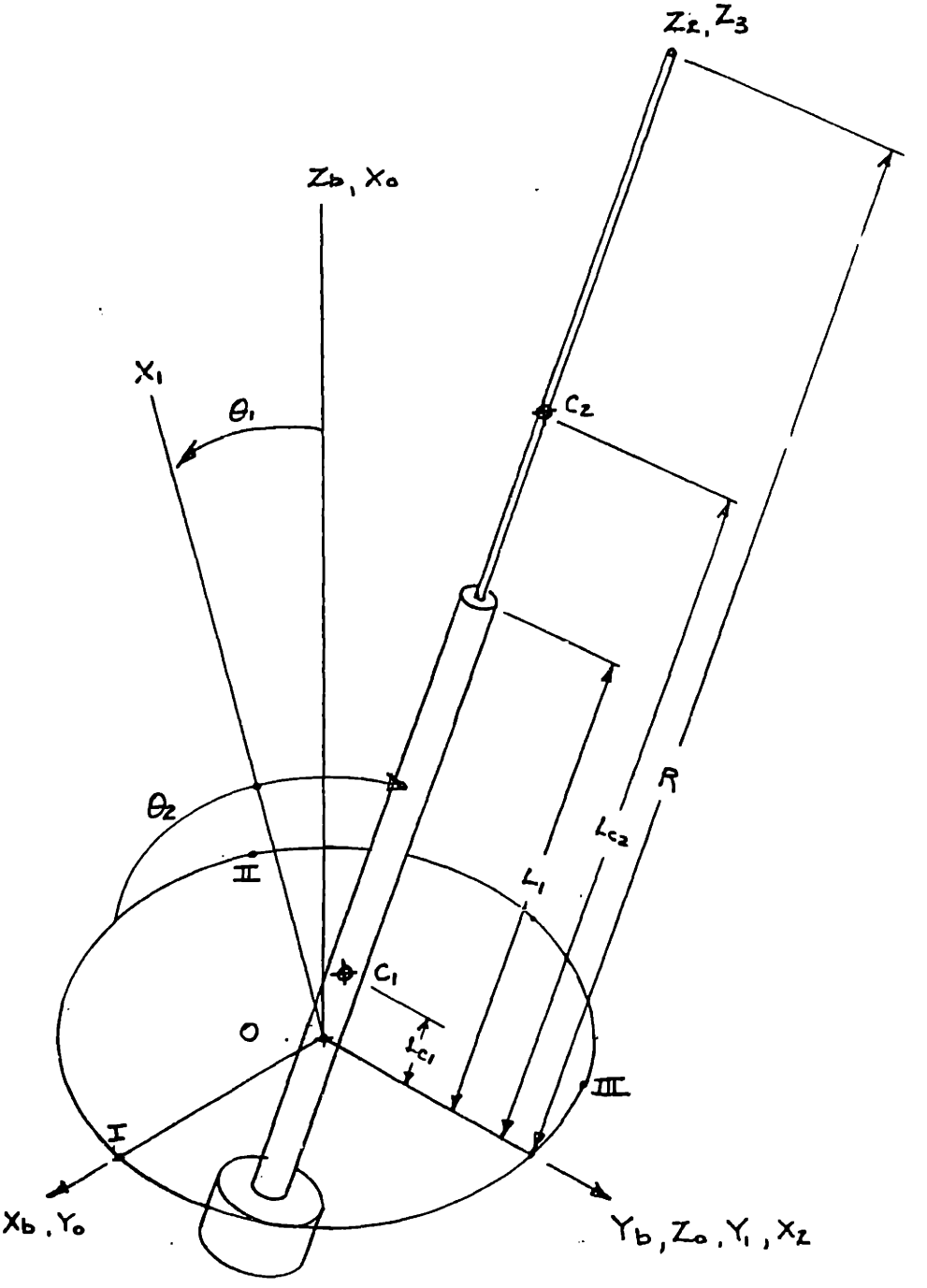

FIGURE 9.2: RIGID SPINE FOR DYNAMICS

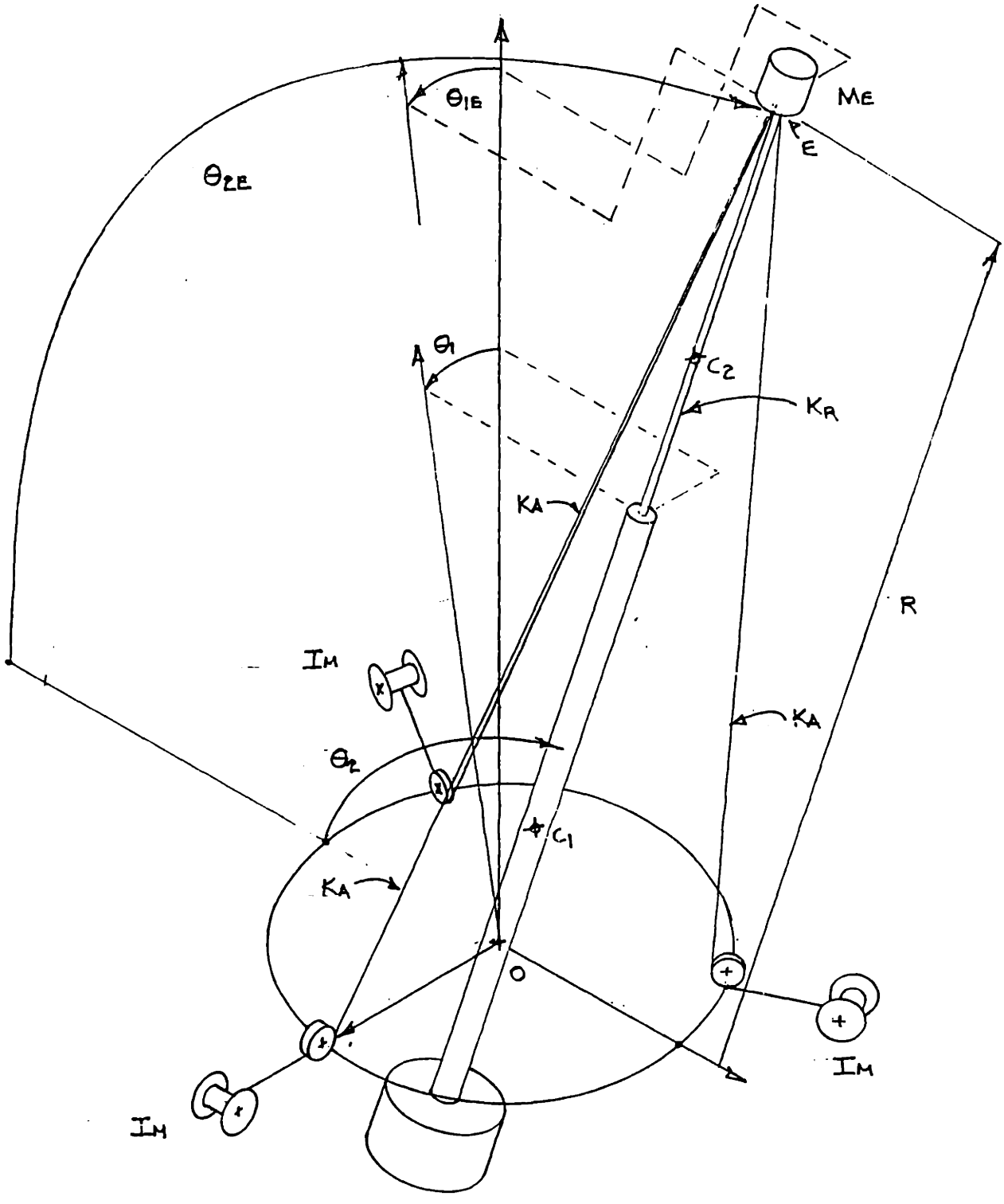

FIGURE 9.3: FLEXIBLE DYNAMIC MODEL

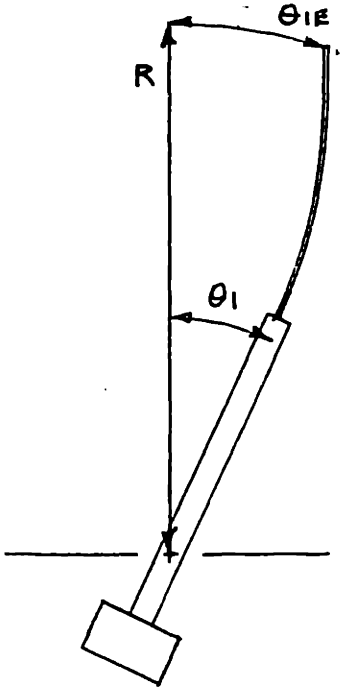

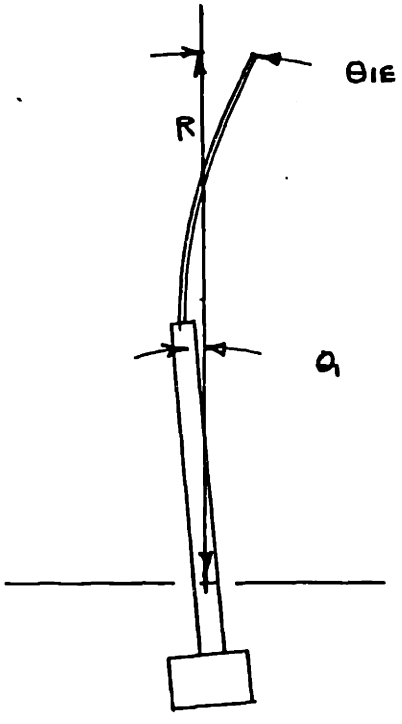

R	f(hz)	$\dot{\theta}_{1E}$	$\dot{\theta}_1$	θ_{1E}	θ_1
80	2.4	.25	1	-.002±.017j	-.008±.066
70	2.7	.27	1	-.002±.016j	-.008±.060
60	3.1	.31	1	-.003±.018j	-.008±.05

INCH

MODE 1

f(hz)	$\dot{\theta}_{1E}$	$\dot{\theta}_1$	θ_{1E}	θ_1
7.3	1	-.14	-.008±.02	.001±.003j
9.5	1	-.08	-.008±.01	.0007±.001j
9.9	1	-.05	-.008±.005	.0004±.0008j

MODE 2

FIGURE 9.4 : PARALLEL ANALYTIC VIBRATORY MODES

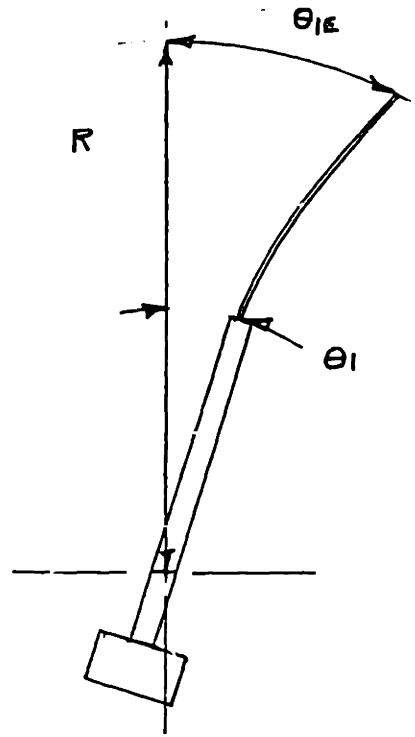

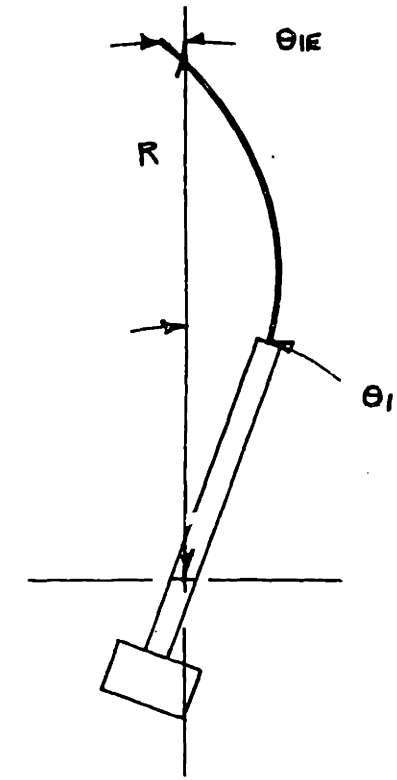

R	f(hz)	$\dot{\theta}_{1E}$	$\dot{\theta}_1$	θ_{1E}	θ_1
80	3.1	1	.27	-.008±.05j	-.002±.013j
70	4.4	1	.34	-.008±.03j	-.003±.012j
60	6.2	1	.59	-.008±.02j	-.004±.01j

INCH

MODE 1

f(hz)	$\dot{\theta}_{1E}$	$\dot{\theta}_1$	θ_{1E}	θ_1
7.7	-.23	1	.002±.004j	-.008±.017j
8.5	-.53	1	.004±.008j	-.008±.015j
9.9	1	-.61	-.007±.01j	.004±.006j

MODE 2

FIGURE 9.5 : SERIAL ANALYTIC VIBRATORY MODES

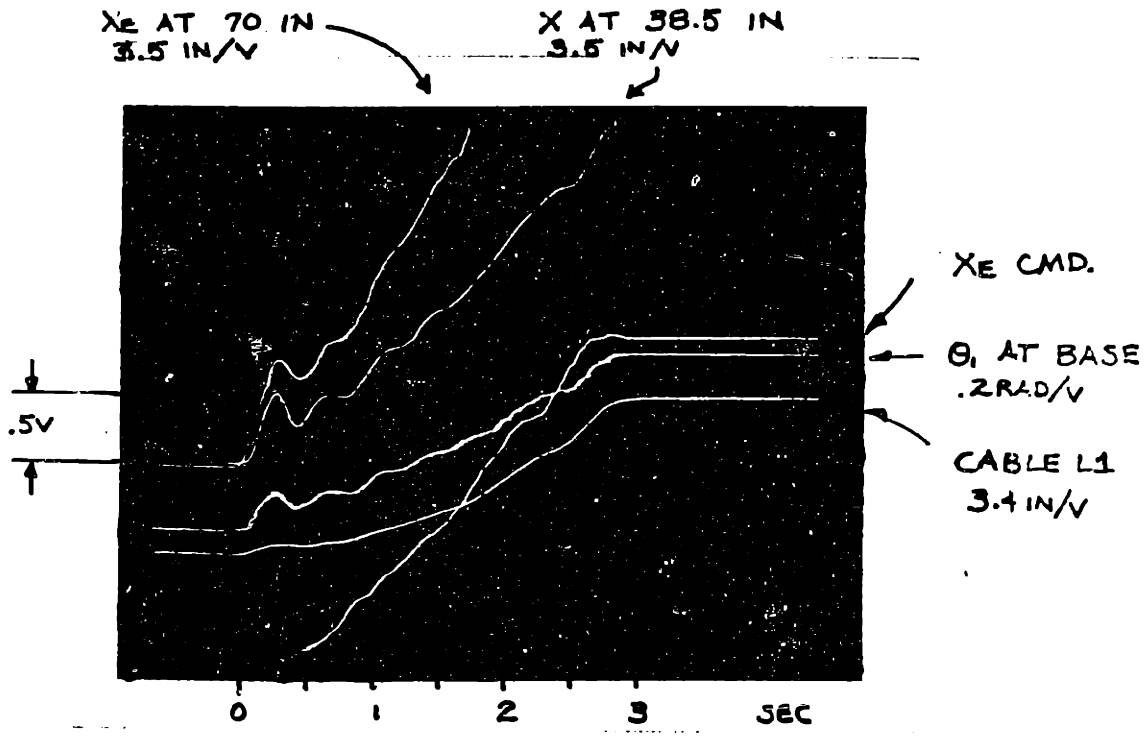

FIG 10.1: X_E RAMP RESPONSE R=70 β=0

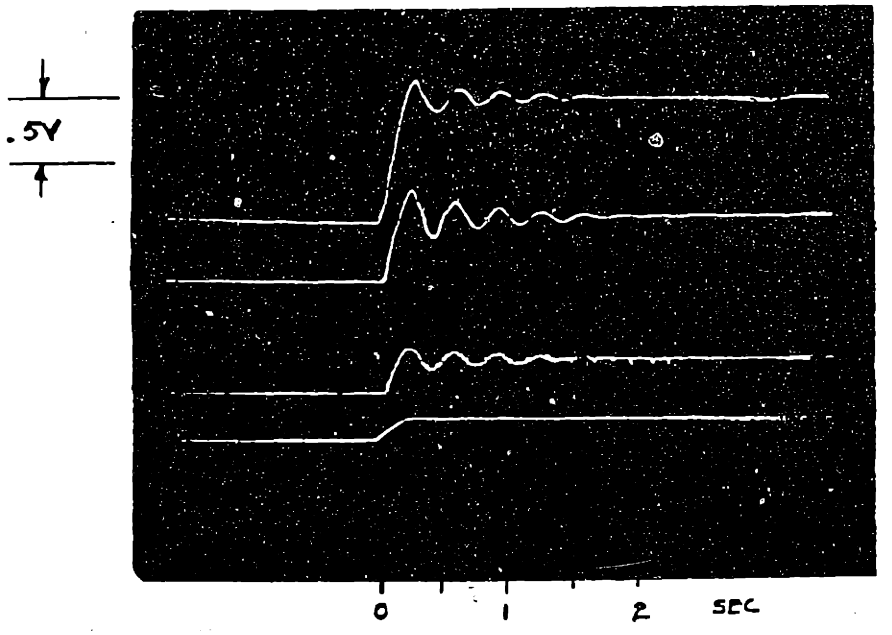

θ_{1E} AT 70 IN.
.05 RAD/V
18% OVERSHOOT

θ_1 AT 38.5 IN.
.09 RAD/V
50% OVERSHOOT

θ_1 AT BASE
.2 RAD/V
50% OVERSHOOT

CABLE L1

ACTUAL

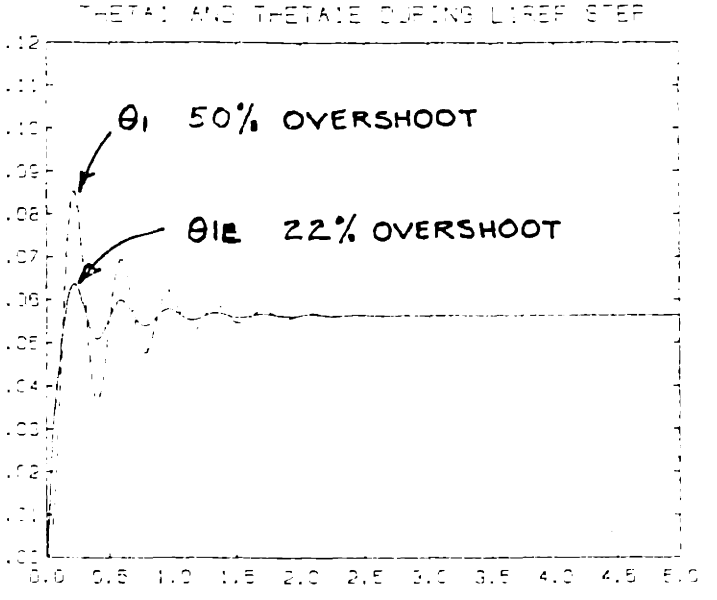

ANALYTIC

FIG 10.2: UNLOADED VIBRATORY MATCH, R=70 ML=0

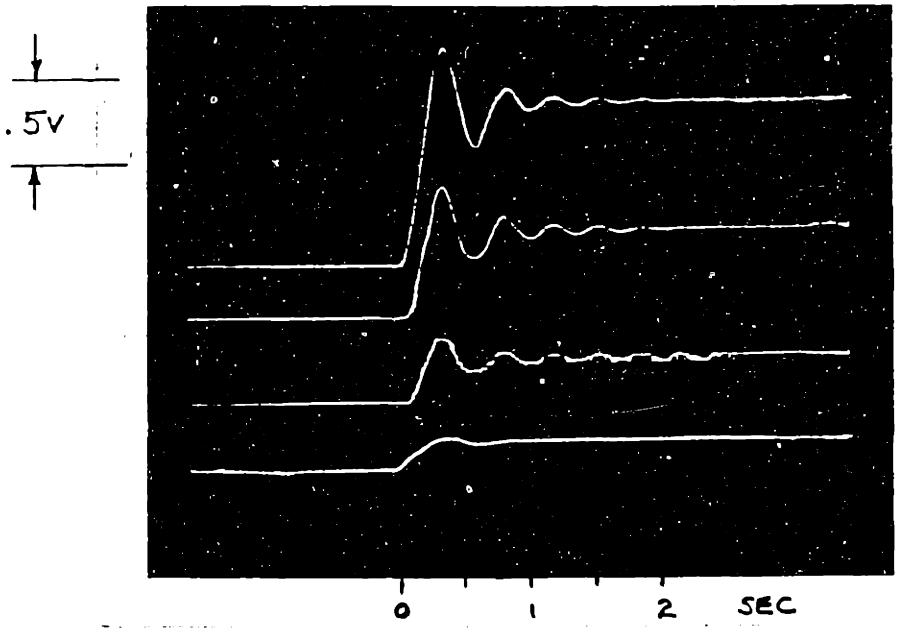

θ_{IE} AT 70 IN.
.05 RAD/V
35% OVERSHOOT

θ_1 AT 38.5 IN.
.09 RAD/V
60% OVERSHOOT

θ_1 AT BASE
.2 RAD/V
65% OVER SHOOT

CABLE L1
3.4 IN./V

ACTUAL

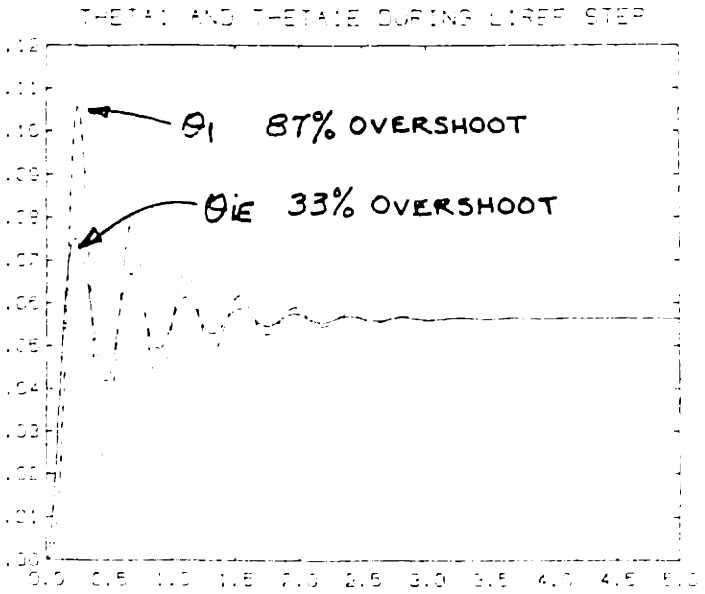

ANALYTIC

FIG 10.3: LOADED VIBRATORY MATCH R=70 ML=2

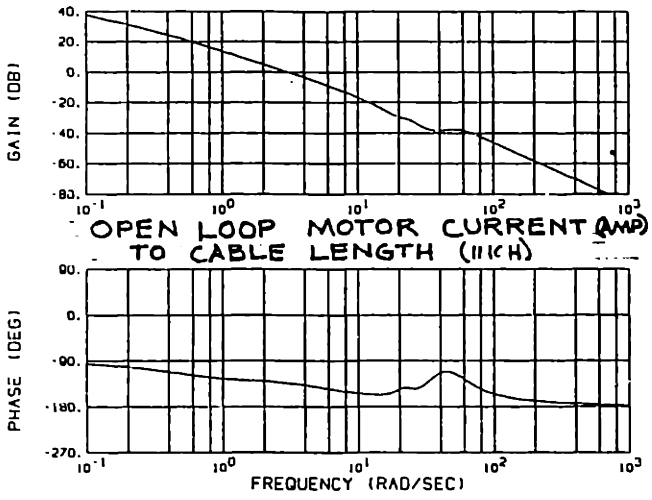

OPEN LOOP MOTOR CURRENT (AMP) TO CABLE LENGTH (INCH)

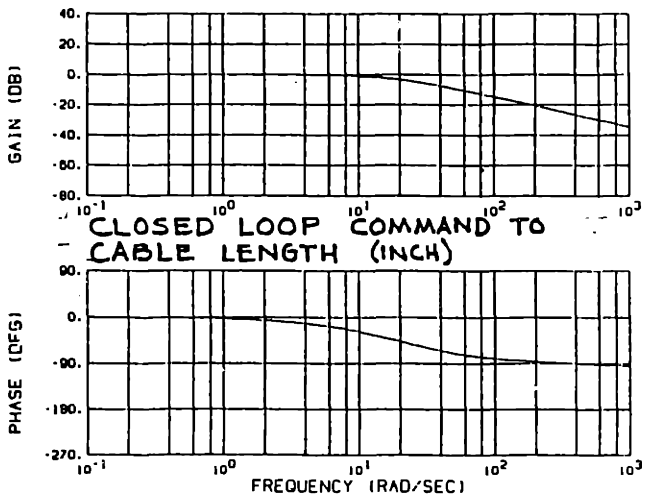

CLOSED LOOP COMMAND TO CABLE LENGTH (INCH)

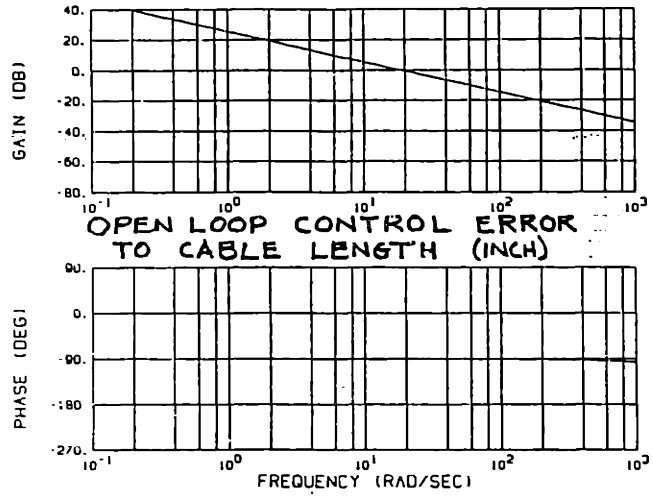

OPEN LOOP CONTROL ERROR TO CABLE LENGTH (INCH)

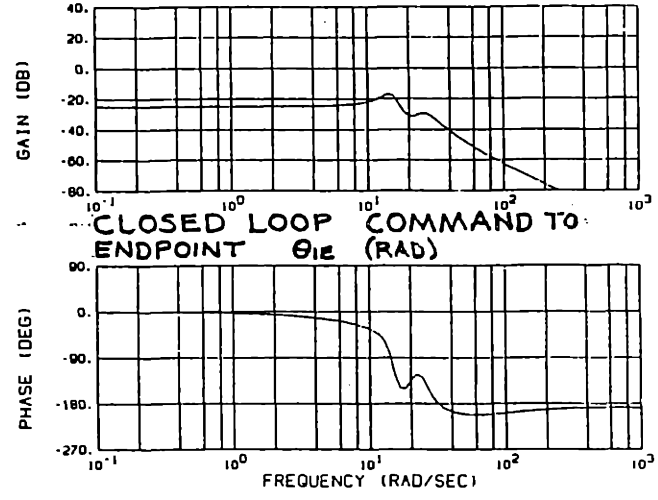

CLOSED LOOP COMMAND TO ENDPOINT θ_{IE} (RAD)

FIGURE 10.4: PARALLEL FREQUENCY RESPONSE ML= 2LBM

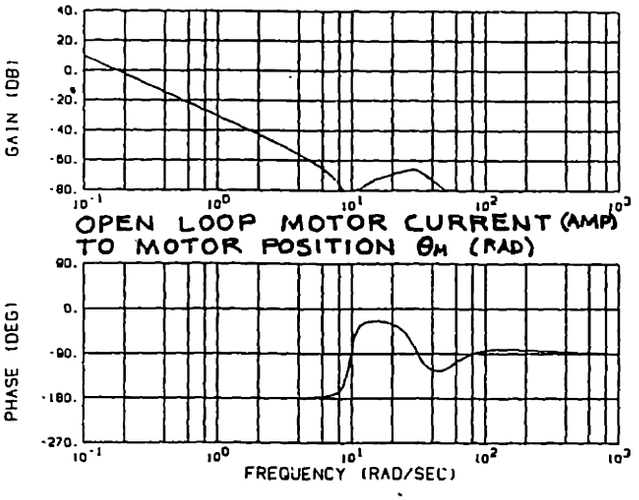

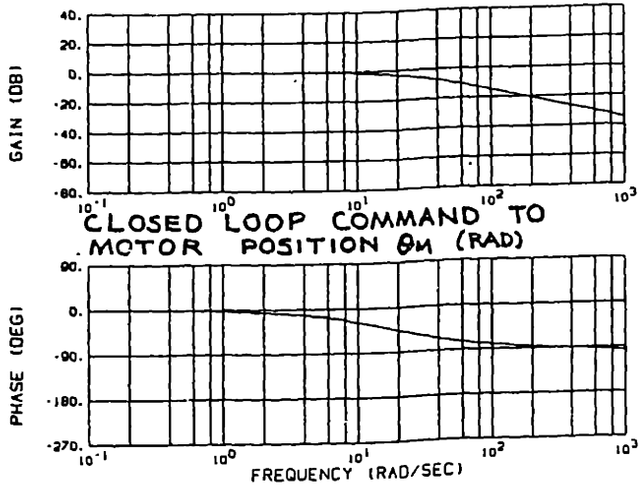

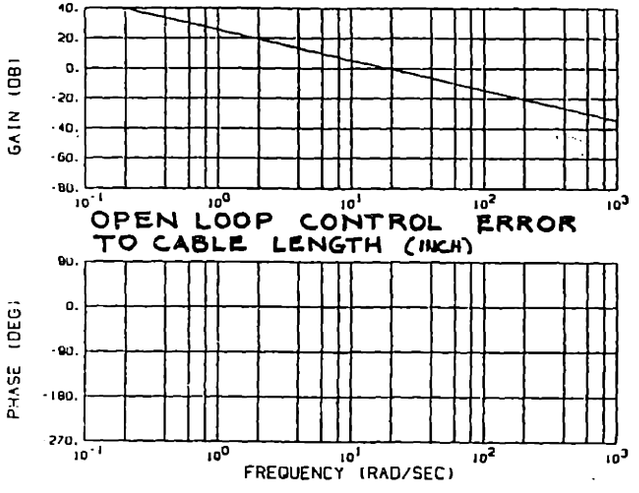

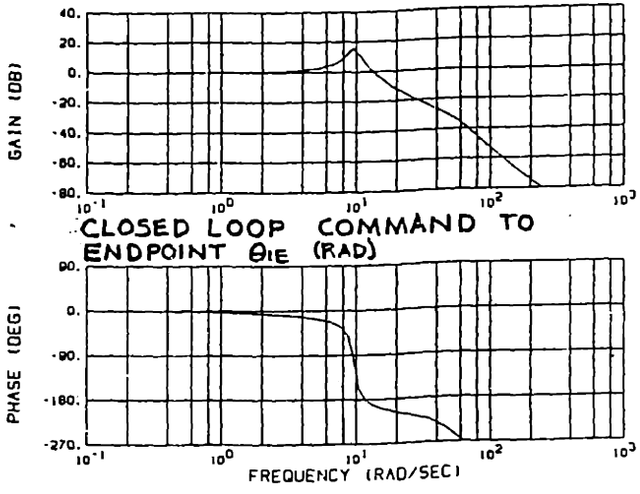

FIGURE 10.5: SERIAL FREQUENCY RESPONSE ML= 2LBM

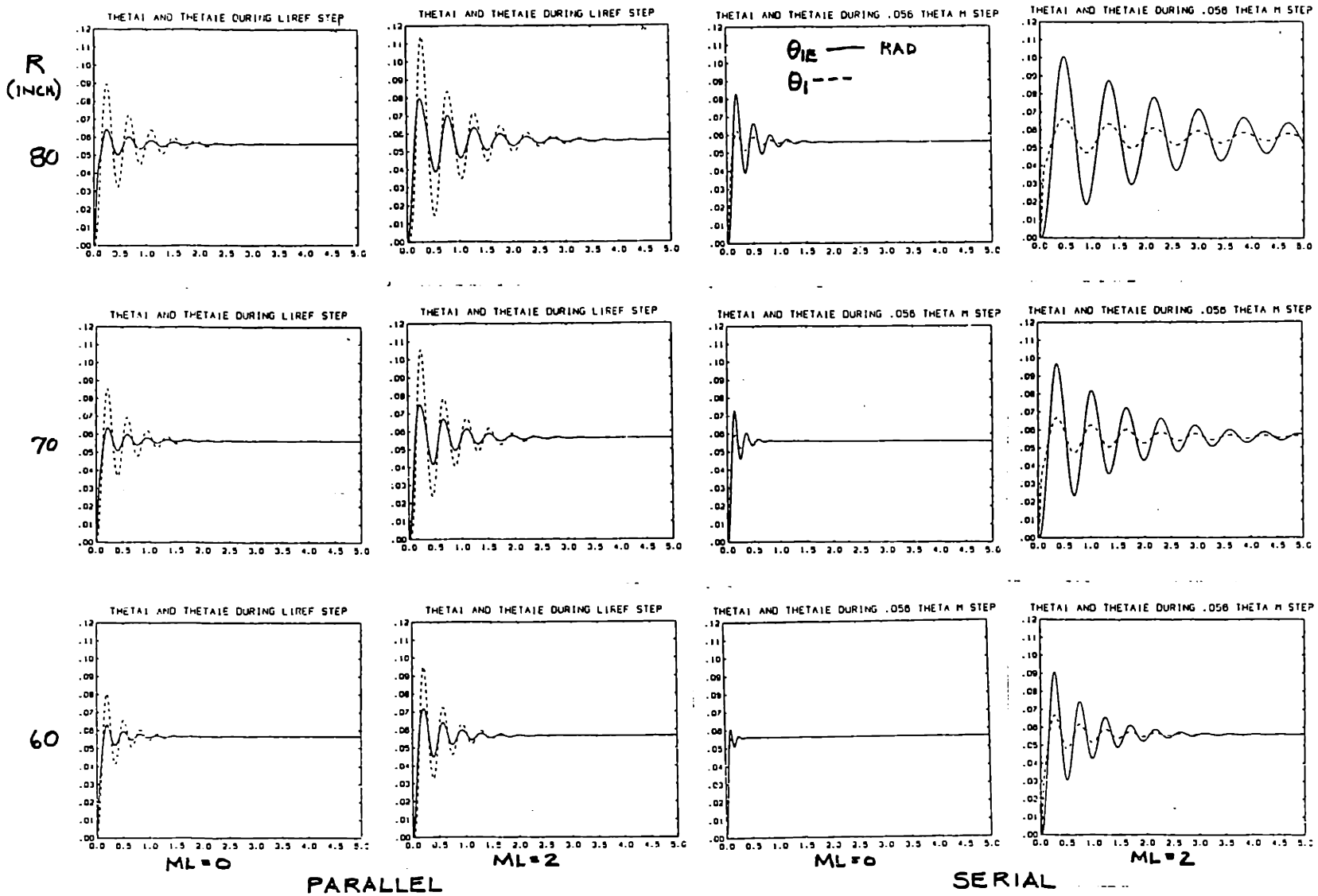

FIGURE 10.6 : PARALLEL AND SERIAL STEP RESPONSE VARY R

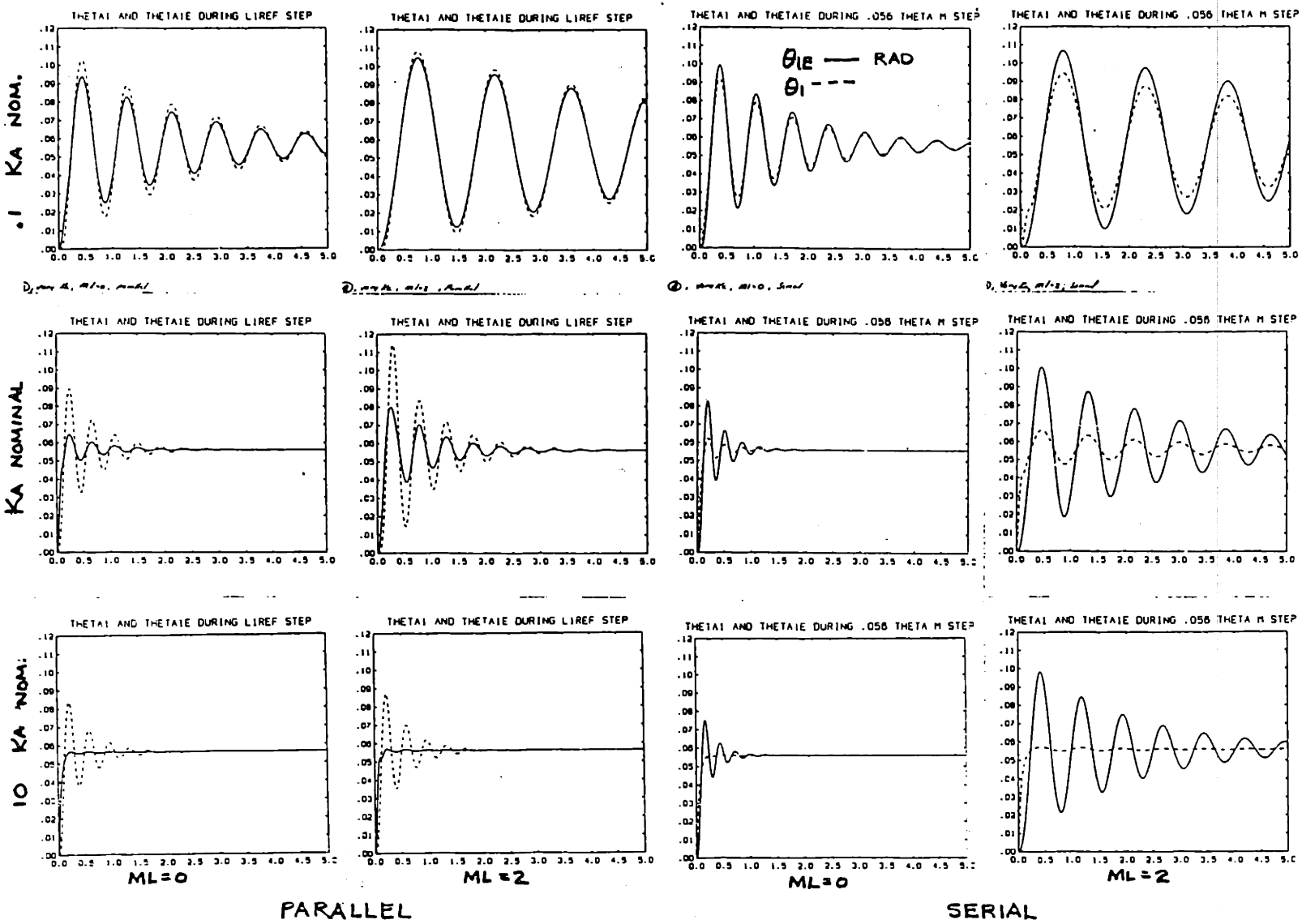

FIGURE 10.7 : PARALLEL AND SERIAL STEP RESPONSE VARY KA

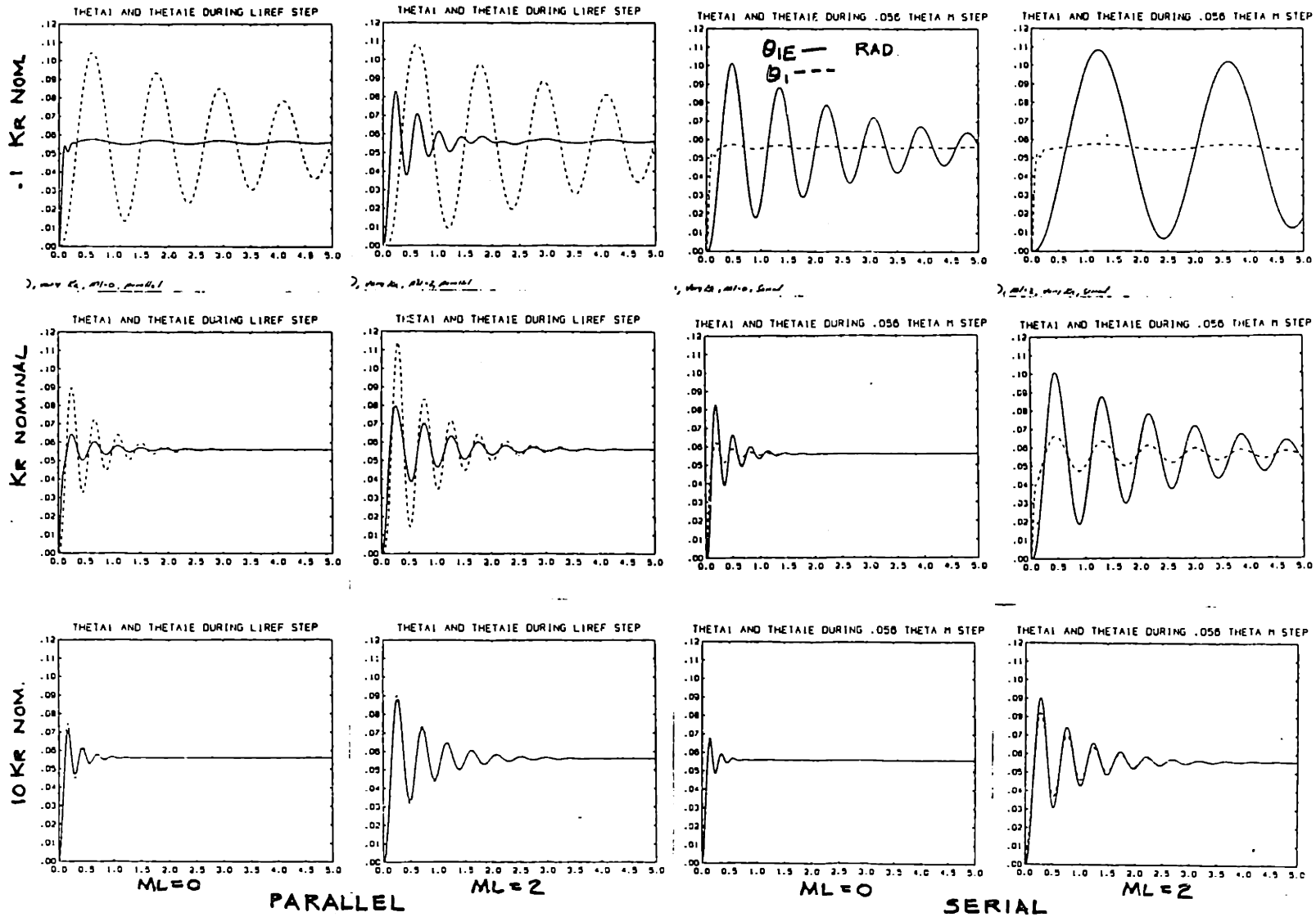

FIGURE 10.8: PARALLEL AND SERIAL STEP RESPONSE VARY KR

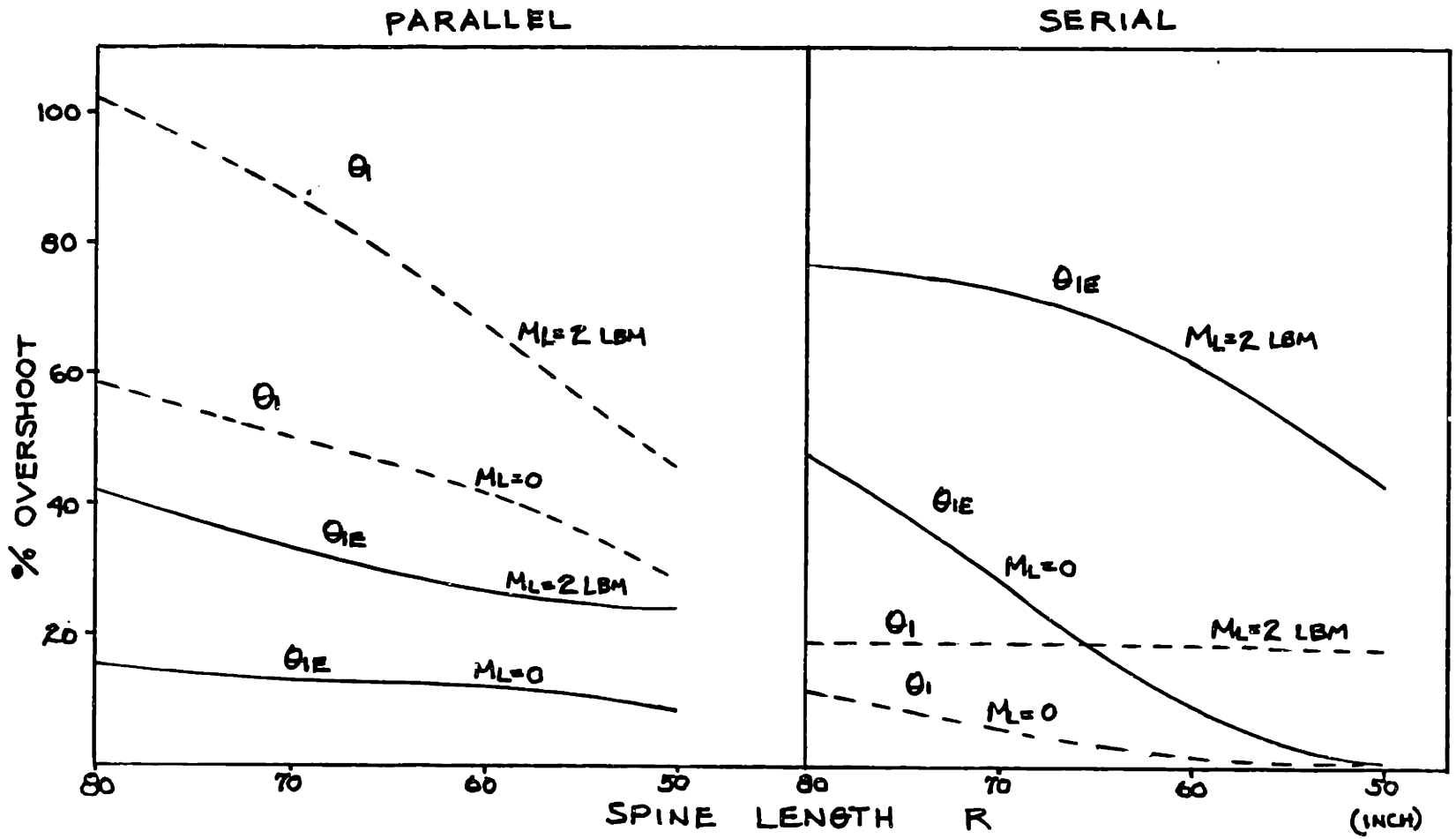

FIGURE 10.9: ENDPOINT AND BASE MAGNITUDES FOR VARYING R

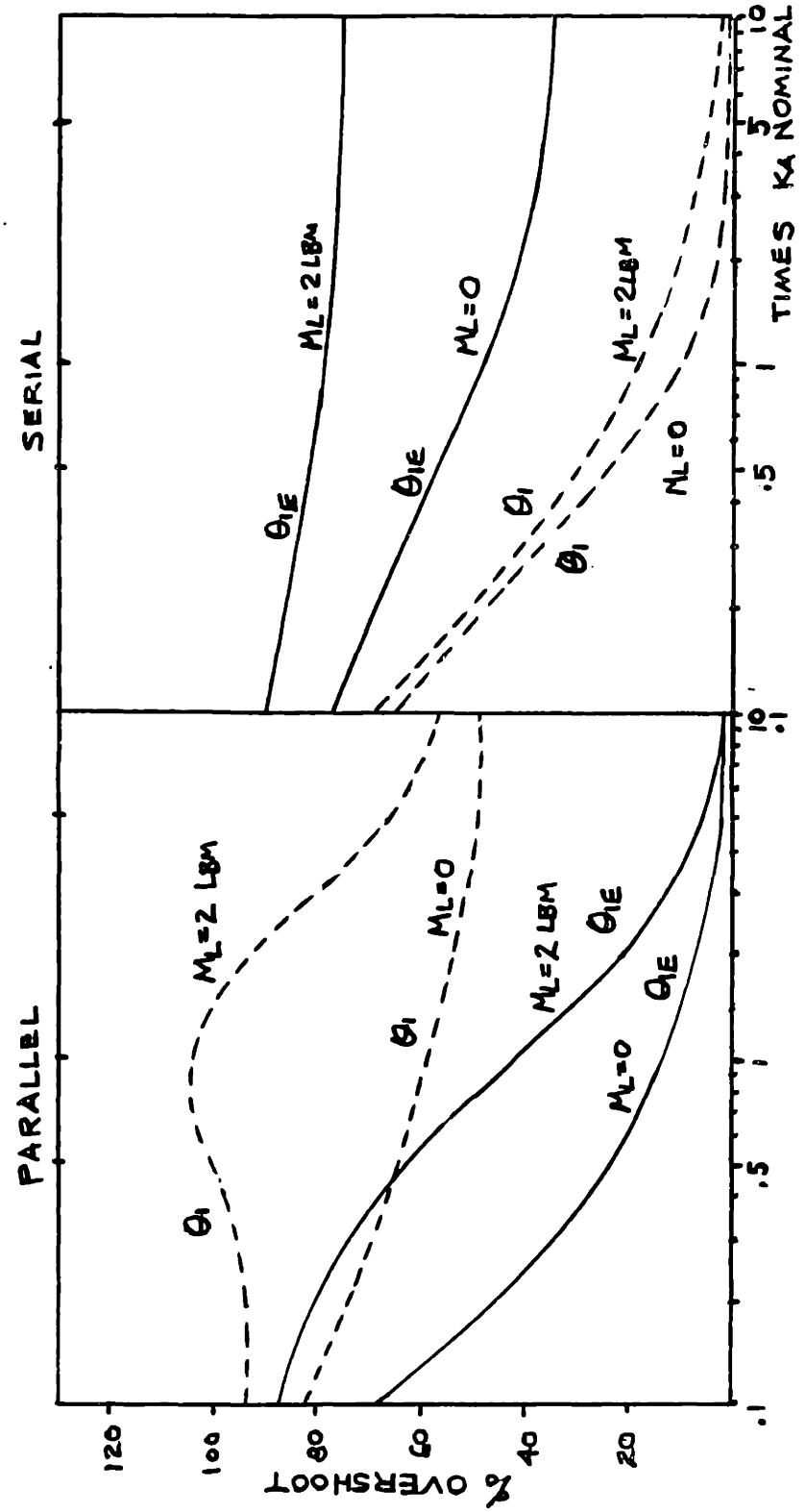

FIGURE 10.10: ENDPOINT AND BASE MAGNITUDES FOR VARYING KA

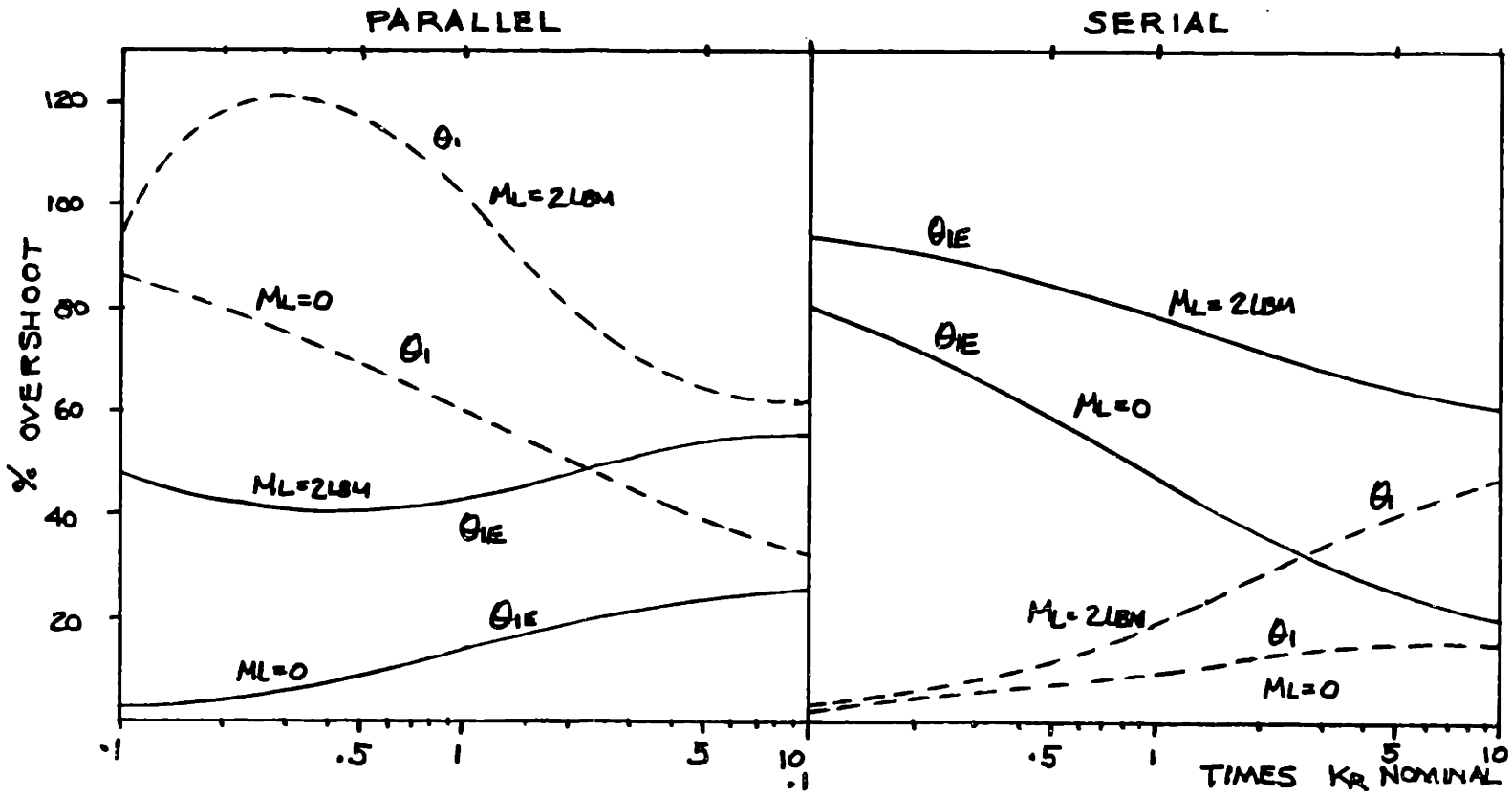

FIGURE 10.11: ENDPOINT AND BASE MAGNITUDES FOR VARYING K_R

Appendix 3.1

CABLE LENGTH TO ENDPOINT KINEMATICS

Cable Length in Terms of Joint Space and End Space

$$L1 = [\ (Xe-Rb)^2 + Ye^2 + Ze^2\ ]^{.5}$$

$$= [\ R^2 - 2\ R\ Rb\ S\theta1\ S\theta2 + Rb^2\ ]^{.5}$$

$$L2 = [\ (Xe + .5\ Rb)^2 + (Ye + \sqrt{3}/2\ Rb)^2 + Ze^2\ ]^{.5}$$

$$= [\ R^2 + Rb\ R\ S\theta1\ S\theta2 - \sqrt{3}\ Rb\ R\ C\theta2 + Rb^2]^{.5}$$

$$L3 = [\ (Xe + .5\ Rb)^2 + (Ye - \sqrt{3}/2\ Rb)^2 + Ze^2\ ]^{.5}$$

$$= [\ R^2 + Rb\ R\ S\theta1\ S\theta2 + \sqrt{3}\ Rb\ R\ C\theta2 + Rb^2]^{.5}$$

Terms for the Jacobian J$_L$

$$\delta L1/\delta R = (R - Rb\ S\theta1\ S\theta2) / L1$$

$$\delta L1/\delta\theta1 = -(R\ Rb\ C\theta1\ S\theta2) / L1$$

$$\delta L1/\delta\theta2 = -(R\ Rb\ S\theta1\ C\theta2) / L1$$

$$\delta L2/\delta R = (R + .5\ Rb\ S\theta1\ S\theta2 - \sqrt{3}/2\ Rb\ C\theta2) / L2$$

$$\delta L2/\delta\theta1 = (.5\ Rb\ R\ C\theta1\ S\theta2) / L2$$

$$\delta L2/\delta\theta2 = (.5\ Rb\ R\ S\theta1\ C\theta2 + \sqrt{3}/2\ Rb\ R\ S\theta2) / L2$$

$$\delta L3/\delta R = (R + .5\ Rb\ S\theta1\ S\theta2 + \sqrt{3}/2\ Rb\ C\theta2) / L3$$

$$\delta L3/\delta\theta1 = (.5\ Rb\ R\ C\theta1\ S\theta2) / L3$$

$$\delta L3/\delta\theta2 = (.5\ Rb\ R\ S\theta1\ C\theta2 - \sqrt{3}/2\ Rb\ R\ S\theta2) / L3$$

Appendix 3.1 con

Terms for Jacobian J{L|X}

$\delta L1/\delta Xe = (Xe - Rb) / L1$

$\delta L1/\delta Ye = Ye / L1$

$\delta L1/\delta Ze = Ze / L1$

$\delta L2/\delta Xe = (Xe + .5\ Rb) / L2$

$\delta L2/\delta Ye = (Ye + \sqrt{3}/2\ Rb) / L2$

$\delta L2/\delta Ze = Ze / L2$

$\delta L3/\delta Xe = (Xe + .5\ Rb) / L3$

$\delta L3/\delta Ye = (Ye - \sqrt{3}/2\ Rb) / L3$

$\delta L3/\delta Ze = Ze / L3$

Appendix 3.2

ENDPOINT TO CABLE LENGTH KINEMATICS

Endpoint Position in Terms of Cable Lengths

$$Xe = (-2\,L1^2 + L2^2 + L3^2) / (6\,Rb)$$

$$Ye = (L2^2 - L3^2) / (2\sqrt{3}\,Rb)$$

$$Ze = [-(L1^4 + L2^4 + L3^4 + Rb^4) / (6\,Rb^2) + (L1^2 + L2^2 + L3^2 - Rb^2)^2 / (6\,Rb^2) + -(L1^2 + L2^2 + L3^2 - 3\,Rb^2)^2 / (9\,Rb^2)\,]^{.5}$$

Terms of Jacobian J_x^{-1}

$$\delta Xe/\delta L1 = -(2\,L1) / (3\,Rb)$$

$$\delta Xe/\delta L2 = L2 / (3\,Rb)$$

$$\delta Xe/\delta L3 = L3 / (3\,Rb)$$

$$\delta Ye/\delta L1 = 0$$

$$\delta Ye/\delta L2 = L2 / (\sqrt{3}\,Rb)$$

$$\delta Ye/\delta L3 = -L3 / (\sqrt{3}\,Rb)$$

$$\delta Ze/\delta L1 = \frac{(-2\,L1^3 + L1\,L2^2 + L1\,L3^2 + 3\,L1\,Rb^2)}{3\,Rb\,[\,AA + BB + CC\,]^{.5}}$$

$$AA = -1.5\,(L1^4 + L2^4 + L3^4 + Rb^4)$$

$$BB = 1.5\,(L1^2 + L2^2 + L3^2 - Rb^2)^2$$

$$CC = -(L1^2 + L2^2 + L3^2 - 3\,Rb^2)^{.5}$$

$$\delta Ze/\delta L2 = \frac{(-2\,L2^2 + L2\,L1^2 + L2\,L3^2 + 3\,L2\,Rb^2)}{9\,Rb^2\,Ze}$$

$$\delta Ze/\delta L3 = \frac{(-2\,L3^2 + L3\,L1^2 + L3\,L2^2 + 3\,L3\,Rb^2)}{9\,Rb^2\,Ze}$$

APPENDIX 5.1

PITMO® D-C SERVO MOTORS

MOTOR SIZE CONSTANTS

ITEM	MOTOR SIZE CONSTANTS	UNITS	SYMBOL	9432, 9532 VALUE	9433, 9533 VALUE	9434, 9534 VALUE
1	PEAK TORQUE (STALL)	OZ-IN	TPK	13.8	31.6	41.2
1a	Peak torque (stall)	mN•m	TPK	97.4	223	291
2	MOTOR CONSTANT	OZ-IN/$\sqrt{W}$	PKO	1.62	2.66	3.00
2a	Motor constant	mN•m/$\sqrt{W}$	PKO	11.4	18.8	21.2
3	POWER FOR PEAK TORQUE	W	PWR	78.1	146	195
4	DAMPING (ZERO SOURCE IMPED.)	OZ-IN/(rad/s)	DPO	1.65×10^{-3}	5.02×10^{-3}	6.37×10^{-3}
4a	Damping (zero source imped.)	mN•m/(rad/s)	DPO	0.131	0.354	0.450
5	DAMPING (INFINITE SOURCE IMPED.)	OZ-IN/(rad/s)	DPI	2.60×10^{-3}	3.20×10^{-3}	3.70×10^{-3}
5a	Damping (infinite source imped.)	mN•m/(rad/s)	DPI	1.8×10^{-1}	2.3×10^{-1}	2.6×10^{-1}
6	NO LOAD SPEED	REV/MIN	SNL	6730	5810	5980
6a	No load speed	rad/s	WNL	705	608	626
7	ELECTRICAL TIME CONSTANT	ms	TCE	0.63	0.84	0.85
8	MECHANICAL TIME CONSTANT	ms	TCM	14.4	9.2	9.3
9	FRICTION TORQUE	OZ-IN	TOF	0.51	0.61	0.69
9a	Friction Torque	mN•m	TOF	3.6	4.3	4.9
10	ARMATURE INERTIA	OZ-IN-s^2	ERT	2.65×10^{-4}	4.64×10^{-4}	5.90×10^{-4}
10a	Armature inertia	kg•m^2	ERT	1.88×10^{-6}	3.28×10^{-6}	4.17×10^{-6}
11	MOTOR WEIGHT	OZ	WGT	6.98	8.9	10.1
11a	Motor mass	kg	WGT	0.20	0.25	0.29
12	THEORETICAL ACCELERATION	rad/s^2	CEL	51900	68100	69800
13	THERMAL TIME CONSTANT	MIN	TCT	7.21	11.1	12.0
14	ULTIMATE TEMP. RISE/WATT	°C/W	TPR	22.7	19.1	17.1
15	MAXIMUM WINDING TEMPERATURE	°C	TMX	155	155	155

WINDING CONSTANTS (other windings available)

MODELS 9432, 9532

	WINDING CONSTANTS	UNITS	SYMBOL	WDG #1	WDG #2	WDG #3	WDG #4
16	VOLTAGE	V	VLT	12.0	19.1	24.0	30.3
17	CURRENT (STALL)	A	AMP	6.52	4.10	3.25	2.59
18	TORQUE CONSTANT	OZ-IN/A	TPA	2.20	3.50	4.40	5.53
18a	Torque constant	mN•m/A	TPA	15.5	24.7	31.1	39.1
19	TERMINAL RESISTANCE	OHMS	RTR	1.84	4.65	7.38	11.7
20	BACK EMF	V/(rad/s)	BEF	0.0155	0.0247	0.0311	0.0391
21	INDUCTANCE	mH	DUK	1.16	2.94	4.64	7.34
22	CURRENT (NO LOAD)	A	INL	0.280	0.163	0.130	0.103

MODELS 9433, 9533

	WINDING CONSTANTS	UNITS	SYMBOL	WDG #1	WDG #2	WDG #3	WDG #4
16	VOLTAGE	V	VLT	12.0	19.1	24.0	30.3
17	CURRENT (STALL)	A	AMP	12.4	7.70	6.10	4.82
18	TORQUE CONSTANT	OZ-IN/A	TPA	2.61	4.20	5.28	6.66
18a	Torque constant	mN•m/A	TPA	18.4	29.6	37.3	47.2
19	TERMINAL RESISTANCE	OHMS	RTR	0.97	2.48	3.94	6.28
20	BACK EMF	V/(rad/s)	BEF	0.0184	0.0297	0.0373	0.0472
21	INDUCTANCE	mH	DUK	0.80	2.08	3.20	5.27
22	CURRENT (NO LOAD)	A	INL	0.256	0.159	0.127	0.100

MODELS 9434, 9534

	WINDING CONSTANTS	UNITS	SYMBOL	WDG #1	WDG #2	WDG #3	WDG #4
16	VOLTAGE	V	VLT	12.0	19.1	24.0	30.3
17	CURRENT (STALL)	A	AMP	16.3	10.3	8.11	6.46
18	TORQUE CONSTANT	OZ-IN/A	TPA	2.59	4.07	5.17	6.50
18a	Torque constant	mN•m/A	TPA	18.2	28.8	36.5	45.9
19	TERMINAL RESISTANCE	OHMS	RTR	0.74	1.85	2.96	4.69
20	BACK	V/(rad/s)	BEF	0.0183	0.0288	0.0365	0.0459
21	INDUCTANCE	mH	DUK	0.63	1.56	2.51	3.97
22	CURRENT (NO LOAD)	A	INL	0.308	0.196	0.154	0.123

TORQUE RATINGS, OZ.-IN.

Ratio	"A" Max.	Rotation*	Gear Efficiency	Standard Gearing	High Torque Gearing	Wide Face Gearing	"B" MAX. GM9412	GM9413	GM9414
5.9:1	1.380	CW	.81	175	N/A	N/A	3.111	3.486	3.686
11.5:1	1.380	CW	.81	175	N/A	N/A	3.111	3.486	3.686

Appendix 6.1

CONTROL VALUES

KO1	=	2000
KO2	=	1000
KO3	=	446
Kv	=	.016 volts / (in/sec)
Ksa	=	1.2 amps / volts
Gr	=	11.5 = gear ratio
Rw	=	.5 inch = winch radius
Kt	=	.406 in lbf / amp = motor torque constant
Klv	=	.297 volts/inch
Meq	=	.094 lbf sec²/inch
Mmotor	=	.020 lbf sec²/inch
Beq	=	.13 lbf sec / inch
Kol	=	KO2 KSA KT Gr / Rw = 11206 lbf/volt
Kfv	=	KO3 Kv/ KO2 = .007 volts / (in/sec)
Kps	=	Kol Klv = 3328 lbf/inch
Kvs	=	Kv KO2 Ksa Gr Kt / Rw = 177 lbf/(in/sec)
Tm	=	.159 sec

Appendix 9.1

NON LINEAR RIGID EQUATIONS

Matrix Form

$$\underline{H}\ \ddot{\underline{q}} + \underline{h(q,\dot{q})} + \underline{G(q)} = \underline{Q}$$

Where: $\underline{q}$ = generalized coordinates
$\underline{Q}$ = generalized forces

$$q = \begin{bmatrix} \theta 1 \\ \theta 2 \\ R \end{bmatrix} \qquad Q = \begin{bmatrix} r\theta 1 \\ r\theta 2 \\ Fr \end{bmatrix}$$

Matrices

$$H(1,1) = (Mp\ Lc1^2 + Mr\ Lc2^2 + Iprx)\ S\theta 2^2 + Iprz\ C\theta 2^2$$

$$H(1,2) = 0$$

$$H(1,3) = 0$$

$$H(2,1) = 0$$

$$H(2,2) = Mp\ Lc1^2 + Mr\ Lc2^2 + Ipry$$

$$H(2,3) = 0$$

$$H(3,1) = 0$$

$$H(3,2) = 0$$

$$H(3,3) = Mr$$

$$h(1,1) = 2\ Mr\ Lc2\ S\theta 2^2\ \dot{R}\ \dot{\theta}1 + 2(Mp\ Lc1^2 + Mr\ Lc2^2 + Iprx - Iprz)\ S\theta 2\ C\theta 2\ \dot{\theta}1\ \dot{\theta}2$$

$$h(2,1) = -(Mp\ Lc1^2 + Mr\ Lc2^2 + Iprx - Iprz)\ S\theta 1\ C\theta 2\ \theta 1^2 + 2\ Mr\ Lc2\ \dot{R}\ \dot{\theta}2$$

$$h(3,1) = -Mr\ Lc2\ S\theta 2^2\ \dot{\theta}1^2 - Mr\ Lc2\ \dot{\theta}2^2$$

Appendix 9.1 con.

$G(1,1) = -(Mp\ Lc1 + Mr\ Lc2)\ g\ S\theta1\ S\theta2$

$G(2,1) = (Mp\ Lc1 + Mr\ Lc2)\ g\ C\theta1\ C\theta2$

$G(3,1) = Mr\ g\ C\theta1\ S\theta2$

Where:
- Mp = cylinder mass
- Mr = rod mass
- Iprx = rod & cylinder moment of inertia around the X1 axis
- Ipry = rod & cylinder moment of inertia around the Y1 axis
- Iprz = rod & cylinder moment of inertia around the Z1 axis

See fig 9.2 for definition of angles and lengths

Appendix 9.2

NON LINEAR FLEXIBLE DYNAMIC EQUATIONS

Equation Form: no external forces

$$d/dt\ \delta T/\delta \dot{L}i - \delta T/\delta Li + \delta U/\delta Li = TLi \qquad i = 1,2,3$$

$$d/dt\ \delta T/\delta \dot{\theta}i - \delta T/\delta \theta i + \delta U/\delta \theta i = 0 \qquad i = 1,2$$

$$d/dt\ \delta T/\delta \dot{R} - \delta T/\delta R + \delta U/\delta R = Fs$$

$$d/dt\ \delta T/\delta \dot{\theta}ie - \delta T/\delta \theta ie + \delta U/\delta \theta ie = 0 \qquad i = 1,2$$

Terms:

$$d/dt\ \delta T/\delta \dot{\theta}1 =$$
$$2\ (Mp\ Lc1^2 + Mr\ Lc2^2 + Iprx - Iprz)\ S\theta2\ C\theta2\ \dot{\theta}1\ \dot{\theta}2 +$$
$$+\ 2\ Mr\ Lc2\ S\theta2^2\ \dot{R}\ \dot{\theta}1 +$$
$$+\ [(Mp\ Lc1^2 + Mr\ Lc2^2 + Iprx)\ S\theta2^2 + Iprz\ C\theta2^2]\ \ddot{\theta}1$$

$$d/dt\ \delta T/\delta \dot{\theta}2 = (Mp\ Lc1^2 + Mr\ Lc2^2 + Ipry)\ \ddot{\theta}2 +$$
$$+\ 2\ Mr\ Lc2\ \dot{R}\ \dot{\theta}2$$

$$d/dt\ \delta T/\delta \dot{R} = (Mr + Me)\ \ddot{R}$$

$$d/dt\ \delta T/\delta \dot{L}1 = (Im / Rw^2)\ \ddot{L}1$$

$$d/dt\ \delta T/\delta \dot{L}2 = (Im / Rw^2)\ \ddot{L}2$$

$$d/dt\ \delta T/\delta \dot{L}3 = (Im / Rw^2)\ \ddot{L}3$$

$$d/dt\ \delta T/\delta \dot{\theta}1e =$$
$$2\ Me\ R\ S\theta2e^2\ \dot{R}\ \dot{\theta}1e + 2\ Me\ R^2\ S\theta2e\ C\theta2e\ \dot{\theta}1e\ \dot{\theta}2e +$$
$$+\ Me\ R^2\ S\theta2e^2\ \ddot{\theta}1e$$

$$d/dt\ \delta T/\delta \dot{\theta}2e = 2\ Me\ R\ \dot{R}\ \dot{\theta}2e + Me\ R^2\ \ddot{\theta}2e$$

$$\delta T/\delta \theta 1 = 0$$

$$\delta T/\delta \theta 2 =$$
$$(Mp\ Lc1^2 + Mr\ Lc2^2 + Iprx - Iprz)\ S\theta2\ C\theta2\ \dot{\theta}1^2$$

Appendix 9.2 con.

$$\delta T/\delta R = Mr\ Lc2\ S\theta2^2\ \dot{\theta}1^2 + Mr\ Lc2\ \dot{\theta}2^2$$

$$\delta T/\delta L1 = 0$$

$$\delta T/\delta L2 = 0$$

$$\delta T/\delta L3 = 0$$

$$\delta T/\delta \theta 1e = 0$$

$$\delta T/\theta 2e = Me\ R^2\ S\theta2e\ C\theta2e\ \dot{\theta}1e^2$$

$$\delta U/\delta \theta 1 = -(Mp\ Lc1 + Mr\ Lc2)\ g\ S\theta1\ S\theta2 - Kr\ (\theta1e - \theta1)$$

$$\delta U/\delta \theta 2 = (Mp\ Lc1 + Mr\ Lc2\ )\ g\ C\theta1\ C\theta2 - Kr\ (\theta2e - \theta2)$$

$$\delta U/\delta R = Mr\ g\ C\theta1\ S\theta2 + Me\ g\ C\theta1e\ S\theta2e +$$

$$-\frac{[Ka\ (L1 - (L1 - L1e)\cdot^5)(2\ R - 2\ Rb\ S\theta1e\ S\theta2e)]}{(2\ L1e)} +$$

$$-\frac{[Ka\ (L2 - (L2 - L2e)\cdot^5)(2R + Rb\ S\theta1e\ S\theta2e - \sqrt{3}\ Rb\ C\theta2e)]}{(2\ L2e)} +$$

$$-\frac{[Ka\ (L3 - (L3 - L3e)\cdot^5)(2R + Rb\ S\theta1e\ S\theta2e + \sqrt{3}\ Rb\ C\theta2e)]}{(2\ L3e)}$$

$$\delta U/\delta \theta 1e = -\ Me\ g\ R\ S\theta1e\ S\theta2e +$$

$$-\frac{Ka\ (L1 - L1e)(-2\ R\ Rb\ C\theta1e\ S\theta2e)}{2\ L1e} +$$

$$-\frac{Ka\ (L2 - L2e)(\ R\ Rb\ C\theta1e\ S\theta2e)}{2\ L2e} +$$

$$-\frac{Ka\ (L3 - L3e)(\ R\ Rb\ C\theta1e\ S\theta2e)}{2\ L3e} + Kr\ (\theta1e - \theta1)$$

$$\delta U/\delta\theta 2e = Me\ g\ R\ C\theta 1e\ C\theta 2e +$$

$$- \frac{Ka\ (L1 - L1e)(-2\ R\ Rb\ S\theta 1e\ C\theta 2e)}{2\ L1e} +$$

$$- \frac{Ka\ (L2 - L2e)(\ R\ Rb\ S\theta 1e\ C\theta 2e + \sqrt{3}\ Rb\ R\ S\theta 2e)}{2\ L2e} +$$

$$- \frac{Ka\ (L3 - L3e)(\ R\ Rb\ S\theta 1e\ C\theta 2e - \sqrt{3}\ Rb\ R\ S\theta 2e)}{2\ L3e} +$$

$$+ Kr\ (\theta 2e - \theta 2)$$

$$\delta U/\delta L1 = Ka\ (L1 - L1e)$$

$$\delta U/\delta L2 = Ka\ (L2 - L2e)$$

$$\delta U/\delta L3 = Ka\ (L3 - L3e)$$

Where:
- Mp = Cylinder mass
- Mr = Rod mass
- Me = Mass lumped at the endpoint, the combination of load and 23% of the rod mass
- Iprx = Rod & cylinder moment of inertia around the X1 axis
- Ipry = Rod & cylinder moment of inertia around the Y1 axis
- Iprz = Rod & cylinder moment of inertia around the Z1 axis
- Ka = Actuator and cable stifness
- Kr = Rod stifness

The cable lengths Li and Lie are defined in Appendix 3.2, Lie uses θie instead of θi. The inertias are defined in Appendix 9.1. The angles and lengths are defined in fig 9.2 and 9.3

Appendix 9.3

LINEAR FLEXIBLE MATRICES

Generalized Coordinates and Generalized Forces

$$\underline{q} = \begin{bmatrix} L1 \\ L2 \\ L3 \\ R \\ \theta 1e \\ \theta 2e \\ \theta 1 \\ \rho 2 \end{bmatrix} \qquad \underline{Q} = \begin{bmatrix} TL1 \\ TL2 \\ TL3 \\ 0 \\ 0 \\ 0 \\ 0 \\ 0 \end{bmatrix}$$

Mass Matrix: this is a diagonal matrix.

$M(1,1) = M(2,2) = M(3,3) = Im/Rw^2$
$M(4,4) = Mr + Me$
$M(5,5) = M(6,6) = Me\ R^2$
$M(7,7) = Mp\ Lc1^2 + Mr\ Lc2^2 + Iprx$
$M(8,8) = Mp\ Lc1^2 + Mr\ Lc2^2 + Ipry$

Stiffness Matrix: this is a symmetric matrix only the upper half will be defined, the terms not mentioned are zero

$K(1,1) = K(2,2) = K(3,3) = Ka$
$K(1,4) = K(2,4) = K(3,4) = -Ka\ R/L$
$K(4,4) = 3\ Ka\ R^2/L^2$
$K(1,5) = Ka\ R\ Rb/L$
$K(2,5) = K(3,5) = -Ka\ R\ Rb/(2\ L)$
$K(2,6) = -\sqrt{3}\ Ka\ R\ Rb\ /(2\ L)$
$K(3,6) = -\ K(2,6)$
$K(5,5) = K(6,6) = 1.5\ Ka\ R^2\ Rb^2/L^2 + Kr$
$K(7,7) = K(8,8) = Kr$
$K(5,7) = K(6,8) = -Kr$

Gain Matrices

$$\underline{Kp} = \begin{bmatrix} Kps & 0 & 0 & 0 & 0 & 0 & 0 & 0 \\ 0 & Kps & 0 & 0 & 0 & 0 & 0 & 0 \\ 0 & 0 & Kps & 0 & 0 & 0 & 0 & 0 \end{bmatrix}$$

$$\underline{Kv} = \begin{bmatrix} Kvs & 0 & 0 & 0 & 0 & 0 & 0 & 0 \\ 0 & Kvs & 0 & 0 & 0 & 0 & 0 & 0 \\ 0 & 0 & Kvs & 0 & 0 & 0 & 0 & 0 \end{bmatrix}$$

Kvs and Kps are defined in Appendix 6.1

Appendix 9.4

LINEAR MATRICES FOR THE SERIAL MANIPULATOR

Generalized Coordinates and Forces:

$$\underline{q} = \begin{bmatrix} \theta m \\ R \\ \theta 1 \\ \theta 1 e \end{bmatrix} \qquad \underline{Q} = \begin{bmatrix} \Gamma m \\ Fr \\ 0 \\ 0 \end{bmatrix}$$

Mass Matrix:

$$\underline{M} = \begin{bmatrix} Im & 0 & 0 & 0 \\ 0 & Mr + Me & 0 & 0 \\ 0 & 0 & Mp\ Lc1^2 + Mr\ Lc2^2 + Iprx & 0 \\ 0 & 0 & 0 & Me\ R^2 + Ie \end{bmatrix}$$

Stiffness Matrix:

$$\underline{K} = \begin{bmatrix} K\theta & 0 & -K\theta & 0 \\ 0 & 0 & 0 & 0 \\ -K\theta & 0 & Kr + K\theta & -Kr \\ 0 & 0 & -Kr & Kr \end{bmatrix}$$

REFERENCES

1) Landsberger, Design and Construction of a Cable-Controlled Parallel Link Manipulator, S.M. Thesis, M.I.T., 1984

2) Asada and Slotine, Robot Analysis and Control, John Wiley and Sons, New York, 1986

3) Pieper, The Kinematics of Manipulators Under Computer Control, Phd Thesis, Stanford University, 1968

4) Cable Manufacturing and Assembly Co., General Products Catalog No. C-83, CMA, New Jersey, 1986

5) Saner, Pittman Servo Motor Application Notes, Pittman, Penn., 1985

6) Youcef-Toumi, Development of a Direct-Drive Arm Using High Torque Brushless Motors, First ISRR, Summer 1983

7) Sunada and Dubowsky, On the Dynamic Analysis and Behavior of Industrial Robotic Manipulators with Elastic Members, ASME trans., March 1983

8) Asada and Yousef-Toumi, The Design of Open-Loop Mainipulator Arms with Decoupled and Configuration Invarient Inertia Tensors, submitted to ASME Journal of Dynamic Systems, Measurement, and Control, 1987

9) Performance Specification Manipulator Arm, SRMS, SPAR-SG 366, SPAR Aerospace Products, Ontario, Canada, 1978